The Pennsylvania State University

The Graduate School

Department of Aerospace Engineering

DESIGN, MANUFACTURE, AND TESTING OF VOLUME SCANNING MECHANISMS FOR A LIDAR AND RADAR SOUNDER

A Thesis in

Aerospace Engineering

by

Thomas E. Manning II

Submitted in Partial Fulfillment
of the Requirements
for the Degree of

Master of Science

August 1993

Thomas E. Manning II

We approve the thesis of Thomas E. Manning II.

Date of Signature

George A. Lesieutre Assistant Professor of Aerospace Engineering Thesis Advisor	
C. Russell Philbrick Professor of Electrical Engineering	
Dennis K. McLaughlin Professor of Aerospace Engineering Head of the Department of Aerospace Engineering	

ABSTRACT

Understanding the physical mechanisms involved in complicated atmospheric processes, such as cloud formation, requires simultaneous measurements of many atmospheric parameters. However, because individual systems such as lidars and radars measure only a few quantities as functions of space and time, complete data sets are rarely obtained and the majority of data acquired by individual instruments is under-utilized. To improve this situation, a group of researchers at Penn State University is building an integrated observing system featuring simultaneous measurements by several instruments. This integrated system is being developed to simultaneously measure condensed water, aerosols, temperature, and water vapor in a volume of the troposphere. The measurements will be made with lidar and radar systems that are mounted on volume scanning mechanisms.

This thesis addresses the development, design, manufacture, and testing of the volume scanning mechanisms for the lidar and radar systems. Design requirements, based on the scientific needs for the project, include a 10 degree per second scanning rate with a 0.1 degree accuracy and reproducibility. Eight initial concepts were developed and reduced to three concepts by preliminary assesments of performance and practicality. The three retained concepts were analyzed for motor sizing, feasibility, and cost to determine the final focus design.

Two identical structures, one for the each of the lidar and radar systems, using micro-stepping motors with 20:1 gear reduction were manufactured to move the atmospheric measuring systems. The motors are controlled with a 4-axis, closed-loop controller that is run from a PC to create motion in the azimuth and elevation coordinates. A test plan was developed to determine the capabilities and limitations of the system.

TABLE OF CONTENTS

LIST OF FIGURES

LIST OF TABLES

NOMENCLATURE

Term	Definition
VSM	volume scanning mechanism
lidar	LIght Detection And Ranging
radar	Radio Acoustic Detection and Ranging
WAVE-LARS	Water and Aerosol Variables in the Environment Lidar And Radar Sounder
DoE	Department of Energy
PSU	Pennsylvania State University
ARL	Applied Research Laboratory
GME	Gear reduction box, Motor, and Encoder combination

ACKNOWLEDGMENTS

Much of the work presented within this thesis could not have been possible without the help of the LARS team. I thank Sumati Rajan, George Evanisko, Mike O'Brian, Brian Mathason, Jim Anuskiewicz, Jim Yurack, David Machuga, and Tim Tyce for their help in teaching me LIDAR principles and assisting me in the writing of this thesis. In addition, I would like to recognize Tim Kane for his helpful and humorous ideas for the work presented.

I am very grateful for the help and guidance provided by my thesis advisor, George Lesieutre. He taught me many things, including that I must be confident in my work and think in a broad and insightful manner. His wisdom and advice allowed me to further grow intellectually and spiritually. He is an excellent person and I applaud him.

I am grateful for the insight and help provided by the manager of this project, C. R. Philbrick. I learned many things from him and respect him very much. I am also thankful to D. K. McLaughlin for allowing me to begin my graduate school under his employment. The practical experience that I learned under him allowed me to receive the research assistantship for the work presented in this thesis.

As I was writing this thesis, I had many times when I wanted to quit. There is one special person that I would like to thank for giving me the drive and love to continue. Tracie's love and support kept me going when the times got hectic. She was there for me when I was getting frustrated when I had to prepare for entry into the U.S. Air Force and try to get all the last details done for my graduation. I love you Tracie.

Finally, I wish to thank my mother for being there throughout my college career. She helped me whenever I needed it, from the time when I first arrived at Penn State as a freshman and to the time when I left as a Master of Science in Aerospace Engineering. I could never have done this without you.

This work was supported by the Department of Energy under grant number DE-FG05-92FR79113.

Chapter 1

INTRODUCTION

The most severe limitation to scientists' knowledge about the climate system is a lack of high quality atmospheric observations of hydrologic variables. The dramatic increase in computing power over the past 20 years has enabled simulation of the atmosphere on time scales ranging from days for forecasting to decades for climate simulation. The decreasing cost in this computing power has made many of these tools accessible to a majority of research scientists. This increase in computing power has shifted most of the experimental research towards the theoretical and computational efforts. The shift has been enhanced by limited funding and the rising cost of building the more sophisticated instruments needed for remote sensing of the atmosphere from the ground and space. Thus, we find that our ability to simulate the variables in the atmosphere and oceans currently far outstrip our ability to measure the same quantities. [1]

Understanding the physical mechanisms involved in complicated processes such as cloud formation requires simultaneous measurements of many atmospheric parameters. However, because individual systems such as lidars (LIght Detection And Ranging) and radars (RAdio Detection And Ranging) measure only a few quantities as functions of space and time, complete data sets are rarely obtained and the majority of data acquired by the individual instruments are under-utilized. To study cloud formation and maintenance comprehensively, it is imperative to study water vapor and aerosol content as a function of both space and time. To improve this situation, a group of researchers at Penn State University are building an integrated observing system featuring simultaneous measurements by several instruments. This integrated system, Water and Aerosol Variables in the Environment Lidar And Radar Sounder (WAVE-LARS), is being developed to measure simultaneously condensed water, aerosols, temperature, and water

vapor in a volume of the troposphere. Also, high resolution water vapor and aerosol data will enable study of the movement of fronts, boundary layers, clouds, etc. The measurements are made with lidar and radar systems mounted on volume scanning mechanisms (VSM) and a lidar system that is pointed in a fixed direction.

1.1 Specific Measurements

Both the lidar and radar systems will measure the liquid/ice phase temperature distribution to map the 3-D aerosol distribution within a cloud structure. The fixed lidar system will measure profiles of water vapor concentration along a chosen line of sight, on the basis of measuring the ratio of the Raman back-scatter intensity profiles (to be discussed later) of water vapor and molecular nitrogen. The 94 GHz radar will map a high resolution 3-D contour of the small droplets that make up the liquid water content. These measurements will enable a study of the boundary moisture fluxes, cumulus formation, cloud base entrainment, and cloud water budgets. These measurements will be made from near surface altitudes to the troposphere.

1.2 Lidar Principles of Operation

The lidar and radar systems operate similarly, (with the primary difference being the wavelength of operation). Although they operate similarly, only the principles of operation of the lidar will be discussed herein as it is slightly more complex. Note that the equipment used for a radar system (antennas, waveguides, and data acquisition) is somewhat simpler than that used for a lidar system (pulsed laser, optical telescope, optics, and data acquisition) because of the longer wavelength involved. The transmitter of the energy for the lidar is usually a pulsed laser. The laser pulses are normally directed to the zenith (perpendicular to horizon) and the backscattered return is monitored. Note that the WAVE-LARS system will not be pointing vertical, but will be pointing at an area of the

sky. There are four scattering processes that make up the measured backscattered light. The relevant processes used in the WAVE-LARS instrument are: 1) Rayleigh scattering, 2) aerosol or particulate scattering, 3) Raman (vibrational and rotational) scattering.[2] The WAVE-LARS system employs polarization techniques to characterize the size and shape distribution of aerosols in the boundary layer and the troposphere. For completeness, the three relevant scattering processes are discussed in what follows.

1.2.1 Molecular Scattering

Molecular scattering is also commonly termed Rayleigh scattering, however the term molecular scattering is preferred since it applies not only to the central unshifted Cabannes line, but to the Stokes and anti-Stokes lines on either side of the Cabannes line.[3] This type of scattering occurs when the scattering molecule is much smaller than the wavelength of the incident light. Molecular scattering is the predominant scattering mechanism at altitudes above 30 kilometers, where aerosol and particle scattering are almost non-existent.[4]

The backscattering cross section for molecular scattering is defined by

$$\sigma_{\pi}^{M}(\lambda) = \frac{\pi^2 (n-1)^2}{N^2 \lambda^4} \qquad (1)$$

where:

n =index of refraction of the transmitting medium
N =number of scatterers
λ =wavelength of the incident light

Equation 1 shows the λ^{-4} dependence of cross section associated with the molecular backscattering process. The backscatter of 355 nanometers (nm) and 532 nm

wavelengths, two of the wavelengths used by the lidar system of the WAVE-LARS project, results in a multiplication of the backscatter cross section by five.

1.2.2 Aerosol (Particulate) Scattering

Aerosol scattering is also commonly called Mie scattering, although Mie scattering only strictly applies to spherical particles. Aerosol scattering also includes the small particle limit of molecular scattering. Aerosol scattering is an elastic scattering process that occurs when the size of the scattering particle is larger than, or on the order of, the wavelength of the incident light.

The use of multiple wavelengths to discriminate between various particle sizes in the lower and middle atmosphere has been studied and found to be a very effective way to characterize the size and shape distribution of aerosols. On the basis of the Mie scattering theory, particles of different shapes alter the polarization of the illuminating light due to internal reflections and scattering. From this, the depolarization observed in the backscatter of the lidar beam is a measure of the different shapes and alignments of the constituent aerosols. The use of multiple wavelengths and polarization information in WAVE-LARS will enable scientific investigation of the aerosol size distribution, which leads to a better understanding of the microphysical and dynamical processes taking place in clouds.[5] Numerical simulations of a multiple wavelength lidar system have indicated that this technique should yield very productive results for cloud formation studies.[6]

1.2.3 Raman Scattering

There are two types of inelastic Raman scattering, vibrational and rotational. The inelastic scattering processes that involve the vibrational states result in a shift on the order of 100's to 1000's cm^{-1} and those involving the rotational states result in a shift of 10's to 100's cm^{-1}. Both processes are species-dependent. Since Raman scattering is unique to

the species, it allows relative concentration measurements of elements independent of aerosol scattering in the lower atmosphere when the laser energy extinction profile can be quantified.

Raman scattering can be understood by considering a molecule in an arbitrary vibrational ground state N_o (Q-branch). This molecule is then illuminated by laser light and elevated to an excited virtual state, M. The molecule may spontaneously decay to another vibrational state, N_1 , that is characterized by a higher energy than N_o. The scattered wavelength has energy $M\text{-}N_1$ ($< M\text{-}N_o$), which results in the characteristic Stokes lines particular to the vibrational energy states of this molecule. If the transition was to state N_{-1} which is lower in energy than N_o , the scattered wavelength would have energy, $M\text{-}N_{-1}$, which is higher energy than the incident light and the transition, referred to as the anti-Stokes line.[5]

Rotational Raman is similar to the vibrational process except that the energy difference for rotational states is smaller than vibrational and the population distribution of the rotational states depend on temperature. Vibrational Raman lines Q-branchs also have rotational Raman lines that surround their central peaks.

1.3 Lidar Equation

With the presence of many different scattering processes, optical elements, lasers, atmospheric conditions, etc., prediction of the performance of a lidar system becomes important not only for modeling a new system, but also when analyzing the returns of an existing system. To quantify most of the factors affecting the return signal, the lidar equation becomes useful. It is a qualitative example of how the performance of a lidar system is measured.

$$N(z) = \frac{E_L}{hc/\lambda_L} * T(\lambda_L, z)T(\lambda_S, z) * \sigma(\lambda_L, \lambda_S)n(z)\Delta z * \frac{\xi(z)A_0}{4\pi z^2} * \xi_{eff}(\lambda_S) \quad (2)$$

(1) (2) (3) (4) (5) (6)

where the grouped terms are: (1) the predicted photon count from range z, (2) the number of transmitted photons from the laser, (3) the one way atmospheric transmission from the ground to the scattering altitude z at the laser wavelength and the scattered wavelength, (4) the probability of scattering in the illuminated volume or range bin, (5) the probability of collecting the scattered photons from altitude z, and (6) the optical efficiency of the detector system. The lidar equation, Equation 2, will not be discussed further in this thesis and the interested reader is referred to [2] for further explanation.

1.4 Radar System

Although lidar systems prove to be a useful tool in understanding of cloud structures and properties, it has its limitations. One of the most obvious is its attenuation in thicker clouds, which will limit its ability to map clouds when the are optically thick. The reason that the WAVE-LARS project incorporates a 94 GHz (3 millimeter wavelength) cloud radar system is to define scattering in heavy clouds. This relatively simple radar system is capable of sensing cloud droplets and penetrating multiple cloud layers, even moderately thick cumulus convection.[7] When cloud particles are small, the 94GHz radar will be in the Rayleigh criteria regime while the lidar will exhibit complicated particle scattering.

The principle by which the radar system detects particles is a radio wave is projected into the atmosphere, and the particle returns a radio wave at a shifted doppler velocity and the time of return is measured to determine its height. This shifted doppler

velocity corresponds to a particle size and this particle size is usually plotted as a function of altitude. This plot will produce a contour map of cross section of a cloud if the radar is vertically pointing and stationary, and will produce a 3-D volume map if the system is scanning as in the present development. The major difference between the radar and lidar systems are the wavelengths and energy levels at which the two operate. These differences enable the simultaneous operation of the two systems.

1.5 Volume Scanning Mechanism

Since Penn State already has a lidar and radar system in operation, the overall configuration of each system will be based on these proven systems. From the predetermined configurations, little variation from the existing configurations is allowed for this project. To be able to scan the two systems, each system's requirements were determined. The result is that the two systems scan simultaneously over a fairly large area of the sky. The systems need to operate in a simple, self-sustaining scanning mechanism that disassembles easily, operated, and maintained. The result of the development, design, manufacture, and testing of the volume scanning mechanism (VSM) leads to a mechanism that is similar to existing azimuth-elevation tables found in experimental structure laboratories. Because of the fairly large size of the lidar and radar systems a VSM for each system was developed.

1.6 Outline of the Thesis

The goal of this work is to develop an operational scanning mechanism for a lidar and radar system. This mechanism must not interfere with the operation of the individual systems but also remain simple. The integrated system is being developed as a tool to measure condensed water, aerosols, temperature, and water vapor in a volume of the troposphere. This tool enables an improvement in the knowledge of about cloud

formation. The WAVE-LARS system will improve forecasts of the weather and environmental condition reports of the atmosphere, resulting in a better database for making decisions for how to improve the situation of the Earth's radiation balance. Based on improved understanding of the radiation balance, it will be possible to make intelligent decisions about the U.S. energy and fuel policies.

The remainder of this thesis discusses the conceptualization, analysis, design, manufacture, assembly, and testing of the two VSM's for the WAVE-LARS project. The conceptual design development and evaluation will be discussed in Chapter 2. Chapter 3 develops the preliminary analysis and design of the VSM's. The manufacture, assembly, and testing of the VSM's are covered in Chapter 4. Summary and recommendations for use of the VSM's in an operational mode are summarized in Chapter 5.

Chapter 2

CONCEPTUAL DESIGN DEVELOPMENT AND EVALUATION

The lidar and radar sounder (WAVE-LARS) is being developed at the forefront of technology to study the atmosphere and cloud dynamics. The entire project is an integrated system that utilizes both radar and lidar technologies. To develop this tool, a definition of the requirements of each subsystem and a task definition of the work to be accomplished was needed. The radar and lidar are considered as self-contained units that will need to scan a volume of the sky. Development of different mechanical scanning concepts and their evaluation are discussed in this chapter, where the reduction of the original eight concepts to one concept was accomplished.

2.1 Task Definition and Requirement List

The task at hand is to develop an operational volume scanning mechanism for both the radar and lidar systems. After defining the task, the requirements of each the volume scanning mechanisms (VSM) were defined. These requirements were made to be the upper limits of the VSM. They are not expected to be used frequently in operation but give the user of the WAVE-LARS system flexibility in planning and executing experiments. The preliminary requirements are listed below.

1. The VSM must be able to scan a 30° (degree) by 30° area in 120 seconds with 'smooth and continuous' motion (scan at 10° per second without including the time for the motion to reverse direction).
2. The VSM must have a pointing accuracy and reproducibility of 0.1°.

3. The VSM must have the ability to scan all parts of the sky, 20° above the horizon.
4. The cost of the VSM must be minimized by cost containment evaluation at each step of development.
5. The two VSM's and all other equipment must fit within a 8' (foot) x 8' x 20' shipping container.
6. The VSM will operate in all weather, except heavy snows and downpours.

2.2 Concept Development

A consultation with all of the people involved in the project produced eight concepts. The concepts are shown in Figures 1-8. Note that the concepts developed do not include any systems to scan the radar system as we had no information of the needs and desires of the group of researchers working on the radar system.

Figure 1 shows the laser on top of the telescope being rotated in three directions by three motors. The laser and telescope rotate about a horizontal axis in a supporting frame to achieve an elevation coordinate (angle above the horizon). The supporting frame of the laser and telescope will be rotated about another horizontal axis, 90 degrees from the previous axis of rotation, to achieve an arcing coordinate in the sky. The structure will be rotated about a vertical axis to get an azimuth coordinate (angle from a reference position, possibly true north), which will only be used to define a reference location for the system. This concept would allow implementation of a large variety of scan profiles, although it would be fairly bulky compared to the other concepts.

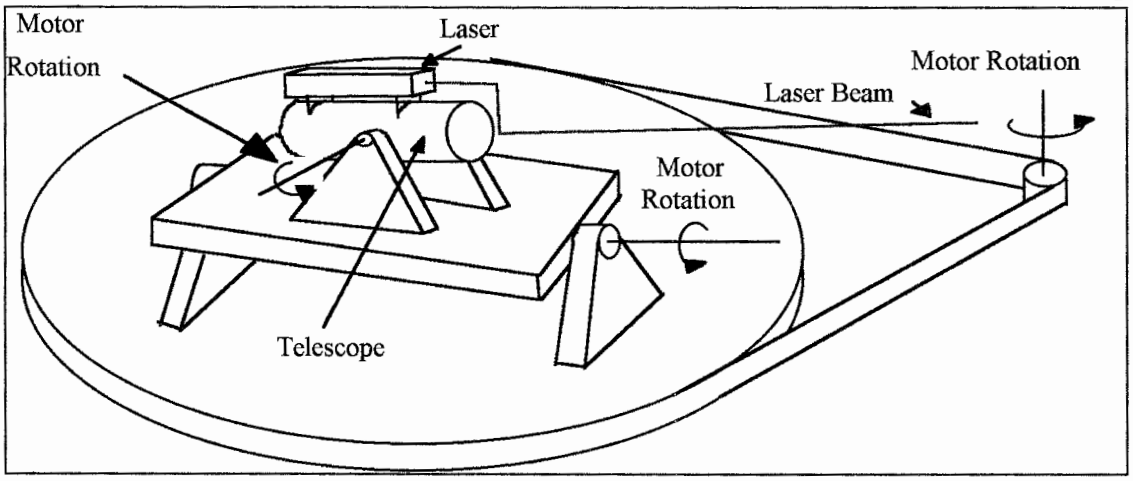

Figure 1: Concept 1

Figure 2 shows concept 2. This meets the requirements well as it is compact, has azimuth and elevation coordinates as its natural coordinates, and scan profiles can easily be implemented in a control scheme. The laser will be supported on top of the telescope and rotated about a horizontal axis as in concept 1, resulting in a natural elevation coordinate. The laser / telescope structure will rotate about a vertical axis resulting in the azimuth coordinate. This concept is expected to require large motors as it must move a large inertia throughout any possible scan profiles. This concept is also very compact compared to the other concepts.

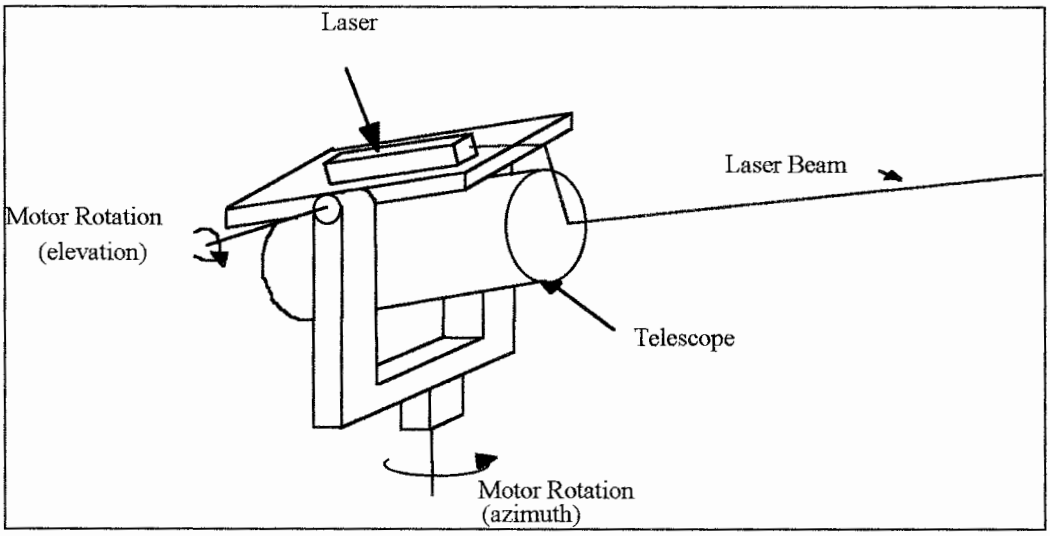

Figure 2: Concept 2

Figure 3 shows concept 3 utilizing a single large mirror The laser and telescope will be mounted on a table that is rotated about a vertical axis to achieve a reference location. The outgoing laser beam will be reflected on an angled large mirror that has a hard core center to enable adequate reflection of the laser beam at the desired angle and allows incoming light to be reflected into the telescope for data analysis. The mirror will rotate to allow for scans to follow a slicing of the sky. The table will lift on one side to allow a semi-elevation coordinate to be achieved. Since lifting of the table can only realistically be achieved by linear actuators, it is expected to require large motors and very strong worm gearing or pistons, detracting from this design.

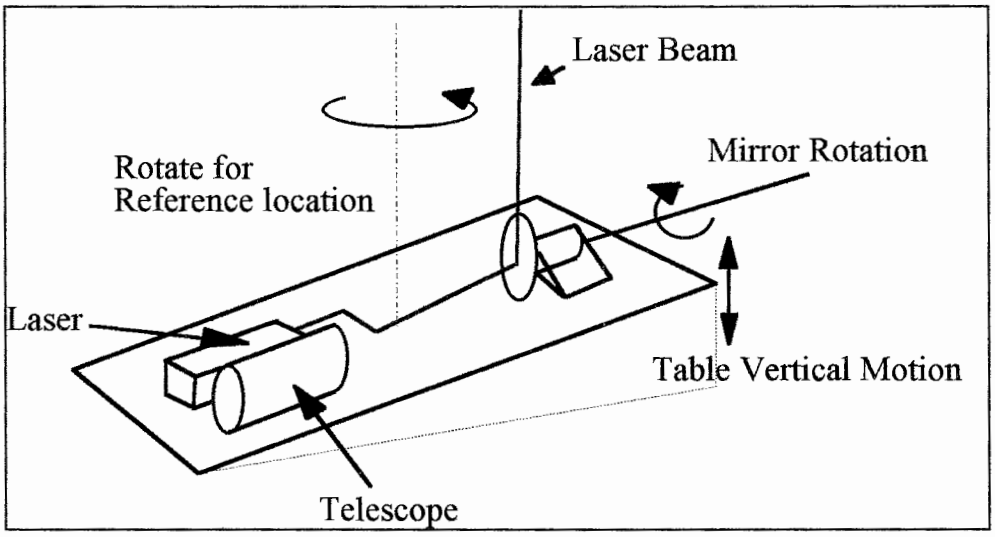

Figure 3: Concept 3

Figure 4 shows the fourth concept developed. It is almost identical to concept 3, except that the laser and telescope are not on the table being elevated. A mirror is along the rotation axis of the table to put the laser beam in the path of the rotating mirror. This was considered because it would require smaller motors and would allow easier alignment

of the laser and telescope combination. It would require the same design effort as concept 3, except that a second mirror is needed.

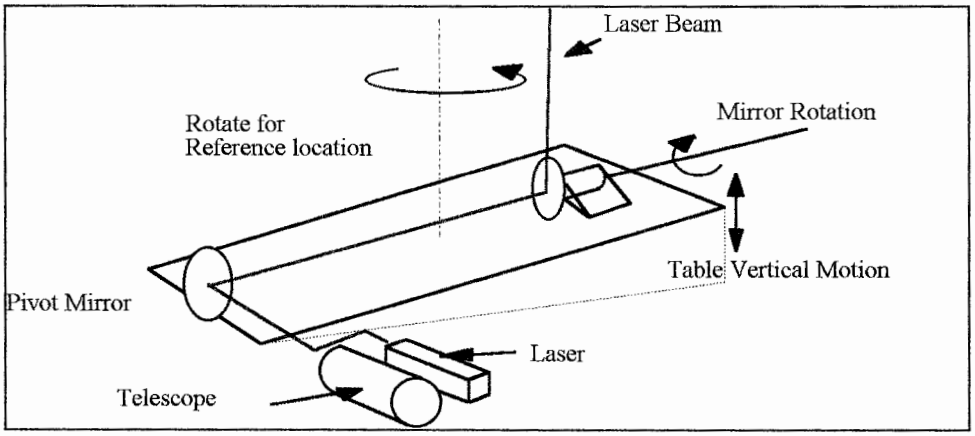

Figure 4: Concept 4

Figure 5 shows the fifth concept, consisting of a mirror that rotates about 2 axes and would be the only portion of the system with controlled motion. This concept is very simple and would require the least design effort compared to the other concepts. The laser and telescope would be permanently mounted to solid structure and the entire system would be rotated for reference locations. A major drawback of this system is that a very large mirror would be needed.

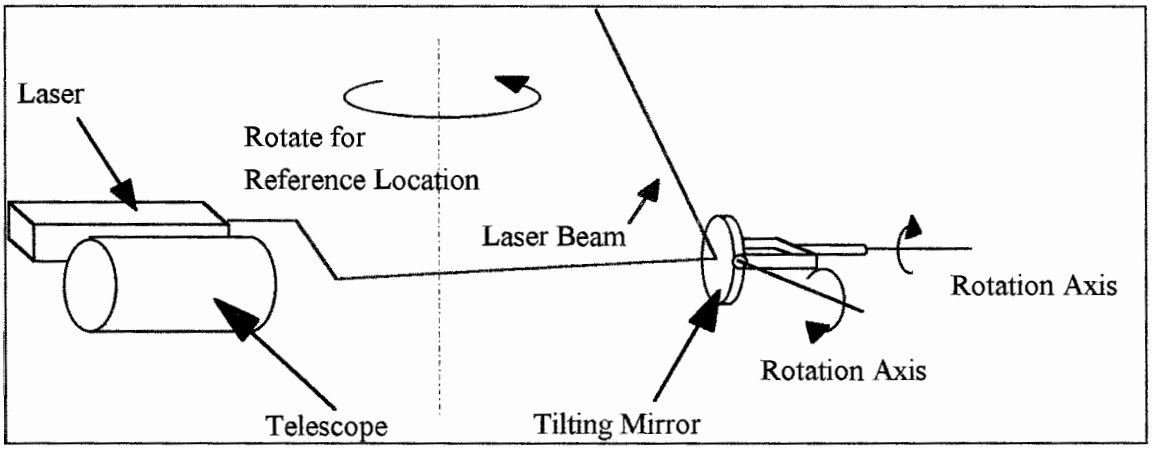

Figure 5: Concept 5

Figure 6 shows concept six. This concept is similar to compound rotary tables found in a metal working machine shops. A rotating table supports the laser and telescope, which establishes the azimuth coordinate by its rotation. The whole system is then lifted on one edge by linear actuators to obtain the elevation coordinate. This system would be very bulky and cumbersome to align.

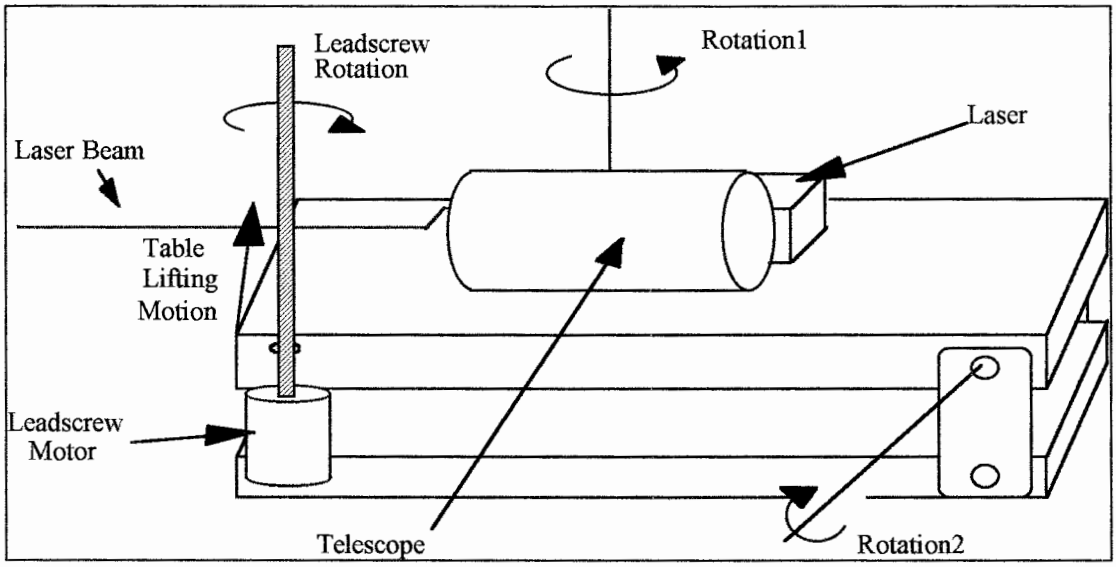

Figure 6: Concept 6

Figure 7 shows a system that would be built into the shipping container. The laser and telescope system will be pointed vertically or the laser beam would be directed to a dual rotation two mirror device. The entire mirror 'capsule' would rotate 360 degrees to establish the azimuth coordinate. The first reflecting mirror would direct the laser beam onto another mirror that would be gimbaled on its sides to slice through the sky with the laser beam. This system allows some advantages over the other concepts, as it will allow more room in the container and it would be simple to implement.

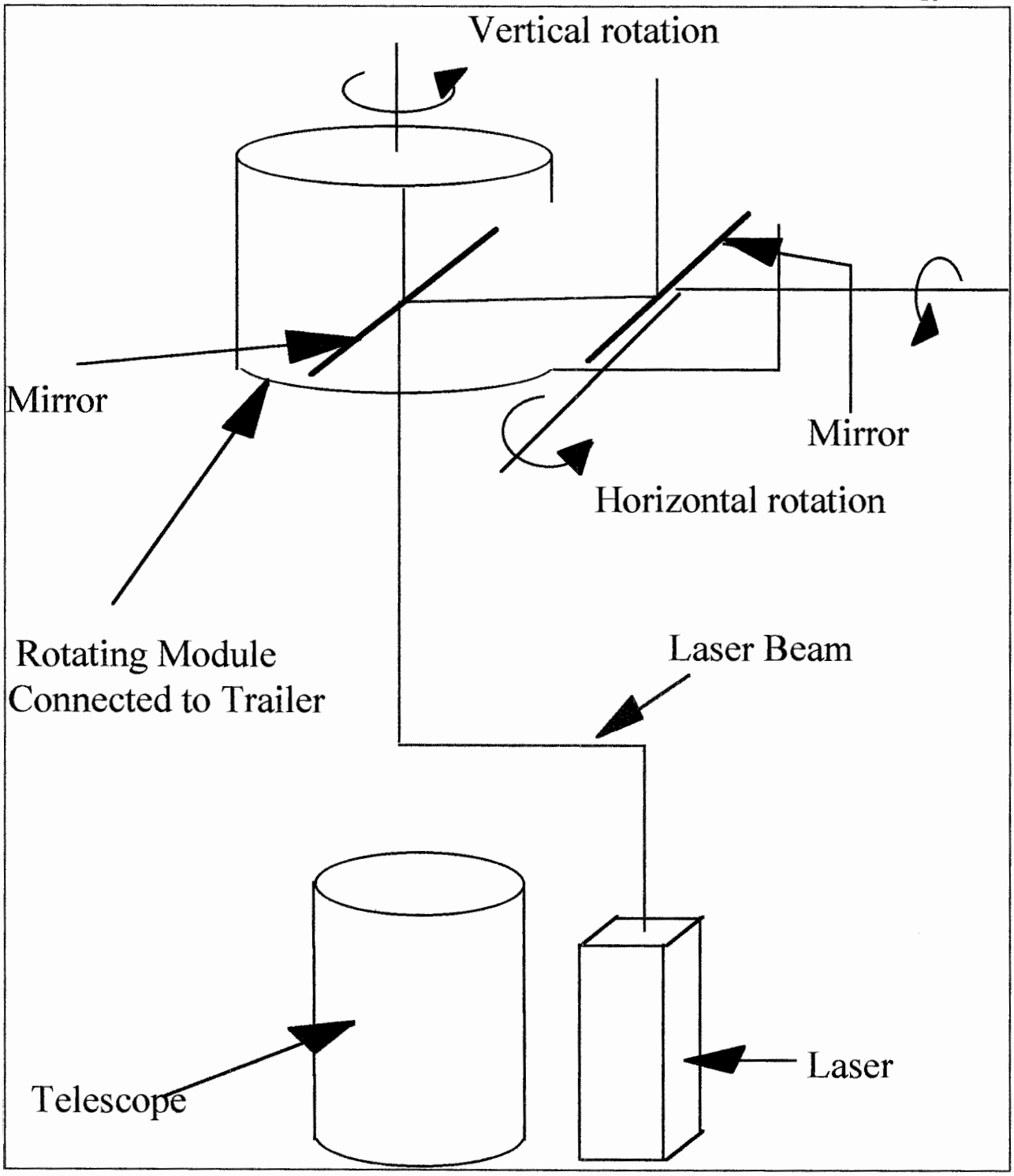

Figure 7: Concept 7

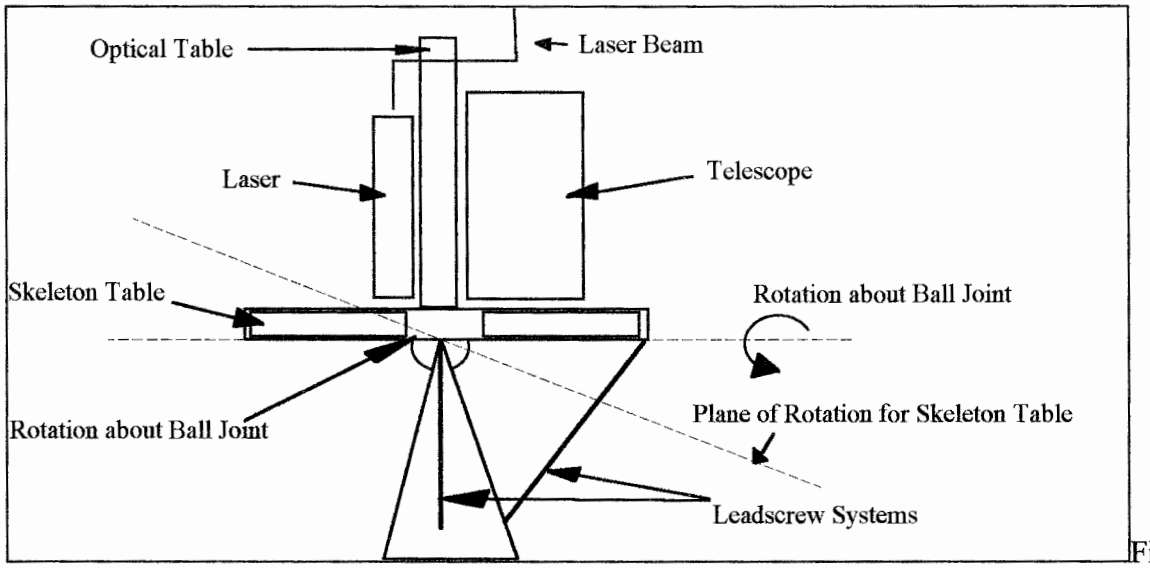

Fi

Figure 8: Concept 8

Figure 8 shows the eighth brainstormed concept. This concept was based on dynamic testing tables used to determine inertia of a system, called Scorsby tables. The laser and telescope would be mounted on a vertical or variable position table, which in turn is mounted on a skeleton frame to allow the system to scan. This skeleton frame is supported at its center by a ball and actuated at two sides by worm gear linear actuators. The control of the motion of this system is quite complicated compared to the other concepts and would dramatically increase the design time. Although it is very complicated, it would allow very easy maintenance and alignment.

2.3 Concept Evaluation and Selection

The previously stated requirements, comments, and additional criterion for design evaluation were considered and the eight initial concepts were evaluated. Table 1 shows how each of the concepts fared in this evaluation. The concepts that used mirrors to move the laser beam and incoming light had the smaller inertia to move which would require small motors for operation. Using large mirrors would dramatically increase the

Table 1: Conceptual Design Evaluation Chart

	Concept							
	1	2	3	4	5	6	7	8
Large Mirrors (#)	No	No	Yes (1)	Yes (2)	Yes (1)	No	Yes (2)	No
Inertia	Large	Large	Medium	Medium	Small	Large	Medium	Large
Observe all the sky?	Yes	Yes	Not easily	Not easily	No	Yes	No	Yes
Easy to Scan?	Yes	Yes	Some what	Some what	Yes	Yes	Yes	No
Complexity	Simple	Simple	Simple-complex	Simple-complex	Simple	Simple	Simple-complex	Complex
Volume & Mass	Medium	Medium	Large	Large	Low	Large	Large	Medium
Cost	Medium	Medium	Medium-High	High	Low-Medium	Medium-High	High	Medium
Compact?	Some what	Yes	Some what	Some what	Yes	No	No	Yes
Consider Further?	No, 3 motors	Yes	No, mirrors, $, radar	No, mirrors, $, radar	No, mirrors, $, radar	Yes	No, mirrors, $, radar	Yes

cost of the system, as the cost of one mirror was approximately $10,000 to 15,000. This decreased the possibility that we would be able to use the systems utilizing large steered mirrors. Also, using mirrors would require that another design would have to be developed to implement the radar in the LARS project. Since the time schedule that was followed was very stringent, developing two distinct designs would be time consuming. All of the above led to the elimination of concepts 3,4,5, and 7 from the list.

This reduced the number of concepts to four. Since concept 1 needed three motors to operate, it would cost more than the other concepts and was also eliminated from consideration. The remaining three concepts, 2,6, and 8, were further evaluated based on motor sizing, cost, and weight. To easily distinguish the remaining three concepts each design was named. Concept 2 was called the fork design; concept 6 was called the compound rotary table; and concept 8 was called the ball & table design.

2.4 Further Evaluation of Three Retained Concepts

To compare the three concepts, an evaluation of the general characteristics of each system was accomplished. Each concept was evaluated based on their cost, design time, manufacturing time, and expected system performance. To avoid any biases that may have occurred in the general evaluation and to insure initial expectations of performance were correct, a more detailed analysis of each system was performed. Since the motors and controls were expected to be the most critical and expensive parts of all concepts, motor sizes, type, and characteristics were determined for each concept. This analysis was used to determine feasibility of each concept, key components of the concepts, and realistic considerations of each design.

2.4.1 General evaluation

Table 2 shows the results of the general evaluation. This evaluation was accomplished by contacting several companies to estimate the cost of the system components. The cost for parts made at Penn State were estimated by speaking with local laboratory and machine shop technicians. The cost evaluation shows that each of the systems should cost less than the budget requirement.

Table 2: Cost and Design Evaluation of Final Conceptual Designs

Option	**Estimated** Cost	Pros	Cons
Compound Angular-Rotary Table	-Table=$16,000 -Prefab controls=$12,000* -In-house controls=$5,000 -Frames/supports=$2,000	-Quickly implemented -Simple design	-High cost -Long controls system development time -Bulky
Fork design	-Materials=$4,000 -Controls=$6,000 -Optical Tables=$6,000	-Simple design -Simple controls -Good scanning capabilities	-Long time to manufacture -Long design time
Ball & Table	-Table & supports=$6,000 -Controls=$8,000 -Optical table=$10,000	-Very flexible operation -Good scanning capabilities	-Complex design -Extremely long design time

* Cost if controls are purchased from the rotary table manufacturer

From Table 2, the fork component was considered as the best choice because of its excellent pros and acceptable cons.

2.4.2 Specific Evaluation

To ensure an unbiased evaluation and determination of feasibility of each of the concepts, an initial motor sizing was accomplished using a common layout of the components of the lidar system. A motor sizing analysis allowed a determination of the size of the motors required, a system layout, and identification of the design flexibilities allowed. Key components of each design were also determined and evaluated to see if the concept was feasible. The inputs to this analysis were a description of the desired scan

profile, the component sizes and masses, and the relative location of the components. The outputs of this analysis are the system layout, the selection and size of the motor (including the possibility of a geared versus direct drive system), the system weight, the table and mount design, a cost estimate, and the system inertia properties. Figure 9 demonstrates the approach taken in this analysis. Steps within the process with design flexibilities were determined and then used to make the torque required for motion smaller. To carry out the analysis, only the lidar component was considered as information about the radar was not known at the time.

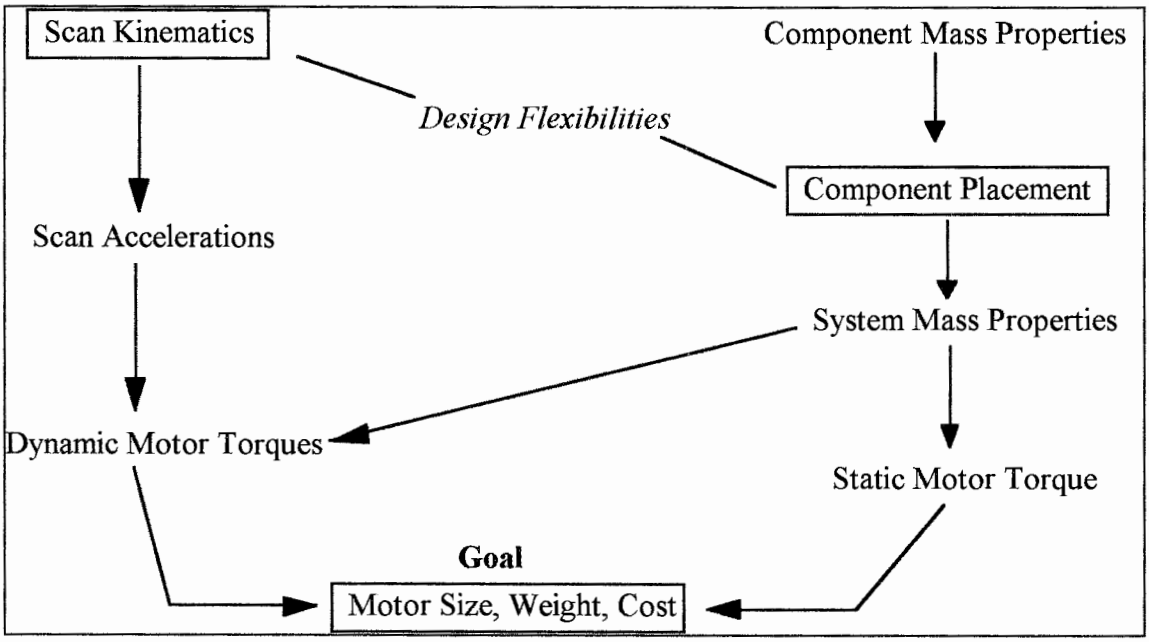

Figure 9: Approach to Key Component Analysis

Before completing any of this analysis, optical design constraints were determined and are listed below.

1. There must be at least 12 inches of table space in front of the laser.
2. There must be 6 inches in front of the telescope.
3. The VSM must not affect the incoming polarized light.

4. The system must be able to have the telescope and laser in a horizontal position when not in use.

The laser, telescope, beam expander, support table, and energy monitor were the components used in the analysis. Since the laser was already ordered at the time of this analysis, its properties, mass and dimensions, were known. The laser that was chosen was a Continuum Surelight II 20 Hz laser, weighing 52 pounds with its center of gravity at the center of the body within one-quarter of an inch and having dimensions of 7 inches wide by 6.25 inches high by 30.3 inches long. (The laser transmits three wavelengths of light at 355 nanometers (nm), 532 nm, and 1064 nm.) To evaluate the telescope, an upper limit of the size and weight of the telescope were defined as a 16 inch diameter Ritchey-Chretien telescope weighing 83 pounds.

A beam expander will be used as part of the optics to spread the beam energy and control the beam divergence. The beam expander was estimated to weigh approximately 15 pounds, having dimensions of 12 inches long by 3 inches wide by 3 inches high, and must be located directly in front the laser. The support table was modeled as a commercially available optical table weighing 175 pounds and dimensions of 4 inches high by 30 inches wide by 60 inches long. The energy monitor will be utilized to determine the energy pulsed to the atmosphere from the three wavelengths of the laser. It will weigh approximately 2 pounds and has dimensions of 5.9 inches long by 3 inches wide by 3 inches high.

2.4.2.1 Motor Type Selection

There were several types of motor available for use on WAVE-LARS. The two types that are most suited for the project are microstepping motors and servo motors. The main difference of the two types is that the servo motors can output larger torque and

require larger amounts of electrical power for operation (25 Amperes), while the microstepping motors output lower torque levels and requires much less power for operation (5 Amperes). The servo motor costs twice as much as the microstepping motor, reducing the likelihood of its application in the VSM. Noting that the total available power to the WAVE-LARS project is about 200 Amperes, the use of 4 servo motors was eliminated because of its power consumption. Using gear reduction boxes would increase the amount of torque available from the microstepping motors, making it the desired motor of use in the VSM application.

2.4.2.2 Fork Analysis

To analyze the fork concept, the layout on the optical table was discussed amongst the WAVE-LARS research team and finally decided upon, as shown in Figure 10. A Microsoft Excel spreadsheet, named inertia.xls and included in Appendix A, was written to determine the mass moment of inertia of each component about their mass centers. The moments of inertia were combined to determine the overall mass moments of inertia about the geometric center (rotation axes) of the optical table. The inertia was then used to determine the torque required to rotate the system about the orthogonal axes centered on the optical table geometric center. These calculations were carried out in a spreadsheet named torque.xls that was linked to inertia.xls (see Appendix A). Throughout this thesis, the units for the mass moments of inertia are given as pound inches-squared. Technically this is not the correct unit for a mass moment of inertia, but when the torque was calculated, the inertia matrix was divided by the appropriate value for the Earth's gravity field.

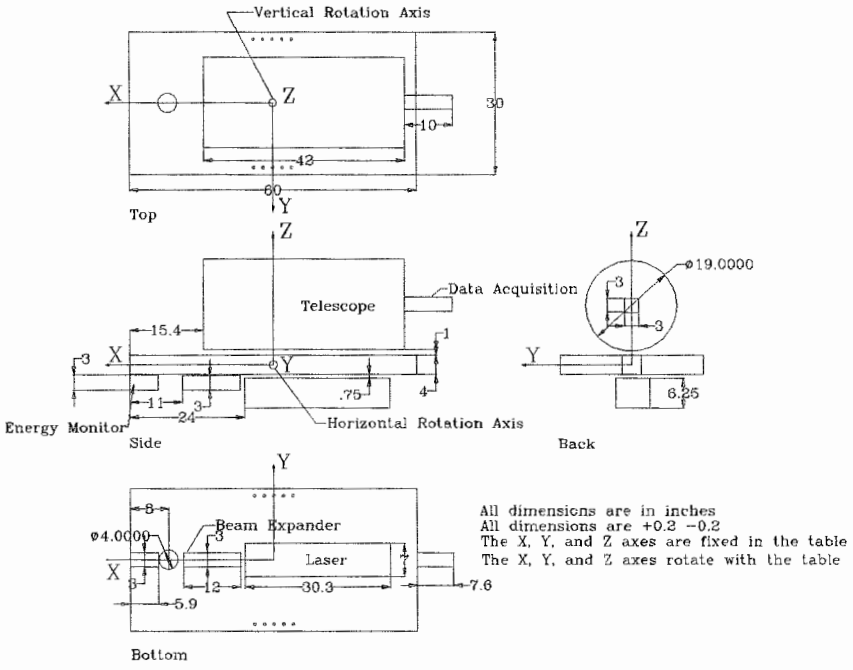

Figure 10: Layout of Equipment on the Optical Table for Fork and Ball & Table Concepts

To determine the mass moments of inertia of each component, the general shape of each component was determined and/or assumed and used to find the equations for the inertia matrices with regular geometric shapes and uniform mass distribution found in [8]. The telescope was modeled as a cylinder with the center of mass located one-third the length from the back of the telescope due to the heavy optics and mountings at the back of the telescope. The laser was modeled as a rectangular box with the center of mass at the center of the box. The location of the laser center of mass was verified by the manufacturer of the laser. The beam expander was modeled as a rectangular box with the center of the mass at the center of the box and was determined from a similar beam expander built for a previous lidar system. The energy monitor was modeled as a rectangular box with its center of mass at the center of the box. The configuration of the energy monitor was determined by knowing that it would be an electronic breadboard with a mirror attached to one end. The mirror at one end of this arrangement would naturally shift the center of mass towards the mirror, but the assumption of the center of mass at the center of the body was made because the size and weight of the energy monitor had an insignificant impact on the overall inertia of the system. Lastly, the optical table was modeled as a rectangular box with the center of mass at the geometric center of the table. The center of mass was assumed to be at the geometric center of the table because the table is symmetric about that point.

The equations used for the telescope cylinder are shown in Equation 3.

$$\begin{bmatrix} I_{xx} & I_{xy} & I_{xz} \\ I_{xy} & I_{yy} & I_{yz} \\ I_{xz} & I_{yz} & I_{zz} \end{bmatrix} = \begin{bmatrix} \frac{1}{2}Wr^2 & 0 & 0 \\ 0 & \frac{1}{12}W\left(3r^2 + L^2\right) + Wu^2 & 0 \\ 0 & 0 & \frac{1}{12}W\left(3r^2 + L^2\right) + Wu^2 \end{bmatrix} \quad (3)$$

where:

I_{ij} =mass moment of inertia about the ij plane
x, y, z =coordinates parallel to the coordinates shown in Figure 10
W =weight of the telescope
r =radius of the telescope
L =length of the telescope
u =distance between the center of the telescope and the offset center of mass location

The equations used for the rectangular box models are shown in Equation 4.

$$\begin{bmatrix} I_{xx} & I_{xy} & I_{xz} \\ I_{xy} & I_{yy} & I_{yz} \\ I_{xz} & I_{yz} & I_{zz} \end{bmatrix} = \begin{bmatrix} \frac{1}{12}W(w^2+h^2) & 0 & 0 \\ 0 & \frac{1}{12}W(L^2+h^2) & 0 \\ 0 & 0 & \frac{1}{12}W(w^2+L^2) \end{bmatrix} \quad (4)$$

where:

I_{ij} =mass moment of inertia about the ij plane
x, y, z =coordinates parallel to the coordinates shown in Figure 10
W =weight of the component
w =width of the component in the y direction
h =height of the component in the z direction
L =length of the component in the x direction

The parallel axis theorem was used to determine the inertia of the entire lidar system. Simultaneous with the inertia calculation of the system, the center of mass of the entire layout about the rotation axis of the layout was calculated. The equation used to

calculate the center of mass is shown in Equation 5. The calculation of the center of mass of the system was taken about the center of the leading edge of the support table.

$$A_{c.m.} = \frac{\sum_i W_i A_{c.m._i}}{\sum_i W_i} \tag{5}$$

where:

$A_{c.m.}$ =center of mass of the entire system in the A direction (i.e. A is the x, y, and z directions) from the leading edge of the optical table

W_i =weight of the i^{th} component

$A_{c.m._i}$ =center of mass of the i^{th} component in the A direction from the leading edge of the optical table

The rotation axis was chosen to coincide with the geometric center of the optical table. To combine the inertia of the components, the mass moments of inertia were moved to the center of mass of the entire system by using the parallel axis theorem and added together. The mass moment of inertia about the center of gravity of the entire system was then shifted to the rotation axes. The equation used to shift the mass moments of inertia of the parts to the product of inertia of the system is shown in Equation 6.

$$\bar{I}_{ii} = I_{ii} + Wd^2 \tag{6}$$

where:

$\bar{I}_{ii}$ =mass moment of inertia about the system center of mass

I_{ii} =mass moment of inertia of a component about its center of mass

W =weight of the component

d =distance from the center of mass of the component to the center of mass of the system

This equation was used for the axes ii = xx, yy, zz. The products of inertia, were calculated using Equation 7.

$$\begin{aligned} \bar{I}_{xy} &= I_{xy} + W\bar{x}\bar{y} \\ \bar{I}_{xz} &= I_{xz} + W\bar{x}\bar{z} \\ \bar{I}_{yz} &= I_{yz} + W\bar{y}\bar{z} \end{aligned} \tag{7}$$

where:

$\bar{I}_{ij}$ =product of inertia about the system center of mass
I_{ij} =product of inertia of a part about its center of mass
$\bar{x}, \bar{y}, \bar{z}$ =distance from component center of mass to the system center of mass in the $x, y,$ and z coordinate directions

Equations 6 and 7 were used for both shifting the mass moments of inertia to the center of gravity of the system and shifting to the rotation axes. The results for the inertia matrix about the center of mass of the entire system for the layout shown in Figure 10 and using the assumptions discussed earlier are shown in Equation 8.

$$\begin{bmatrix} \bar{I}_{xx} & \bar{I}_{xy} & \bar{I}_{xz} \\ \bar{I}_{xy} & \bar{I}_{yy} & \bar{I}_{yz} \\ \bar{I}_{xz} & \bar{I}_{yz} & \bar{I}_{zz} \end{bmatrix} = \begin{bmatrix} 17{,}548 & 0.000 & 25{,}257 \\ 0.000 & 75{,}447 & 0.000 \\ 25{,}257 & 0.000 & 88{,}383 \end{bmatrix} \text{lb-in}^2 \tag{8}$$

The results for the inertia matrix about the rotation axes for the entire system are shown in Equation 9.

$$\begin{bmatrix} I_{xx} & I_{xy} & I_{xz} \\ I_{xy} & I_{yy} & I_{yz} \\ I_{xz} & I_{yz} & I_{zz} \end{bmatrix} = \begin{bmatrix} 20{,}042 & 0.000 & 29{,}467 \\ 0.000 & 85{,}049 & 0.000 \\ 29{,}467 & 0.000 & 95{,}491 \end{bmatrix} \text{lb-in}^2 \tag{9}$$

It is noted that the only product of inertia that exists is the I_{xz} term. This so because all the elements were aligned with the x and z axes. This helps to decrease the torque that will be required to rotate both axes of rotation (y and z) simultaneously.

To determine the torque required by the motors to perform the scans, a description of the desired scan profiles is necessary. Figure 11 shows a few scans that are of interest to the radar and lidar systems. The critical part of each scan is when the direction of the scan is reversed. This is when one motor decelerates and then accelerates immediately after the motor has decelerated to zero velocity. The other motor will do the same motion in reverse direction.

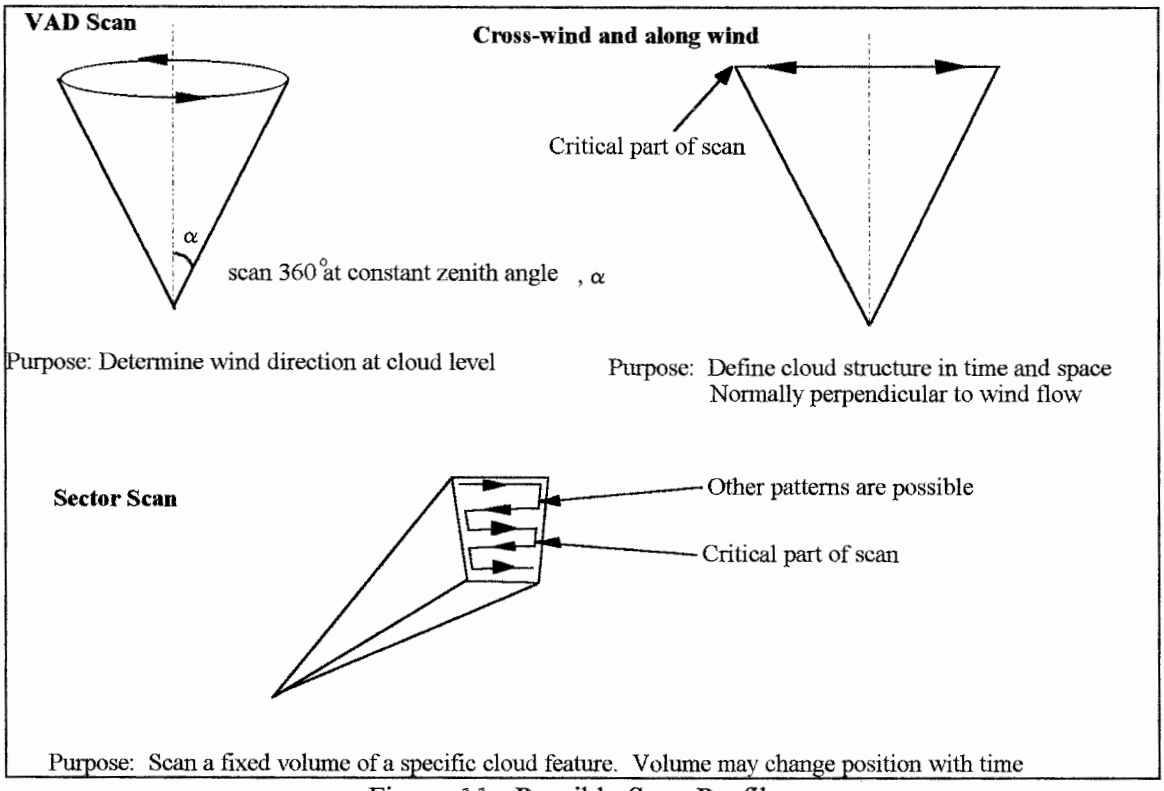

Figure 11: Possible Scan Profiles

Critical parts of the scan profiles, reversing direction, cause the highest accelerations that the VSM will encounter during operation. These motion loads will be considered as the largest experienced loads the VSM will encounter for this concept

evaluation. The equation used to determine the torque for this motion is given in Equation 10.

$$M_{ii} = J_{ii}\alpha \tag{10}$$

where:

M_{ii} =motor moment or torque required to accomplish the desired motion

$J_{ii} = \frac{I_{ii}}{N} + NJ_{motor} + \frac{J_{gearbox}}{N}$

I_{ii} =mass moment of inertia of the system in the ii direction (ii = xx, yy, and zz)

J_{motor} =mass moment of inertia of the motor

$J_{gearbox}$ =mass moment of inertia of the gearbox (referred to output)

$\alpha = \frac{2\omega}{t_{rev}}$, the acceleration of table due to motor reversal

ω =angular velocity of the scan motion in table coordinates (10° / second)

t_{rev} =time for motor reversal to occur

N =gear ratio of the gearbox

A gear reduction box was included in the analysis to increase the speed of the motor shaft rotation, decrease the torque seen by the motor, and decrease the load to motor inertia ratio. Since the manufacturers of the microstepping motors recommended that the motor shaft be rotating at a minimum 5 revolutions per second, the gear reduction box was considered essential in this design. The load to motor inertia ration is the ratio of the load as seen by the motor divided by the motor inertia. A high ratio indicates that the speed the driven system can operate is slow and its likelihood for unstable motion is high.

A Microsoft Excel spreadsheet, torque.xls in Appendix A, was linked to inertia.xls to calculate the torque required for the scan motion. To calculate the torque applied to

the table, a gear reduction ratio of 1 was used. The scan rate was kept fixed at 10 degrees per second and the time for motor reversal was changed between 0.1 and 0.5 seconds. A manufacturer factor of safety of 1.5 was applied to the calculated values to account for maintenance and wear of the motor. The inertia of the motor and gearboxes were found in catalogs from the manufacturers. The results of the analyses are shown in Table 3.

Table 3: (Fork) Motor Torque Requirement to Accomplish Scan Profile

Motor reversal time (sec)	Gear Ratio 1:1 Torque(in-lb)	Gear Ratio 20:1 Torque(in-lb)
0.1	1,166	59
0.2	583	30
0.5	233	12

The results indicate that a gear reduction box is necessary to accomplish any reasonable scan profiles, because the peak output torque of any commercially available microstepping motor is about 118.75 inch-pound (in-lb). Although the torque output from the motor is quite large in comparison to the required torque with a gear reduction box, this reduction box is necessary to bring the load to motor inertia ratio below 200. The calculated load to motor inertia ratio for the fork system, found in torque.xls, is 66.1 for the geared system and 26,458 for the ungeared system. A ratio of 100 to 200 is recommended by most motor manufacturers for slow moving, high precision scientific measuring instruments. The low calculated ratio indicates that this system will respond quickly and in a stable regime. These calculations did not include the fork supporting frame; and, including it is expected to increase the torque required for motion.

An additional torque that needed to be calculated and is not affected by the non-inclusion of the supporting frame is the static torque created by the center of mass of the

system not being located on the rotation axes. The static torque was calculated, found in torque.xls, to be 94.14 inch-pounds. Since the motors that were being considered have a permanent magnet as part of their design, the magnets help to create a "daytime torque" to account for any static torque that is encountered whenever the motor is not powered. The technical support personnel at Compumotor quoted the motors under consideration to have a "daytime torque" of 62.5 inch-pounds. The quoted "daytime torque" is below what is expected and safe to assume that counter balances may be added to move the center of gravity towards the center of the optical table.

2.4.2.3 Ball & Table Analysis

The layout of the Ball & Table design on the optical table with equipment was assumed to be exactly the same as for the fork design. The table with the large holes, shown in Figure 8, is termed the skeleton table as it just provides a means of transforming the linear actuator forces to torques at the ball support to accomplish the possible scan. The rotation axes of interest are the x and z axes as shown in Figure 10, but shifted to the back of the optical table. All the calculations and equations used for the fork analysis were repeated. The major difference is that the torques required to achieve the motions were converted to axial forces applied to the skeleton table edges. These forces were then converted to torque capabilities of commercially available leadscrew/motor systems.

The inertia matrix about the center of mass of the system is identical to that computed for the fork analysis and is found in Equation 8. The inertia matrix about the rotation axes was computed using inertia.xls and is shown in Equation 11.

$$\begin{bmatrix} I_{xx} & I_{xy} & I_{xz} \\ I_{xy} & I_{yy} & I_{yz} \\ I_{xz} & I_{yz} & I_{zz} \end{bmatrix} = \begin{bmatrix} 20,042 & 0.000 & 667 \\ 0.000 & 320,435 & 0.000 \\ 667 & 0.000 & 330,877 \end{bmatrix} \text{lb-in}^2 \qquad (11)$$

Notice the very large increase in I_{yy} and I_{zz} and very large decrease in I_{xz} compared to Equation 8. This large increase in the mass moment of inertia of the rotation axes of interest may make this concept unrealistic. The low product of inertia will decrease the torque required to rotate both axes at the same time but will probably still be too large for a standard linear actuator to handle.

The skeleton table's inertia was computed assuming that the skeleton table is a solid square prism with dimensions 36 inches wide by 36 inches long by 4 inches high. The table was assumed to have one-third the weight of a solid aluminum table of the same dimensions (172.8 pounds). The mass moment of inertia of the skeleton table about the similar axes of the optical table with equipment is shown in Equation 12.

$$\begin{bmatrix} I_{xx} & I_{xy} & I_{xz} \\ I_{xy} & I_{yy} & I_{yz} \\ I_{xz} & I_{yz} & I_{zz} \end{bmatrix} = \begin{bmatrix} 37,325 & 0.000 & 0.000 \\ 0.000 & 18,893 & 0.000 \\ 0.000 & 0.000 & 18,893 \end{bmatrix} \text{lb-in}^2 \qquad (12)$$

The total inertia to be moved is the sum of Equations 11 and 12, which is shown in Equation 13.

$$\begin{bmatrix} I_{xx} & I_{xy} & I_{xz} \\ I_{xy} & I_{yy} & I_{yz} \\ I_{xz} & I_{yz} & I_{zz} \end{bmatrix} = \begin{bmatrix} 57,367 & 0.000 & 667 \\ 0.000 & 339,328 & 0.000 \\ 667 & 0.000 & 349,769 \end{bmatrix} \text{lb-in}^2 \qquad (13)$$

To calculate the torque required to accomplish the scan profiles, an equation similar to Equation 10 is used but does not include the motor or gearbox inertia and reduction. The equation that is used to calculate the torques is shown in Equation 14.

$$M_{ii} = I_{ii}\alpha \qquad (14)$$

where:

M_{ii} =moment or torque required to accomplish the desired motion
I_{ii} =total inertia to be moved
$\alpha = \frac{2\omega}{t_{rev}}$, the acceleration due to motor reversal
ω =angular velocity of the scan motion in
table coordinates (10° / second)
t_{rev} =time for motor reversal to occur

The result of the torque calculation is shown in Table 4. The torque shown is the maximum torque required to achieve the desired motion (about the z axis).

Table 4: (Ball & Table) Rotation Torque to Accomplish Scan Profiles

Motor reversal time (sec)	Torque(in-lb)
0.1	4,357
0.2	2,179
0.5	871

To convert these torques to usable forces required for the linear actuators that will accomplish the scan profiles, the torques are divided by the moment arm created by using the skeleton table for support. The moment arm is 18 inches, as the skeleton table is supported at its geometric center. The forces from this calculation are shown in Table 5.

Table 5: (Ball & Table) Force on LeadScrew to Accomplish Scan Profiles

Motor reversal time (sec)	Force(lb)
0.1	242
0.2	121
0.5	48

To convert these linear forces to torques that are required by a motor, a leadscrew system will be used as the linear actuator. Equation (15) was used to convert the linear forces to torques.

$$T = \frac{F}{2\pi pe} \tag{15}$$

where:

T =torque output of motor (in - lb)
F =linear force acting along the leadscrew (lb)
p =pitch of the leadscrew (number of revolutions per inch)
e =efficiency of the leadscrew (%)

The torques were calculated assuming the leadscrew pitch to be 5 revolutions per inch and its efficiency to be 85% (values obtained for a stainless steel ball-nut, lubricated leadscrew system). The calculated torques are found in Table 6.

Table 6: (Ball & Table) Motor Torque Requirement to Accomplish Scan Profile

Motor reversal time (sec)	Torque(in-lb)
0.1	9.06
0.2	4.53
0.5	1.81

Since the maximum torque output of a micro-stepping motor is 118.75 in-lb, a motor without gearing is possible. Looking at the load to motor inertia ratio, this concept

will be very slow and unstable as the ratio is 247. Because of the load to motor inertia problem, the ball & table concept was eliminated.

2.4.2.4 Compound Rotary Table Analysis

The layout of the compound rotary table was determined based on the needs previously discussed. Since all components will be located on one side of an optical table there will be no hole drilled through the table. The layout of the components is shown in Figure 12. The size and weight of the components are the same as assumed and/or known from the previous analyses. Inertia.xls was used to calculate the inertia of the entire system about the pivot axes shown in Figure 12. The inertia matrix of the system about the axis of rotation 1 shown in Figure 12 is in Equation 16.

$$\begin{bmatrix} I_{xx} & I_{xy} & I_{xz} \\ I_{xy} & I_{yy} & I_{yz} \\ I_{xz} & I_{yz} & I_{zz} \end{bmatrix}_1 = \begin{bmatrix} 22{,}565 & -12{,}005 & 31{,}123 \\ -12{,}005 & 87{,}807 & -6{,}828 \\ 31{,}123 & -6{,}828 & 96{,}415 \end{bmatrix} \text{lb-in}^2 \qquad (16)$$

The inertia matrix about the system about the axis of rotation 2 shown in Figure 12 is in Equation 17.

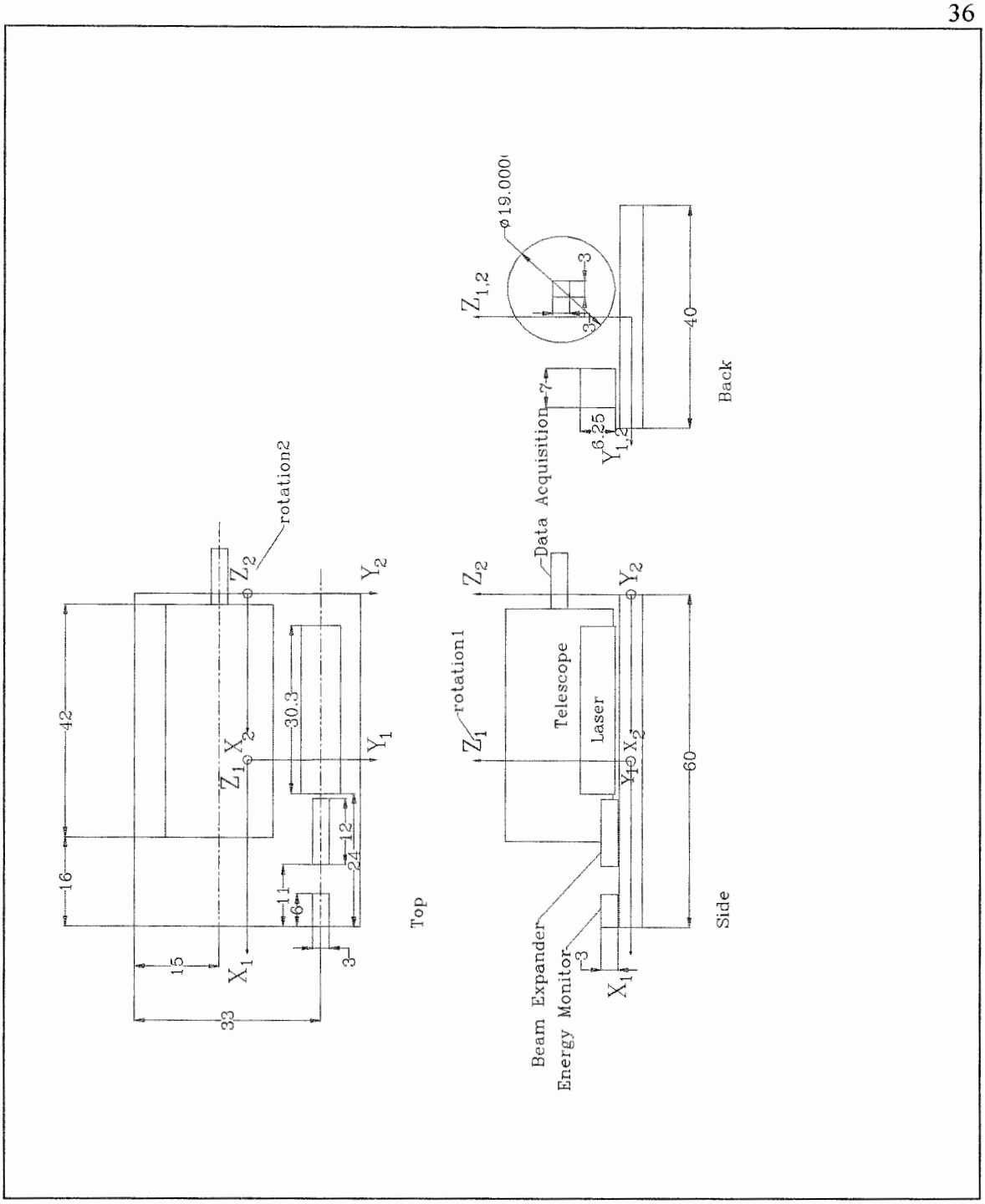

Figure 12: Layout of Equipment on the Optical Table for the Compound Rotary Table Concept

$$\begin{bmatrix} I_{xx} & I_{xy} & I_{xz} \\ I_{xy} & I_{yy} & I_{yz} \\ I_{xz} & I_{yz} & I_{zz} \end{bmatrix}_2 = \begin{bmatrix} 22{,}565 & -22{,}715 & -8{,}297 \\ -22{,}715 & 319{,}305 & -6{,}828 \\ -8{,}297 & -6{,}828 & 327{,}913 \end{bmatrix} \text{lb-in}^2 \qquad (17)$$

Rotation 1 is a direct drive system and is analyzed similar to the rotations for the fork conceptual design. Rotation 2 is semi-linear drive system and is analyzed similar to the rotations for the Ball & Table conceptual design. The torques required to accomplish the scan profiles were calculated using Equation 10 for rotation 1 and Equations 14 and 15 for rotation 2. The length of the compound rotary table used to create the moment arm for the leadscrew system to lift the table is 60 inches, the same as the length of the optical table used to support the equipment. The pitch and efficiency of the leadscrew system are assumed to be the same as analyzed for the Ball & Table design. The torques required to accomplish the rotations about the axes of interest (rotation 1 and rotation 2) are shown in Table 7. These torques are those required by the motors and include a torque calculation for a 20 to 1 gear reduction box for the direct drive rotation.

Table 7: (Compound Rotary Table) Motor Torque Requirement to Accomplish Scan Profile

Motor reversal time(sec)	Torque (in-lb) for rotation 1 (20:1 gear reduction)	Torque (in-lb) for rotation 2
0.1	1,307 (66)	2.71
0.2	654 (33)	1.36
0.5	262 (13)	0.54

The torques shown in Table 7 suggest that this concept will be the easiest to accomplish with the previously mentioned motors. As mentioned in the fork analysis, the load to motor inertia ratio has to be between 100 and 200. For rotation 1, the ratio is 27,000 for an ungeared system and 67.5 for a 20 to 1 gear reduction. For rotation 2, the ratio is 100,896. Since the load to motor inertia ratio for rotation 2 is well above that recommended for our type of system, it is expected that the system will operate too slowly and be susceptible to motor stall. This factor eliminated this concept from further consideration.

2.5 Conceptual Design Selection

After the initial eight concepts were developed, the amount of concepts to be further considered was reduced to three. This reduction was accomplished with many reasons in mind. First, the concept that required three motors to operate was eliminated from considered. Second, the remaining concepts that were eliminated were done so because of the extreme cost that would be required to have the large mirrors and to have a second VSM for the radar system.

After the number of concepts was reduced to three, these conceptual designs were analyzed on the basis of cost, expected performance, design time, and expected time for manufacture. This analysis pointed in the direction of selecting the fork concept. Further detailed analysis was accomplished to determine the feasibility of each design and the corresponding size, type, and cost of motor for its development. The results of the single axis rotation analysis pointed out that the ball & table concept and the compound rotary table concept were not feasible. They would be susceptible to slow scan rates and motor stall. The fork concept prevailed and microstepping motors with gear reduction boxes resulted in a feasible volume scanning mechanism.

Both the general evaluation and the motor sizing analysis pointed to the selection of the fork concept. The design flexibilities that were identified in the motor sizing analysis -- the height that the telescope is above the support table and the time for the motion to reverse direction -- will be used to increase system performance. Since the fork concept was selected by analysis and was the preferred concept, it was chosen as the concept to design and manufacture. The preliminary and detailed design, manufacture, and testing are discussed in the remainder of the thesis.

Chapter 3

PRELIMINARY ANALYSIS AND DESIGN

Once the concept was chosen, a more detailed analysis of the design was required to enable designs of the components of the VSM to be produced. More detailed information about the components (lidar and radar) was determined. Analysis of the VSM with both axes of rotation (table and fork), a dual axis rotation, was accomplished to insure of correct loading conditions, correct motor selection, shaft design, shaft - motor coupling selection, and bearing selection. Preliminary performance analysis was accomplished to determine if the VSM needed to be modified to improve performance. A deflection analysis of the entire fork and individual components was accomplished using the finite element method. Angular deflection analysis of the critical components was done to determine the source of the largest pointing error. Modal vibration analysis of the rotating components was performed to determine any possible dynamic flexibility problems with selected scan profiles. After these tasks were accomplished, the parameters for the detailed design of the VSM were known.

3.1 Detailed Component Information

Before any more analysis could have been completed, more information about the components was required. This information came from decisions on the purchase of items for the project, designs that were near completion, and better communication between the lidar and radar groups.

3.1.1 Lidar Components

As was already mentioned, the laser was purchased at the time of the conceptual analysis and its properties were given in Chapter 2. Near the end of the conceptual analysis the telescope was determined to be a 16 inch Ritchey-Chretien telescope, with a 19 inch tube

diameter and weighing approximately 83 pounds. The mounting apparatus for the telescope raises the bottom of the telescope 3 inches from the top of the optical table. The beam expander, energy monitor, and data acquisition (an optical system consisting of lenses, a beam splitting prism, and two 1 millimeter diameter fiber optic cables) were still not completed and the previously mentioned sizes and weights were set as the upper limits of their designs. The optical table had the dimensions previously mentioned (30 inches by 60 inches by 4 inches). Knowing that the telescope is now going to be 3 inches above the optical table, rather than the initial 1 inch, the inertia matrix about the rotation axis is shown in Equation 18.

$$\begin{bmatrix} I_{xx} & I_{xy} & I_{xz} \\ I_{xy} & I_{yy} & I_{yz} \\ I_{xz} & I_{yz} & I_{zz} \end{bmatrix} = \begin{bmatrix} 20,979 & 0.000 & 33,128 \\ 0.000 & 85,986 & 0.000 \\ 33,128 & 0.000 & 95,491 \end{bmatrix} \text{lb-in}^2 \qquad (18)$$

Selection of the optical table was accomplished by talking with several manufacturers. The possibility of building the optical table out of composite materials was considered in the selection because of the outstanding characteristics available. If the optical table was made from metal and was purchased from an optical table company, the optical table could be made to meet specifications for equipment mounting by having it built with standard 1/4-20 tap holes on one inch centers on both sides of the optical table and brackets for the shaft to rotate the table. If the table was made out of composite materials, a more detailed design would have to be accomplished. Since composite materials cannot be threaded to accept bolts, mounting plates would have to be attached to the surface. Due to the size, cost, and fabrication time, the use of composite materials was eliminated. This decision is better outlined in Table 8. To clarify Table 8, the two companies considered to manufacture the composite table were the Penn State Applied Research Laboratory (ARL) and M.C. Gill. ARL was the only facility available to do the post fabrication, i.e., attach the mounting plates ans shaft. Aerotech, a metal optical table manufacturer, was the cheapest company that could

manufacture the ready-made metal optical table to meet the requirements. The row in the table that is labeled as risk can be better explained as the risk in having the table made and the risk that the table may not perform to standards, i.e., it may fracture under the extreme temperature changes and corrosive environments that are expected.

Table 8: Optical Table Decision Chart

	Composite Table		Metal Table
Table Fabrication	ARL ~$8,000 4-6 weeks (Risky- No Experience)	M.C Gill $1,520 6 weeks	Aerotech $2,475 3-4 weeks
Post Fabrication	ARL ~$2,000 2-3 weeks	ARL ~$2,000 2-3 weeks	None
Design Time	2 weeks	1 week	1 day
Cost	~$10,000	$3,520	$2,475
Total Time	8-11 weeks	9-10 weeks	3-4 weeks
Weight (pounds)	30	30	160
Risk	High	Medium	None

3.1.2 Radar System

It was not until the choice of the VSM concept that more details on the radar system became available. The radar was chosen to be a 94 GHz radar system that is made of a housing unit to hold the electronics, a graphite transmitting antenna, and a graphite receiving antenna, as shown in Figure 13.

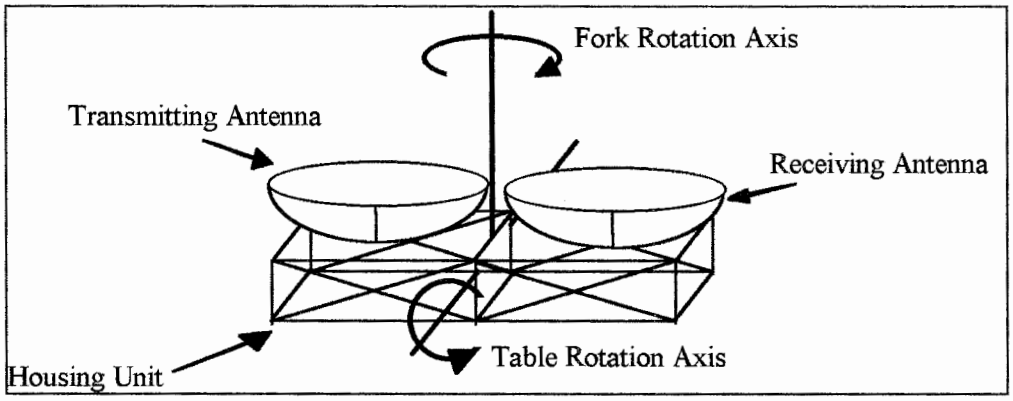

Figure 13: Radar System

The radar has a total weight of 250 pounds. The housing unit has dimensions of 14 inches high by 26 inches wide by 62 inches long. The antennas are identical and have dimensions of 36 inch diameter and have a 18 inch height, weighing approximately 10 pounds. Since the housing unit is made of aluminum and is the only sturdy part of the radar, this was decided to be the location for the mounting brackets to interface with the VSM. From Equation 5, the center of gravity was calculated to be 1.28 inches above the geometric center of the housing unit. Using the equations for a rectangular box to determine the inertia matrix of the housing unit and the equations for a cylinder to determine the inertia matrix of the antennas, the inertia matrix of the radar system about its center of mass is shown in Equation 19.

$$\begin{bmatrix} \bar{I}_{xx} & \bar{I}_{xy} & \bar{I}_{xz} \\ \bar{I}_{xy} & \bar{I}_{yy} & \bar{I}_{yz} \\ \bar{I}_{xz} & \bar{I}_{yz} & \bar{I}_{zz} \end{bmatrix} = \begin{bmatrix} 23,584 & 0.000 & 0.000 \\ 0.000 & 84,304 & 0.000 \\ 0.000 & 0.000 & 97,093 \end{bmatrix} \text{lb-in}^2 \qquad (19)$$

Similarly, from the lidar table analysis, the mass moment of inertia about the rotation axes needed to be computed. Knowing that the researchers working with the radar wish to rotate the radar about an axis 2 inches below the top of the housing unit, the mass moment of inertia about the rotation axis is found in Equation 20.

$$\begin{bmatrix} I_{xx} & I_{xy} & I_{xz} \\ I_{xy} & I_{yy} & I_{yz} \\ I_{xz} & I_{yz} & I_{zz} \end{bmatrix} = \begin{bmatrix} 25,072 & 0.000 & 0.000 \\ 0.000 & 85,792 & 0.000 \\ 0.000 & 0.000 & 97,093 \end{bmatrix} \text{lb-in}^2 \qquad (20)$$

Note that the inertias in Equations 20 are on the same order as Equation 18, those for the lidar system. Also note the Equation 20 does not have any products of inertia. This is because of the assumption that all the radar components lie along the centerline of the housing unit. To

insure that this assumption has some validity, it was requested to the group of researchers that are building the radar that most heavy components be along the centerline of the housing unit. Because of the comparability of the inertias of the two systems, the dual axis analysis was carried out with both systems in mind.

3.1.3 Fork System

To complete a analysis for the torque required for motion with both axes of rotation rotating simultaneously, the mass moment of inertia of the fork system needed to be completed. The configuration for the fork component is shown in Figure 14. The dimensions assumed for the fork are: the "u-shape" portion will consist of aluminum square tubing with dimensions of 6 inches by 6 inches by a quarter inch thick walls; the "u-shape" will have overall dimensions of 55 1/4 inches wide, and 54 inches high; the base of the "u-shape" will be a 10 inch diameter solid cylinder, 12 inches long; a motor with a gear reduction box will be located at the top of one of the legs of the "u-shaped" portion of the fork system; the motor will weigh 40 pounds and have dimensions of 5 inches wide by 5 inches high by 18 inches long.

Using the previously stated dimensions, the center of mass of the fork was calculated to be located at 21 inches from the ground and shifted 4 inches from the centerline of the fork towards the motor. The inertia matrix about the center of mass of the fork was calculated and is shown in Equation 21.

$$\begin{bmatrix} \bar{I}_{xx} & \bar{I}_{xy} & \bar{I}_{xz} \\ \bar{I}_{xy} & \bar{I}_{yy} & \bar{I}_{yz} \\ \bar{I}_{xz} & \bar{I}_{yz} & \bar{I}_{zz} \end{bmatrix} = \begin{bmatrix} 72{,}612{,}615 & 0.000 & 0.000 \\ 0.000 & 40{,}130 & 63{,}656 \\ 0.000 & 63{,}656 & 77{,}578 \end{bmatrix} \text{lb-in}^2 \qquad (21)$$

The inertia matrix of the fork system about the rotation axis was calculated using the equations as discussed in Chapter 2 and is shown in Equation 22.

$$\begin{bmatrix} I_{xx} & I_{xy} & I_{xz} \\ I_{xy} & I_{yy} & I_{yz} \\ I_{xz} & I_{yz} & I_{zz} \end{bmatrix} = \begin{bmatrix} 72,618,515 & 0.000 & 0.000 \\ 0.000 & 161,846 & 86,840 \\ 0.000 & 86,840 & 81,994 \end{bmatrix} \text{lb-in}^2 \qquad (22)$$

Although these values seem large, the I_{zz} component is the one of significance in the single axis analysis. The other components of the inertia matrix will add only a small amount to the required torques, as will be seen in the dual axis analysis.

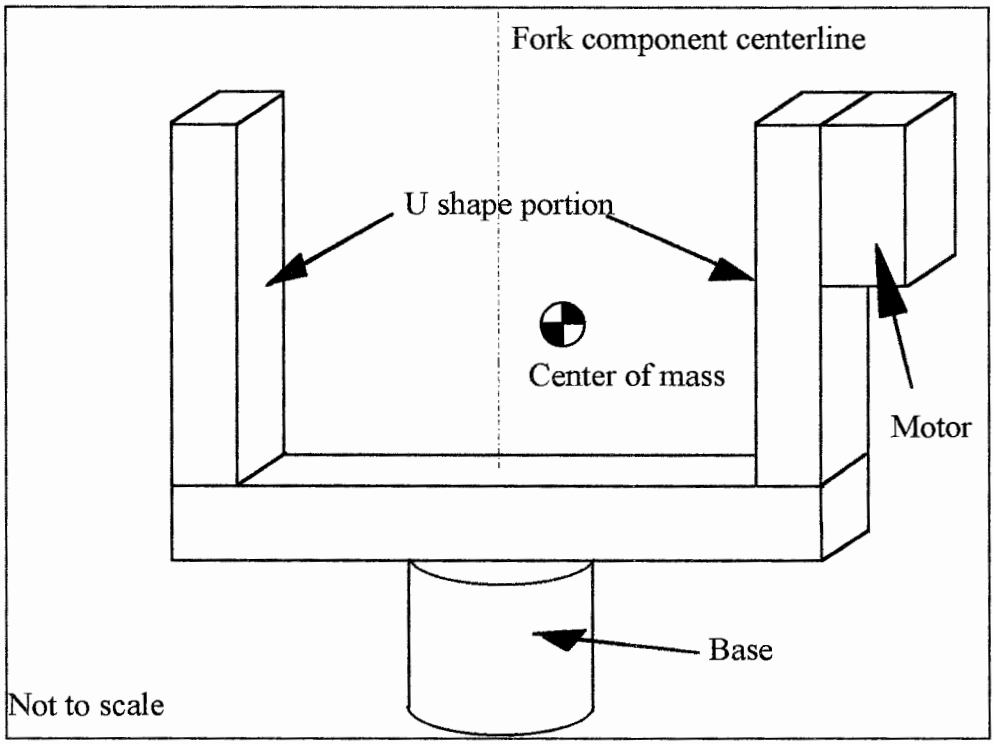

Figure 14: Fork System

3.2 Dual Axis Rotation Analysis

A dual axis rotation analysis was done to determine the torque required to achieve the desired scan rates for two axes rotating simultaneously. Note that throughout this analysis the term "table" refers to the lidar or radar system. This analysis was accomplished using the time derivative of the angular momentum of the fork system in motion.[8] Before the analysis was

done, coordinate systems were determined and are shown in Figure 15. The torques that were calculated in the $\hat{t}_2$ axis are the same as the torques experienced by the elevation motor. The torques that were calculated in the $\hat{f}_3$ axis are the same as the torques experienced by the azimuth motor. Note that the $\hat{t}_1$ direction in Figure 15 coincides with the lidar system line of sight and that $\hat{t}_3$ coincides with the radar system line of sight.

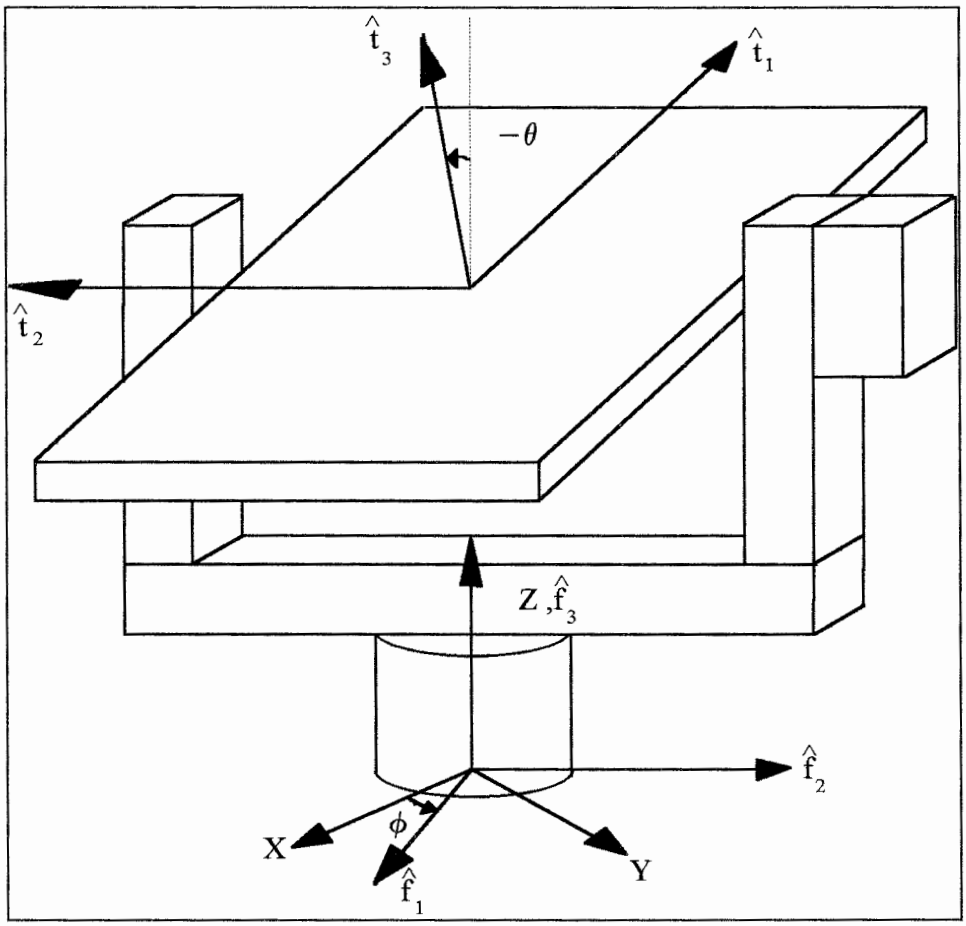

Figure 15: Coordinate Systems for Dual Axis Rotation Analysis

The coordinates shown in Figure 15 are unit vectors fixed in:

$\hat{t}_1, \hat{t}_2, \hat{t}_3$ =table frame of reference

$\hat{f}_1, \hat{f}_2, \hat{f}_3$ =fork frame of reference

X, Y, Z =inertial frame of reference

The inertia matrix of the major components are defined as:

$[I]_t$ =inertia of the table in table reference frame (defined in equation (18))

$[I]_f$ =inertia of the fork in fork reference frame (defined in equation (22))

The angular velocity of the table in an inertial frame resolved in the table reference frame is:

$$\hat{\Omega}_t = -\dot{\phi}\sin\theta\hat{t}_1 - \dot{\theta}\hat{t}_2 + \dot{\phi}\cos\theta\hat{t}_3 \tag{23}$$

Similarly, the inertial angular velocity of the fork resolved in the fork reference frame is:

$$\hat{\Omega}_f = \dot{\phi}\hat{f}_3 \tag{24}$$

To determine the torque needed for rotation of the lidar and radar systems, the angular momenta of the table and fork component must be determined. The following analysis yields the motor torque required at the table shaft and the constraint forces between the fork and the table. The angular momentum of the table component resolved in the table frame is:

$$\{\vec{H}_t\}_t = \begin{bmatrix} I_{xx} & -I_{xy} & -I_{xz} \\ -I_{xy} & I_{yy} & -I_{yz} \\ -I_{xz} & -I_{yz} & I_{zz} \end{bmatrix}_t \begin{Bmatrix} -\dot{\phi}\sin\theta \\ -\dot{\theta} \\ \dot{\phi}\cos\theta \end{Bmatrix} \tag{25}$$

Now that the angular momentum has been determined in one coordinate system, the external moments can be determined by taking the time derivative of the angular momentum in

an inertial frame and assuming that the table rotates approximately about its mass center, as shown in Equation 26.

$$\{M_t\}_t = \left\{\dot{\vec{H}}_t\right\}_t + \left\{\hat{\Omega}_t\right\} \times \{\vec{H}_t\}_t \tag{26}$$

Note Equation 26 was determined by knowing the derivative of the inertia matrix of the table is zero, $\left[\dot{I}\right]_t = 0$. This true because the table inertia is fixed in the table frame and is constant. Note that M_{t_2} is the torque required for the table rotation from Equation 26.

Expanding Equation 26 yields:

$$\begin{aligned} M_{t_1} = & -I_{xx_t}\left(\ddot{\phi}\sin\theta + \dot{\phi}\dot{\theta}\cos\theta\right) + I_{xy_t}\ddot{\theta} - I_{xz_t}\left(\ddot{\phi}\cos\theta - \dot{\phi}\dot{\theta}\sin\theta\right) \\ & -\dot{\theta}\left(I_{xz_t}\dot{\phi}\sin\theta + I_{yz_t}\dot{\theta} + I_{zz_t}\dot{\phi}\cos\theta\right) \\ & -\dot{\phi}\cos\theta\left(I_{xy_t}\dot{\phi}\sin\theta - I_{yy_t}\dot{\theta} - I_{yz_t}\dot{\phi}\cos\theta\right) \end{aligned} \tag{27}$$

$$\begin{aligned} M_{t_2} = & I_{xy_t}\left(\ddot{\phi}\sin\theta + \dot{\phi}\dot{\theta}\cos\theta\right) - I_{yy_t}\ddot{\theta} - I_{yz_t}\left(\ddot{\phi}\cos\theta - \dot{\phi}\dot{\theta}\sin\theta\right) \\ & +\dot{\phi}\sin\theta\left(I_{xz_t}\dot{\phi}\sin\theta + I_{yz_t}\dot{\theta} + I_{zz_t}\dot{\phi}\cos\theta\right) \\ & +\dot{\phi}\cos\theta\left(-I_{xx_t}\dot{\phi}\sin\theta + I_{xy_t}\dot{\theta} - I_{xz_t}\dot{\phi}\cos\theta\right) \end{aligned} \tag{28}$$

$$\begin{aligned} M_{t_3} = & I_{xz_t}\left(\ddot{\phi}\sin\theta + \dot{\phi}\dot{\theta}\cos\theta\right) + I_{yz_t}\ddot{\theta} + I_{zz_t}\left(\ddot{\phi}\cos\theta - \dot{\phi}\dot{\theta}\sin\theta\right) \\ & -\dot{\phi}\sin\theta\left(I_{xy_t}\dot{\phi}\sin\theta - I_{yy_t}\dot{\theta} - I_{yz_t}\dot{\phi}\cos\theta\right) \\ & +\dot{\theta}\left(-I_{xx_t}\dot{\phi}\sin\theta + I_{xy_t}\dot{\theta} - I_{xz_t}\dot{\phi}\cos\theta\right) \end{aligned} \tag{29}$$

where:

θ =angular coordinate describing the position of the table w.r.t. a reference elevation angle of 0 degrees

ϕ =angular coordinate describing the position of the fork w.r.t. a reference azimuth direction

$\dot{\theta}$ =angular velocity of the table

$\dot{\phi}$ =angular velocity of the fork

$\ddot{\theta}$ =angular acceleration of the table

$\ddot{\phi}$ =angular acceleration of the fork

I_{ab_c} =mass moment of inertia w.r.t. the a-b axes direction of the c component in the body-fixed c-frame (i.e. c = table or fork)

To determine the torque needed for rotation of the fork component, the angular momentum of the combined fork and table system must be determined. The following analysis yields the motor torque required at the fork shaft and the reaction torques applied to the ground from the fork component. The angular momentum of the system becomes:

$$\{\bar{H}_s\} = \underbrace{\begin{bmatrix} I_{xx} & -I_{xy} & -I_{xz} \\ -I_{xy} & I_{yy} & -I_{yz} \\ -I_{xz} & -I_{yz} & I_{zz} \end{bmatrix}_t \begin{Bmatrix} -\dot{\phi}\sin\theta \\ \dot{\theta} \\ \dot{\phi}\cos\theta \end{Bmatrix}}_{\text{resolved in table frame}} + \underbrace{\begin{bmatrix} I_{xx} & -I_{xy} & -I_{xz} \\ -I_{xy} & I_{yy} & -I_{yz} \\ -I_{xz} & -I_{yz} & I_{zz} \end{bmatrix}_f \begin{Bmatrix} 0 \\ 0 \\ \dot{\phi} \end{Bmatrix}}_{\text{resolved in fork frame}} \tag{30}$$

Resolving Equation 30 so that the entire equation is in the fork frame:

$$\{\bar{H}_s\}_f = \left\{ [{}_tT_f] \begin{bmatrix} I_{xx} & -I_{xy} & -I_{xz} \\ -I_{xy} & I_{yy} & -I_{yz} \\ -I_{xz} & -I_{yz} & I_{zz} \end{bmatrix}_t [{}_tT_f]^T \right\} \left\{ [{}_tT_f] \begin{Bmatrix} -\dot{\phi}\sin\theta \\ \dot{\theta} \\ \dot{\phi}\cos\theta \end{Bmatrix} \right\} + \begin{bmatrix} I_{xx} & -I_{xy} & -I_{xz} \\ -I_{xy} & I_{yy} & -I_{yz} \\ -I_{xz} & -I_{yz} & I_{zz} \end{bmatrix}_f \begin{Bmatrix} 0 \\ 0 \\ \dot{\phi} \end{Bmatrix} \tag{31}$$

where:

$$\left[{}_{t}T_{f}\right]=\begin{bmatrix}-\cos\theta & 0 & \sin\theta\\ 0 & -1 & 0\\ \sin\theta & 0 & \cos\theta\end{bmatrix}$$ transformation matrix from table reference to fork reference

$$\left[I_{t}(\theta)\right]_{f}=\left[{}_{t}T_{f}\right]\begin{bmatrix}I_{xx} & -I_{xy} & -I_{xz}\\ -I_{xy} & I_{yy} & -I_{yz}\\ -I_{xz} & -I_{yz} & I_{zz}\end{bmatrix}_{t}\left[{}_{t}T_{f}\right]^{T}$$ transformed inertia matrix of table in fork reference

$$\left\{\Omega_{t}\right\}_{f}=\left[{}_{t}T_{f}\right]\begin{Bmatrix}-\dot{\phi}\sin\theta\\ -\dot{\theta}\\ \dot{\phi}\cos\theta\end{Bmatrix}$$ transformed angular velocity of table in fork reference

Now that the angular momentum has been determined in the fork reference frame, the reaction moments can be determined by taking the time derivative of the angular momentum, as shown in Equation 32.

$$\left\{\vec{M}_{s}\right\}_{f}=\left\{\dot{\vec{H}}_{s}\right\}_{f}+\left\{\hat{\Omega}_{f}\right\}\times\left\{\vec{H}_{s}\right\}_{f} \tag{32}$$

Carrying out the derivative and cross product in Equation 32 and separating terms yields Equations 33, 34, and 35. Note that is the torque required by the fork motor to achieve the desired motion.

$$\begin{aligned}M_{f_1}=&-\dot{\theta}\sin\theta\left(-I_{xx_t}\dot{\phi}\sin\theta-I_{xy_t}\dot{\theta}-I_{xz_t}\dot{\phi}\cos\theta\right)+\dot{\theta}\cos\theta\left(I_{xz_t}\dot{\phi}\sin\theta-I_{yz_t}\dot{\theta}+I_{zz_t}\dot{\phi}\cos\theta\right)\\&-I_{xz_f}\ddot{\phi}-\cos\theta\left(-I_{xx_t}\left(\ddot{\phi}\sin\theta+\dot{\phi}\dot{\theta}\cos\theta\right)+I_{xy_t}\ddot{\theta}-I_{xz_t}\left(\ddot{\phi}\cos\theta-\dot{\phi}\dot{\theta}\sin\theta\right)\right)\\&+\sin\theta\left(I_{xz_t}\left(\ddot{\phi}\sin\theta+\dot{\phi}\dot{\theta}\cos\theta\right)+I_{yz_t}\ddot{\theta}+I_{zz_t}\left(\ddot{\phi}\cos\theta-\dot{\phi}\dot{\theta}\sin\theta\right)\right)\end{aligned} \tag{33}$$

$$\begin{aligned}M_{f_2}=&-I_{xy_t}\left(\ddot{\phi}\sin\theta+\dot{\phi}\dot{\theta}\cos\theta\right)+I_{yy_t}\ddot{\theta}+I_{yz_t}\left(\ddot{\phi}\cos\theta-\dot{\phi}\dot{\theta}\sin\theta\right)-I_{yz_f}\ddot{\phi}\\&-2I_{xy_t}\dot{\phi}\dot{\theta}\cos\theta-I_{yz_t}\dot{\phi}\dot{\theta}\sin\theta-I_{xz_t}\dot{\phi}\dot{\theta}\sin\theta\end{aligned} \tag{34}$$

$$
\begin{aligned}
M_{f_3} =& \dot{\theta}\cos\theta\left(-I_{xx_t}\dot{\phi}\sin\theta - I_{xy_t}\dot{\theta} - I_{xz_t}\dot{\phi}\cos\theta\right) - \dot{\theta}\sin\theta\left(I_{xz_t}\dot{\phi}\sin\theta - I_{yz_t}\dot{\theta} + I_{zz_t}\dot{\phi}\cos\theta\right) \\
& + I_{zz_f}\ddot{\phi} + \sin\theta\left(-I_{xx_t}\left(\ddot{\phi}\sin\theta + \dot{\phi}\dot{\theta}\cos\theta\right) + I_{xy_t}\ddot{\theta} - I_{xz_t}\left(\ddot{\phi}\cos\theta - \dot{\phi}\dot{\theta}\sin\theta\right)\right) \\
& + \cos\theta\left(I_{xz_t}\left(\ddot{\phi}\sin\theta + \dot{\phi}\dot{\theta}\cos\theta\right) + I_{yz_t}\ddot{\theta} + I_{zz_t}\left(\ddot{\phi}\cos\theta - \dot{\phi}\dot{\theta}\sin\theta\right)\right)
\end{aligned} \tag{35}
$$

where all the variables are as defined for Equations 27, 28, and 29.

If the torques that the ground will experience are known, then the stability of the entire fork system during operation can be evaluated. This will enable a design of the base that is able to withstand the moments that will be occurring during the scan profiles. The moments in the fork reference are transformed to an inertial system and are shown in Equation 36.

$$
\begin{Bmatrix} M_1 \\ M_2 \\ M_3 \end{Bmatrix} = \begin{bmatrix} \cos\phi & -\sin\phi & 0 \\ \sin\phi & \cos\phi & 0 \\ 0 & 0 & 1 \end{bmatrix} \begin{Bmatrix} M_{f_1} \\ M_{f_2} \\ M_{f_3} \end{Bmatrix} \tag{36}
$$

Equations 27 through 29 were solved with a FORTRAN program called momentt.for and Equations 33 through 36 were solved with a FORTRAN program called momentf.for; Appendix B includes listings of both programs. These programs were executed using the times for motor reversal as used in Chapter 2, to solve for the torques. The angular position of the table, θ, was varied between 0 and 180 degrees. The variation of angular position of the fork, ϕ, was found not to affect the torque required to achieve the motion for both the table and fork analyses, but was varied to determine the largest reaction torque experienced by the ground. The angular acceleration used in the program was calculated as shown in Equation 37.

$$
\left(\ddot{\phi},\ddot{\theta}\right) = \frac{2\left(\dot{\phi},\dot{\theta}\right)}{t_{rev}} \tag{37}
$$

where:

t_{rev} =time for motor reversal
$\dot{\theta}, \ddot{\theta}, \dot{\phi}, \ddot{\phi}$ =as defined previously

The torques were solved for both axes rotating, and the two axes rotating independently. It was determined that the largest torques occurred when both axes were rotating simultaneously and occurred for the fork motor on the lidar system. A check of the calculations was accomplished by comparing the single axis rotation analysis from the inertia.xls spreadsheet to the results for a single axis rotation in the momentt.for and momentf.for programs. To simplify design time, the largest torque calculated was used as the torque required for each motor to operate successfully. This torque was that needed at the shaft of the gear reduction box. Table 9 shows the largest torques needed for the motor scan profile for both the table and fork dual axis rotation analyses, including the manufacturer's reccommended margin of safety of 50% for the motor torques. Note that it was found that the lidar component had the largest torques for the table rotation and the radar component had the largest torques for the fork rotation.

Table 9: Largest Torques for Dual Axis Rotation

Motor Reversing Time (sec)	Torque for Fork Rotation (in-lb)	Torque for Table Rotation (in-lb)	Reaction Torque at Ground (in-lb)
0.1	2369	1172	1281
0.2	1185	590	644
0.5	475	239	261

3.2.1 Improved Motor Selection

Comparing the results from the dual axis rotation analysis, Table 9, to the single axis rotation analysis for the fork concept, Table 3, the torques to rotate the table are equivalent for the dual axis rotation analysis and the single axis rotation. Also, the torque required to rotate the VSM at the fork motor is approximately two times that required for the single axis rotation. This is because of the larger combined table and fork inertia.

3.2.1.1 Motor Torques

With the use of the motors and gear reduction boxes that were previously selected, the torque requirement for the scan profiles can be easily met. The use of Equation 38 determines the torque required to be output by the motor to achieve the torques for the scan profile listed in Table 9.

$$T_{motor} = T_{scan} N \frac{1}{\eta} \tag{38}$$

where:

T_{motor} =torque required by the motor
T_{scan} =torque required for the scan
N =gear reduction box ratio
η =efficiency of the gear reduction box

Since the efficiency of the gear reduction box under consideration is 85% and the gear reduction box ratio is 1/20, the maximum torque needed by the motor for the fork rotation is 139.35 in-lb, with a motor reversing time of 0.1 seconds. This torque requirement exceeds the output capabilities of the motor by approximately 17%, which suggests that a motor reversing time of 0.1 seconds is not possible. Duplicating the above analysis, a motor

reversing time of 0.2 seconds will yield a required motor torque of 69.71 in-lb for the fork rotation. Similarly for the table rotation, a required motor torque of 69.12 in-lb is required for the table rotation with a 0.1 second reversal time. This determines that the quickest possible time for reversing the motors is 0.2 seconds at the fork rotation and 0.1 seconds at the table rotation. With this in mind, Equation 39 can be used to determine the effective load inertia for the dual axis rotation.

$$I_{effective} = \frac{1}{N}\eta T_{motor}\frac{t_{rev}}{2\dot{\phi}_{scan}} \tag{39}$$

where:

$I_{effective}$ =effective inertia of the component
$\dot{\phi}_{scan}$ =angular velocity of the component
t_{rev} =motor reversing time

The effective inertia for the fork rotation is 222,881 lb-in^2. Using this value the load to motor inertia ratio can be calculated and used to determine the effectiveness of the motor in moving the system. The ratio is 172 for the S106-205 Compumotor microstepping motor and RA-115-20 Bayside Precision Controls Gearbox. This signifies that the system may be close to to instability and may have motor stall. To keep the motor in the stable region and prevent possible motor stall, an increase in the time for the motor to reverse direction may be necessary. Experimental testing of the completed system will provide a better understanding of the conditions surrounding the load to motor inertia ratio. Similarly for the table rotation, the effective mass moment of inertia was calculated to be 130,004 lb-in^2 with a load to motor inertia ration of 100. This defines the upper limit of the VSM to be: the system can scan at 10 degrees per second and can only reverse direction in no less than 0.2 seconds from the time of

the start of the motor deceleration to the point at which the 10 per second scan rate is achieved in the opposing direction for the fork rotation. A similar statement can be made for the table rotation except to use a 0.1 second criteria.

3.2.1.2 Static Torque

The static torque for the lidar system was found to be 1,974 in-lb without a gear reduction box and 99 in-lb with a gear reduction box for the table layout previously mentioned. The static torque is for the center of mass being 5 inches from the rotation axis. Since the static torque only affects the motor that rotates the table, this will be studied more. As previously stated, the "daytime torque" is 62.5 in-lb and counter masses may have to be added to move the center of mass of the system towards the rotation axis. Knowing that the maximum weight of the table will be 370 pounds (for the lidar system) and that gear reduction ratio is 1/20, the maximum allowable distance that the center of mass of the system can be from the rotation axis is 2.9 inches. This will allow for the static torque to always be counter acted by the magnet. Because the possibility that a safety radar system may be added to the lidar system, it was suggested that this be used as the counter balance. It has also been suggested that the telescope be moved forward on the optical table. This is because the previously mentioned turning mirror that will be mounted on to the secondary of the telescope may not need as much room as previously thought.

3.2.1.3 Additional Parts

Besides scanning the systems through portions of the sky, knowing the positions in time on the computer network is necessary to calculate the size of the data range bins for both of the lidar and radar systems. The addition of Compumotor 106-P incremental encoders to the motor met this need. In addition, these encoders add a closed loop control of the system to allow more accurate motion in the scan profiles.

To control the motors in a reasonable and economical fashion, a controller had to be selected. For our needs, a Compumotor AT6400, 4 axis controller was selected. It is able to 4 axes of rotation simultaneously and independently. The controlling software for this system was based on the Microsoft Windows environment, which is the environment that the LARS data acquisition computers will use. All the motion controlling equipment was purchased from Compumotor, 4 S106-205 microstepping motors, 4 106-P incremental encoders, 4 Bayside RA-115-20 planetary gearheads, breakout boards for emergency shutdown, and a AT6400, 4 axis controller.[9] Because of the early purchase of the motors, gear reduction boxes, encoders, and motion controlling equipment, all further designs were done to meet the motor and gear reduction box interfaces.

3.2.2 Shaft Design

Having the motors and gear reduction boxes selected, the preliminary design of the shafts that enable the rotation of both the table (lidar and radar systems) and the fork component had to be accomplished. First, a shaft sizing based on shear stress from applied torques was done and then a sizing based on deflection due to dead weight acting on the shafts. The final size of the shaft was determined by the bearing that could withstand the expected loading conditions, which will be discussed later.

3.2.2.1 Shear Stress Analysis

Determination of the absolute minimum of the shaft diameters for each rotation was done by analyzing the size that would have experience the yield shear stress within the shaft. The maximum torque experienced by the shaft rotating the fork will be 1185 in-lb. Using an aluminum shaft, which has a yield shear stress of 20,000 pounds per square inch (psi) and a shear modulus of 3,700,000 psi, the size of the shaft to reach yielding can be calculated using Equation 40.[10]

$$r = \sqrt[3]{\frac{2T_{scan}}{\pi \tau_{yield}}} \qquad (40)$$

where:

r =radius of circular shaft
T_{scan} =torque required to accomplish the scan profile
τ_{yield} =yield shear stress

The radius that will have the material begin yielding under the applied torque was calculated to be 0.34 inches. Thus, the diameter of the shaft will be 0.67 inches for the shaft rotating the fork component. Similarly, the size of the shaft rotating the table component can be calculated. The total torque experienced by the shaft is 2,661 in-lb. The diameter was found to be 0.88 inches. Note that these diameters were calculated to provide a minimum diameter of each shaft. This minimum diameter will not be approached to avoid any fatigue problems that may occur in the material.

3.2.2.2 Compression and Tension Stress Analysis

The shaft rotating the fork component will only experience compression and torsion during operation; and since the torsion analysis has already been covered, the compression analysis will be covered here. The size of the shaft required to keep the aluminum shaft below its yield compression stress of 37,000 psi was calculated using Equation 41. This equation was determined from Hooke's law for an isotropic material.[10]

$$r = \sqrt{\frac{W_{vsm} + W_{table}}{\pi \sigma_{yield}}} \qquad (41)$$

where:

r =radius of the shaft
W_{vsm} =weight of the volume scanning mechanism
W_{table} =weight of the table
σ_{yield} =compression yield stress

From Equation 41 the radius of the shaft rotating the fork component, for a VSM weight of 300 pounds and a table weight of 370 pounds, is 0.076 inches. Since this radius is so small in comparison to the size to meet the torque requirement it was ignored.

The shaft rotating the table will experience torsion and bending. Since torsion was already covered, bending will be discussed here. From simple beam bending theory [10], the equation to determine the size of a circular shaft in bending is shown in Equation 42. This equation was determined by assuming that the shaft goes straight through the table, is pinned at both ends the weight of the table is concentrated at the center of the shaft, and that the length of the shaft is 40 inches, which is a very extreme assumption.

$$r = \sqrt[3]{\frac{2W_{table}L}{\pi\sigma_{yield}}} \tag{42}$$

where:

r =radius of the shaft
W_{table} =weight of the table
L =length of shaft
σ_{yield} =compression / tension yield stress

Using the weight of the table as 370 pounds, the radius of the shaft was calculated as 0.63 inches, thus, the diameter is 1.26 inches. Since this is larger than that required for the torsion and the assumptions are extreme, this diameter will provide an additional margin of safety.

3.2.3 Shaft to Motor Coupling Selection

Because the height of the VSM must be less than 7 feet, the use of a coupler at the connection between the gear reduction box and the shaft to rotate the fork component was eliminated. Instead, a direct connection between the two was chosen. The aluminum was designed to be fitted with a stainless steel fitting to match the keyed shaft at the output of the gear reduction box. Stainless steel was chosen for two reasons: 1) to decrease any chance of material wear due to cyclic loading, and 2) to reduce any galvanic corrosion between two dissimilar metals. The use of aluminum for this fitting was eliminated because of reason 1. The size of the fitting was designed to meet the size of the shaft, which will reduce the stress levels of the fitting compared to an aluminum fitting since it is a stronger material.

For ease of assembly, a coupling device was chosen to be used for the interface of the gear reduction box and the table component shaft. Several types of couplers evaluated and considered and due to size constraints and cost limitations, a helical power coupler was chosen. This device allows for no maintenance, no wear of moving parts, no lubrication, no backlash, bi-directional capabilities without torque loss, and no vibration with misalignment. The power coupler can withstand a 0.037 inch parallel misalignment, has a maximum torque of 719 in-lb., has a torsional stiffness of 18,400 in-lb/radian, and has a weight of 2.31 pounds. The coupler is made to accept keyed shafts at either end. The power coupler selected was a PL6200-36K5-24K8. The size of the shafts accepted are a 1 inch shaft with a .315 inch keyway on one end and a 1 1/8 inch shaft with a 1/4 inch keyway at the other end. Assembly is accomplished by inserting the shafts until they are just visible in the helical section and the set screw located just above the key is tightened to a recommended torque. This will allow easy assembly of the shaft to gear reduction box at the table location.

The allowable torque on the power coupler dictates that the center of mass of the table must be within 0.35 inches from the rotation axis for motor reversal time of 0.2 seconds. For a motor reversal time of 0.5 seconds the distance is increased to 1.3 inches. The distance was

computed by subtracting the expected dynamic torque of 590 in-lb for 0.2 second motor reversing time from the allowable torque on the power coupler. The remaining torque is the allowable static torque. For the known weight of the table being 370 pounds, the maximum distance of the center of mass from the rotation axis was computed by dividing the maximum allowable static torque by the weight of the table. Note that the largest distance is 1.9 inches for a VSM not in operation.

3.2.4 Bearing Selection

Before the selection of the bearings could be carried out, several unknowns had to be defined. One of these was, what type of bearing to use for the shafts. Another concern was how to have the bearings attached to the shafts. After skimming through several catalogs for the different types of bearings available, the selection of the types of bearings were reduced to self-centering bearings mounted on a flange for the table shaft; and, angular contact or radial bearings for the fork shaft. After consulting the engineering section of a bearing catalog [10], the use of radial bearings was decided more suitable to our needs as it required no lubrication and was easier to install.

On the basis of the expected maximum dead load weight of 370 pounds from the table and the force created by the moment, M_{t_3} which has a maximum of 914 in-lb from the dual axis rotation, the radial load that is expected to act on the bearings for the table shaft is 208 pounds. The size of the shaft must be at least 1.26 inches in diameter. An SCJ series cast iron flange cartridge with a YA108-RRB non-relubricatable bearing was selected for the job. It can withstand 4000 pounds of static loading and can easily be mounted to a flat surface with four 1/2 inch bolts. As recommended by the manufacturer, the load rating was cut by two-thirds to allow for wear and a bearing life increase; reducing the load rating to 1333.33 pounds. Although the load rating is well above that expected, it provides a large factor of

safety. The main reason that this bearing was selected is that it is the only size greater than the calculated 1.26 inch diameter minimum required to prevent yielding in the shaft.

To help prevent tipping of the fork component, two radial bearings were chosen for use on the shaft rotating the fork component. These bearings were arbitrarily chosen to be at a distance of 6 inches apart from one another, in a vertical shaft configuration. In this configuration, the bearings will be experiencing a thrust load from the weight of the entire system and radial loads induced by their separation and the reaction moments acting on the ground. These loads were calculated to be approximately 650 pounds for the thrust load and 395 pounds for the radial load. A concern in the design of the base portion of the fork component was that if the base was not wide enough the VSM may tip over. For this reason, the diameter of the shaft rotating the fork component was chosen to be 3 inches instead of the calculated 0.67 inch to prevent yielding in the material. From this, four 316WDD radial bearings were purchased. They have a bore diameter (shaft clearance) of 3.1496 inches; have a radial static load rating of 30,000 pounds; are shielded on both sides to prevented dirt and unwanted debris from entering the bearings; and they are prelubricated and do not require lubrication for 20-30 years. Again the load rating was reduced from the quoted value to one-third the quoted value, 10,000 pounds, to measure its margin over the expected load. To calculate the thrust load, the reduced load capacity was reduced by one-half, 5,000 pounds. These bearings will carry all expected loads with ease and should increase the life of the VSM. The installation of these bearings is covered in detail in the service catalog and the are going to be press fit onto the shaft rotating the fork component.

3.3 Preliminary Performance Evaluation

To insure that further design of the VSM is credible, very simple performance evaluations of the design were accomplished. Several methods were used to perform the analysis. First, a finite element analysis of the VSM was performed to determine the

deflections and rotations at the support points of the table shaft. Second, an angular deflection analysis of the table and fork shafts, gear reduction boxes, and interfaces was done to determine the largest angle that the pointed system would be in error due to material deflections. Finally, a modal vibration analysis of the rotating systems was accomplished to compare the scanning frequencies with scan profiles to determine if dynamic amplification of deflections would occur.

3.3.1 Finite Element Analysis

A finite element analysis was done to find the deflections that the fork component would encounter when operating at the peak torques. The analysis was done with the previously determined fact that a 0.2 second motor reversing time enables the motors to move the fork component and that 0.2 seconds is an allowable reversing time for the table rotation. To define the static loading condition, a gravity field was defined for the fork system to include the effect of the weight of the fork component. The external loading input to the analysis is that shown in Figure 16. The motor and gear reduction box were modeled as distributed point masses along the side of the fork component. The torques in the table coordinates were reduced to point loads in the appropriate direction. To apply boundary conditions, the bottom of the base of the fork component is considered to be cantilevered.

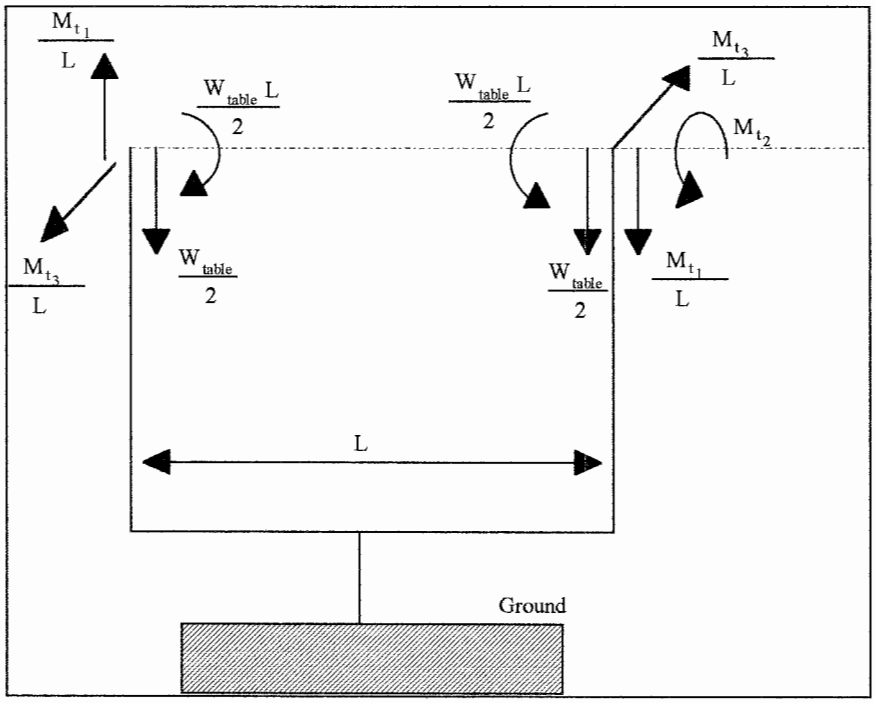

Figure 16: Load Condition for the Volume Scanning Mechanism

From the torques resulting from the dual axis analyses and the weight of the table the numerical values for the loads are shown in Equation 43.

$$M_{t_2} = 590 \text{ in-lb},\ \frac{M_{t_1}}{L} = 7 \text{ lb},\ \frac{M_{t_3}}{L} = 18 \text{ lb}$$
$$\frac{W_{table}}{2} = 185 \text{ lb},\ \frac{LW_{table}}{2} = 7{,}400 \text{ in-lb, and } L = 40 \text{ in} \tag{43}$$

An ANSYS finite element analysis [12], shown in Appendix C, was executed and the deflections and rotations at the support points were found. The results are shown in Table 10. Looking closely at the results, one can see that the largest component of the total deflection is in the x direction. This deflection will add an approximate 0.008 inch error in the alignment of the components of the VSM in the azimuth direction,. The next largest deflection occurs in the z direction, that acted on by gravity. This deflection will not add any significant errors in pointing since it just makes the entire fork component drop approximately 0.0037 inches. The

relative deflection in the y direction is very small, 0.0001 inches. This relative deflection moves the entire table component in the y direction, along with the fork component at the connection point. This deflection is very insignificant in the realm of all expected errors.

The rotation at the two points supporting the table component in the x direction, θ_x, represents the angle at which the table shaft rotates because of the bending of the shaft due to the weight of the table component. Because the values are very small they are not considered important in the pointing error of the VSM. The rotation difference between the two support points in the y direction directly adds to the pointing error in the elevation direction. The difference between the two points shows that there is a lagging between the torque applied at the motor and the support at the other end of the shaft. Although the lagging angle is 0.007 degrees, it is expected that the true lagging angle will be smaller because the "true" shaft between the two points will be made of the stainless steel honeycomb optical table, a very strong interface, and two 5 inch long aluminum shafts at either side of the optical table. Also, the shaft will not be constrained as it was in the finite element model, but allowed to rotate freely in the bearings. The remaining rotational deflection, θ_z, represents the angle at the ends of the shaft. Because the shaft will actually be pinned at the connection to the fork component, the true angle should be much smaller than that resulting here. The total deflection within the table component resulting from this bending should average out and not have a large contribution to the pointing error of the VSM.

Because the finite element analysis included the static loading condition, the reaction forces were expected to be higher than those resulting from the dual axis analysis. Table 11 shows the results and proves that this was true. The F_z term is equivalent to the weight of the VSM with the lidar system, 648.5 pounds. Table 11 also shows that the torque required to

Table 10: Finite Element Deflection and Rotation Results

Deflection and Rotation	Top of fork without motor	Top of fork with motor
u_x (inches)	0.0021	-0.0059
u_y (inches)	0.0014	0.0013
u_z (inches)	-0.0032	-0.0043
θ_x (degrees)	-0.0231	0.0200
θ_y (degrees)	0.0021	-0.0050
θ_z (degrees)	0.0062	0.0063

achieve the scan profile from the output of the gear reduction box is 1,440 in-lb, M_z. Because the point where this reaction torque occurred was considered cantilevered, no rotations and no deflections occur; therefore this torque is probably higher than what will actually occur. This is probably true since the system will be on bearings to enhance rotating capabilities and the mechanical connection will have some deflection and rotation. Note that this torque is slightly less than that calculated with the dual axis rotation in Table 9.

Table 11: Finite Element Reaction Forces Results

Reaction Force	Base location on ground
F_x (lb)	22.5
F_y (lb)	0
F_z (lb)	648.5
M_x (in-lb)	1,330
M_y (in-lb)	871
M_z (in-lb)	-1,440

3.3.2 Angular Deflection Analysis

Due to the all the parts that make up the connection between the motor and the system being moved, deflections of these parts will occur. The determination of the part that contributes the largest angular deflection will enable a better design of the final VSM. Considering the fork and table rotations as two separate analyses, each analysis was broken into several parts. First, the table rotation angular deflections were made up of the gear reduction box, power coupler, and the shaft. Second, the fork rotation angular deflection was made of the gearbox, the steel fitting between the shaft and the gear reduction box, and the aluminum shaft.

To determine the angular deflection that the table connection will undergo, the torsional stiffness was calculated using Equation 44.

$$k_\theta = \left(\frac{1}{k_{gearbox}} + \frac{1}{k_{coupler}} + \frac{1}{k_{shaft}} \right)^{-1} \qquad (44)$$

where:

k_θ =total torsional stiffness of the connection
$k_{gearbox}$ =torsional stiffness of the gear reduction box at the output (15,000 in - lb / degree)
$k_{coupler}$ =torsional stiffness of the power coupler (321 in - lb / degree)
k_{shaft} =torsional stiffness of the shaft (6,419 in - lb / degree)

The total torsional stiffness was calculated to be 300 in-lb/degree, with a table shaft section of 5 inches long and a diameter of 1.5 inches. Note that the power coupler contributes the largest portion of the torsional stiffness and is the 'weak link' in the connection. To determine the largest angular deflection under the expected load, Equation 45 is used.

$$\theta = \frac{T}{k_\theta} \tag{45}$$

where:

θ =angle that the connection is deflected
T =applied torque

From the expected maximum dynamic torque of 590 in-lb for the shaft to rotate the table component, the angular deflection is 1.97 degrees. Although this is above the required accuracy of 0.1 degrees, this is a deflection that occurs when the system reverses direction. When the system is reversing direction, it will deflect through this angle as the system is decelerating and the deflect through the opposite direction as it is accelerated. After the reversing direction maneuver is accomplished, the scan will require a near zero torque and, in a quasi-static steady state, deflect less than the required maximum of 0.1 degrees.

The torsional stiffness of the fork was calculated similarly to Equation 44, except that the value of the shaft torsional stiffness increases to 62,174 in-lb/degree, for a 10 inch long 3 inch diameter shaft. The power coupler torsional stiffness is replaced by the stainless steel coupling. The fitting was assumed to be 3 inches in diameter and 2 inches long for the analysis. The torsional stiffness for this assumption became 735,594 in-lb/degree. The torsional stiffness for the connection was then calculated to be 11,889 in-lb/degree. From this, the angular deflection at the time of motor reversal was calculated to be 0.099 degrees from an expected torque of 1,185 in-lb for the fork rotation. As stated earlier, this will not degrade from the performance of the VSM. Since this is smaller than the angular deflection of the table rotation, the fork rotation is expected to point in a direction closer to that directed during direction reversing than the table rotation.

3.3.3 Frequency Analysis

A comparison of the frequency of the scan rates and the natural vibration torsional frequency of the connections between the motor and rotating table and the motor and fork component is necessary to determine if dynamic amplification of any deflection will occur. The equation used to determine the natural torsional frequency of the connection is shown in Equation 46.

$$\omega_{connection} = \sqrt{\frac{k_\theta}{I_\theta}} \tag{46}$$

where:

$\omega_{connection}$ =natural torsional frequency of the connection (radian / sec)
k_θ =torsional stiffness of the connection (in - lb / radian)
I_θ =torsional inertia of the body being moved (in - lb - sec^2)

The torsional stiffnesses of both connections were given in the angular deflection analysis and just were converted to in-lb/radian for this calculation. The torsional inertia of the body being moved were calculated by taking the effective mass moment of inertias, calculated in the dual axis rotation, and dividing by gravity, 386.2 in/sec^2. In doing this, the natural (motor-fixed) torsional frequency of the table connection was determined to be 8.79 rad/sec. The period for the table connection frequency becomes 0.715 seconds using Equation 45. Similarly for the fork connection, the natural torsional frequency was calculated as 38.52 rad/secand and the period was calculated as 0.163.

The frequency of the scan profiles was calculated using Equation 47.

$$\omega_{scan} = \frac{2\pi}{P_{scan}} \tag{47}$$

where:

ω_{scan} =scan frequency
P_{scan} =period of the scan profile

The period of the scan profile will vary between 6 and 300 seconds for scan rates varying between 10 and 0.2 degrees per second. This large range of scan periods is because of the need to scan between 0.1 and 10 degrees per second over a 60 degree cycle, motion for a scan portion to leave and return to the original angular position. With these values the scan frequency ranged from 0.020944 to 1.047198 radians per second. Since the scan frequency range does not overlap the connection frequencies, dynamic amplification of deflections during one scan direction may occur, but with very small amplification factors. Since the vibration period of the connection (0.163 to 0.715 seconds) falls within the period for the time to reverse the motor direction (0.1 to 0.5 seconds), dynamic amplication may occur near the point when the scan direction is reversed. Two solutions are possible; 1) adjustment of the time for reversal of the motor direction to a point of deadbeat control and 2) increase the time for motor reversal to a time greater than 0.715 seconds. Because of the amount of data that will be transferred from measuring equipment to a data acquisition computer during the time of the scanning direction change, the second solution will be a more advantageous one. So, the minimum time for motor reversal was set to be one second to avoid dynamic amplification of deflections.

3.4 Preliminary Design Conclusions

The VSM containing the lidar system will experience the highest loads and torques required for a scan profile. The highest loads occur when both the table and fork components are rotating simultaneously. The selected motors, Compumotor S106-205, with a 20:1 gear

reduction box can handle the loads with the only stipulation being that the time for the scan profile to change directions must be greater than 0.2 seconds for the fork and table rotations. To prevent the static torque from over loading the motors and power coupler, the center of mass of the table may be within 0.35 inches of the rotation axis. To prevent yielding of the aluminum, the size of the shaft to rotate the table components is 1.5 inches in diameter, while the shaft to rotate the fork component is 3 inches in diameter.

Based on the preliminary performance analysis, the system should have a very small pointing errors due to elastic deflections (not including backlash, alignment, and other possible errors) in the regions when the VSM is not approaching or leaving a change of direction. Due to possible vibration amplification during the time when the scan directions are reversed, the time for the motor to decelerate, stop then accelerate to the desired scan rate must be greater than 1 second. With these criteria for further design, the detailed design, manufacture, and testing of the VSM are discussed in the rest of this thesis.

Chapter 4

DETAILED DESIGN, MANUFACTURE, AND TESTING

After the preliminary design, the detailed design of the volume scanning mechanism was accomplished. Various details of the design were determined and detailed drawings developed. These drawings were prepared for use by a machinist. The final drawings, parts and assembly, were submitted to the Penn State Machine Shop for manufacturing. After all the pieces were manufactured, the pieces were carefully assembled. Tests to evaluate the performance of the VSM were recommended. Performance aspects of interest include acceleration rates, time for direction reversal, scan rates, and scan profiles. Such tests will also help to identify operating limits . These limits would be programmed into the controlling software. The final VSM was completed and turned over to the technician responsible for its operation. Recommendations for future use are discussed in the next chapter.

4.1 Important Details of the Final Design

Figure 17 shows a front view of the VSM final design. Several areas of the design were analyzed in detail to insure that the components could withstand the expected loads, be easily assembled, and be easily manufactured. These areas include motor mounting, motor to shaft interfaces, shaft to table (lidar and radar instruments) interfaces, and bolt strength. Throughout these analyses, a goal of simplicity (manufacture, assembly, disassembly, and maintenance) was pursued. The detailed drawings of every part and the associated assembly drawings are found in Appendix D.

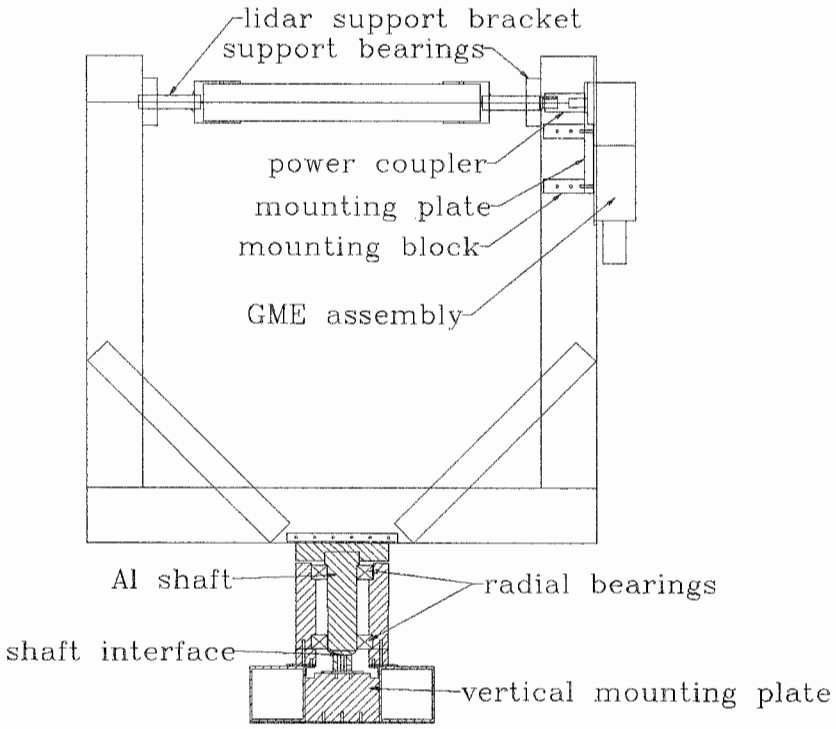

Figure 17: Front View of the VSM Assembly

4.1.1 Motor Mounting

Because the square tubing for the u-shaped portion of the fork component had already been selected, the design of the mount for the motor to turn the table component was designed to fit within the tubing. To securely mount the motor, a bolt hole pattern matching that on the gear reduction box was placed on a mounting plate (part number 13 in Appendix D). The gear reduction box, motor, and encoder combination (GME) were

bolted to the mounting plate and the mounting plate was attached to the tubing. To decrease the amount that the motor will extend from the square tubing, a section of the tubing wall was cut (see part number 16 in Appendix D). Mounting blocks (part number 12) were placed within the open section of the tubing so the mounting plate with the GME can be firmly mounted. The power coupler linked the shaft protruding from the GME and the shaft attached to the table component. The combination of the GME, mounting plate, and mounting blocks was very simple to manufacture and assemble.

The GME that rotates the fork component is mounted using a plate similar to that for the table rotation. The fork mounting plate (part number 4), smaller than the table mounting plate, attaches to a vertical plate (part number 3) that attaches to a plate that lies on the floor (part number 2). The plate that lies on the floor attaches to two 40 inch long square tubes (part number 5) that is identical to the ones used for the u-shaped portion of the fork component. This arrangement should have the motor mounted sturdily and transfer the reaction loads to the ground efficiently. The assembly of this arrangement was done carefully as to insure that the shaft protruding from the GME does not carry the weight of the entire system.

4.1.2 Motor to Shaft Interfaces

The interface between the GME shaft and the table component was designed using the previously selected power coupler. The GME combination mounts within the tubing. The shaft that protruded from the GME combination attaches to the power coupler. The power coupler had enough room to fit between the tubing and the motor mounting plate. There was enough room for a hex key to fit within the tubing to allow tightening of the set screws at either end of the power coupler. The GME combination mounts to the square tubing with the power coupler attached to the shaft that protruded from the combination. After the GME assembly (GME combination and motor mounting plate) is attached, the

shaft from the table component slips through the table support bearings and slides 1.1 inches within the power coupler to have the set screws tightened.

The interface between the GME shaft and the fork component was designed knowing that the interface, made of stainless steel, attaches to the three inch aluminum shaft (part number 10). The interface had a keyed bore hole for easier manufacture of the piece. The interface (part number 10a) also has a set screw over the key, similar to the power coupler assembly.

4.1.3 Shaft to Table Interfaces

Once the mount of the motor to rotate the table was designed, the link between the shaft protruding from the power coupler and the lidar and radar instruments was designed. To keep the design of the two brackets simple, the shafts extending from the support bearings mounted on the fork component were identical, except for length, for both systems (part numbers 18,19,21, and 22). The width of the two systems, lidar and radar, only differ by 4 inches. The brackets that mounted directly to the lidar and radar instruments were designed independently of each other. The bracket for the lidar (part number 24) was designed to clamp the optical table on both sides with ten 1/2 inch steel alloy bolts. The design of the brackets for the radar (part number 23) was designed to bolt to a plate that permanently mounts on the housing unit of the 94 GHz system. Eight 1/2 inch aluminum alloy bolts were used to support the radar instrument in the VSM.

4.1.4 Bolt Strength Analysis

As is seen in Figure 17, there are many bolts used in the design of the VSM. To ensure that the bolts can withstand the expected loading, a shear analysis of the critical bolts was accomplished. Several bolts are critical to the design. They clamp the lidar instrument to its support bracket, bolt the radar instrument to its supporting brackets,

attach the stainless steel interface for the fork rotation to the fork rotation aluminum shaft, and bolts the angle that is holding the u-shaped portion of the fork component to the base. The selected bolts were alloy steel socket caps with a tensile strength of 190,000 pounds per square inch (psi) and a shear strength of 95,000 psi.

The 1/2 inch bolts that are used to hold the radar and lidar instruments can withstand a shear loading of 23,750 pounds. Since the largest average shear loading per bolt expected was 37 pounds for the lidar and 31.25 pounds for the radar, these bolts will not have any strength problems. Five bolts selected to attach the shaft interface to the fork shaft are 1.35 inches from the rotation, which results in 176 pounds of shear force per bolt. These bolts are also not susceptible to strength failure. The remaining bolts, the ones attaching the base to the u shaped portion of the fork component, experience 100 pounds in tension and 56 pounds in shear. These bolts will also not experience any strength problems.

4.2 Manufacture and Assembly

After deciding the details of the design, the drawings for manufacture were produced. All the drawings for the 24 parts are included in Appendix D. After many iterations these final drawings were submitted to the Penn State Machine Shop. It took 6 weeks for the parts to be produced and partial assembly to be completed. Parts were numbered for assembly. Testing of the VSM for the lidar system was accomplished first, as the radar system was not expected to be ready for operation until the end of the year.

4.3 Testing Plan

The VSM tests include: verification of torsional stiffness of the connection of the table component and associated motor, measurements of static deflections of the connections that were analyzed in Chapter 3, torque levels on the shafts, stresses in the

shafts, and motion capabilities. These measurements will define safe operating levels for the VSM. Although analytical operating levels were computed, experimental results would verify the analyses.

Each axis of the VSM should be tested independently before simultaneous testing of the axes is accomplished. Because of the value of the components mounted on the optical table of the lidar system, the VSM with the optical table should be tested with mass simulators to simulate the weight, inertia, and center of mass location of the layout. The mass simulators are expected to be just large pieces of metal mounted on the optical table to simulate the properties of all of the components.

4.3.1 Torsional Stiffness and Deflections of the Connections

The torsional stiffness and static deflections of the connection between the motor and the table component need to explored. The experimental torsional stiffness will give better values for a modal vibration analysis of the connection between the table component and its associated motor. To study the torsional stiffness, the motor of the shaft should be locked in place. With this, a known torque can be applied to the shaft connected to the table component with a torque wrench. The measured angular deflection will determine the torsional stiffness of the connection. The experimental stiffness can be used to repeat the modal vibration analysis to determine if vibration amplification will occur before any motion experiments are done.

In conjunction with the torsional stiffness, the calculation of the static angular deflection due to the offset of the center of mass with the rotation axis of the table component can be accomplished. The center of mass can be calculated from experiment by placing all the equipment on the optical table and letting the layout freely rotate. The layout should come to rest at an angle. Geometry can be used to determine the approximate location of the center of mass. Knowing the total weight of the table

component, 370 pounds for the lidar system, the static deflection can be calculated. The weight of the table component creates a torque of the weight times the distance from the rotation axis to the center of mass of the table component. This torque can be divided by the torsional stiffness of the connection to determine the angular deflection that will always be present with a center of mass offset from the rotation axis. Also, counter balances can be added such that the table comes to rest in the horizontal position. This will decrease the static deflection due to gravity because the center of mass of the layout will almost coincide with the rotation axis.

4.3.2 Torque and Stresses on the Shafts

Torque and stress on the shaft will play an important role. Large torques induce high stress levels in the shaft. Although the expected stress levels of 890 and 224 psi for the table and fork shafts respectively are well below the yield strength of the aluminum, the actual stress levels should be measured during the testing phases to insure safe operation of the VSM. The high stress levels can propagate fatigue damage within the shaft and decrease the life of the shaft. To measure the stress levels of the shafts, a strain rosette or an angle measuring device can be used. The best method of measuring the stress levels is with the strain rosette. Using a rosette may be difficult as the shaft will be rotating. If the rotation of the shaft is kept at small rotations, i.e., less than 45 degrees, then this might be a beneficial tool. The use of an angle measuring device may be difficult to implement, but may not be restricted to certain shaft rotations. In addition, an angular measuring device would add the knowledge of how much deflection is occurring in a scan profile. The choice of measurement has not been selected as of yet. Either way, the stresses will be recorded during the motion capabilities testing and compared to the yield strength of the aluminum shafts. If the stress levels are too high, within 20% of the yield

strength of aluminum, then the angular accelerations will have to be reduced or a fatigue analysis will be necessary.

4.3.3 Motion Capabilities

Experimental verification of the motion capabilities of the VSM must be accomplished. The main areas of the motion capabilities that must be known are the acceleration, reversing, and scanning capabilities of the VSM. The acceleration verification includes determining the maximum acceleration rate of the optical table that will not experience motor stall or system tip over. The reversing experiment determines the fastest time that the motors can reverse direction without stalling. The scan profile validation determines the fastest scan rate that the VSM can undergo without experiencing motor stall and tip over.

4.3.3.1 Acceleration Verification

The experiment consists of accelerating a component about an axis from zero to 1 degree per second, scan rate, in Y seconds. The time for the acceleration, Y, is decreased until motor stall is observed. The scan rate is increased by 1 degree per second increments. The experiment is then run again to determine the fastest acceleration rate. This procedure is repeated until a maximum scan rate is determined. The procedure will determine the acceptable acceleration rates that the VSM can undergo.

4.3.3.2 Reversing Validation

This experiment determines the fastest time that the motors can reverse directions without experiencing motor stall or VSM tip over. The accelerations from the previous experiment will be used as baseline accelerations for this experiment. A component will be accelerated from zero to a predetermined scan rate and allowed to rotate for 30

degrees about an axis. When 30 degrees has been reached, decelerate the axis until a scan rate of zero degrees per second has been reached. At this point begin immediate acceleration of the axis in the opposite direction until the predetermined scan rate has been reached. During this maneuver, any tipping, large stress levels, or large vibrations of the system should be noted. Motor stalls should not occur because the accelerations used will not exceed those obtained from the previous experiment. This procedure is repeated with a faster scan rate. The fastest time that the system can achieve this motion is recorded. The entire procedure is repeated with a faster scan rate to find an envelope of operation for the turn around times and scan rates.

4.3.3.3 Scan Profile Validation

The scan profile experiment is done as a mock-up of a run in the field with an operational lidar system. Simple scan profiles, consisting of only one axis rotating at a time, are run with a large time for motor reversal and a slow scan rate (1 degree per second). The time for motor reversal is decreased until the "safe" time determined in the previous experiment is encountered. Tip over, motor stalls, motor overheating, large stress levels, or any other problems are noted and used to help determine a safe scan rate for a profile. The scan rate is increased for the same scan profile and repeated to find the safe operating motor reversing time. The scan rate with the fastest motor turn around time that does not experience motor stall, motor overheating, tip over of the VSM, or large vibration amplitudes, will be considered the upper limit of the VSM.

The procedure is repeated for the other axis and for the VSM to scan about both axes simultaneously. The safest scan profiles will be used as programmed into the scanning profiles as limits of operation. These soft and hard limits, as well as an emergency shutdown switch, will provide adequate protection that the system will not stall, tip over, over heat, or fatigue during operation.

4.4 Summary

The detailed design was carried out based on the preliminary design discussed in Chapter 3. The bolts used in the manufacturing of the VSM were determined to be able to hold the structure together reliably. The details of the assembly of the critical parts of the VSM were developed through several iterations and were designed to be simple to assemble and manufacture. Testing of the VSM was planned to determine safe operating levels to prevent any undesirable operating characteristics, (motor stall, dynamic amplification of deflections, tip over, over heating, large deflections, large stresses, and large torque's), and damage to the instruments. Insight in the design suggests that the VSM will outperform the design requirements presented in Chapter 2.

Chapter 5

SUMMARY AND RECOMMENDATIONS

5.1 Summary

At the beginning of this project, a volume scanning mechanism that would enable lidar and radar systems to scan the sky was desired. This would enable the systems to map 3-D contours of many hydrologic parameters. Eight initial concepts were considered and reduced to three final concepts. These final three concepts were further evaluated. The evaluations were based on general characteristics of each concept and calculations to determine the feasibility of each concept. The concept that prevailed against all the other concepts was the fork concept. This concept had easy maintenance, easy implementation of scan profiles, a fairly simple design, and was inexpensive in comparison to other concepts.

The preliminary design of the fork concept showed that microstepping motors with planetary gearheads are able to move the VSM. Sizes for all critical components were determined. Preliminary performance analysis suggests that the system will have small pointing errors due to elastic deformation of the rotating shafts. The final design of the volume scanning mechanism was easily assembled. Insight in the design suggests that the final design will perform better than that stipulated at the beginning of the project.

Every critical component of the VSM was analyzed. The only portion of the VSM that may create problems would be the connection between table component and the motor shaft. This "weak" connection may produce dynamic amplification of elastic deformations during scan reversing manuevers. To prevent this problem from occuring, the time for the motor to reverse direction must either be tuned or the time must be

greater than 1 second. The volume scanning mechanism should outperform that required for successful operation.

5.2 Recommendations

To insure successful operation, the recommended tests of the system should be done before any atmospheric measurements are taken. These tests will identify any problems that might hinder the operation of the VSM in the field. Also, it is recommended that the time for the motors to reverse direction be at least 1 second.

When components of the lidar system are mounted to the optical table, placement of temporary supports to the optical table is highly suggested. The supports should be pressed between the optical table and the ground to allow the optical table to remain in the horizontal position. At least three people should be present when the optical table is rotated for mounting to the opposite side. All three people should hold the VSM to insure that tip over does not occur.

Decreasing the maximum allowable scan rate from 10 degrees per second to a slower rate, maybe 5 degrees per second, will allow for faster motor reversal times. It will also allow for the position of the center of mass of the layout relative to the rotation axis to become 1.4 inches, for 5 degrees per second, instead of 0.35 inches when the scan rate was 10 degrees per second.

Static balancing of the lidar components for the previously discussed layout must be done in order to have the center of mass of the layout be within the stipulated distance.

REFERENCES

1. Philbrick, C.R., "Water, Aerosol, Vapor Experiment-LIDAR and RADAR Sounder," Proposal to the U.S. Department of Energy (Program Notice DE-PS05-92ER79054), Office of Energy Research, December 9, 1991.

2. Machuga, D.W., "Daytime Performance of the LAMP Rayleigh/Raman Lidar System," MS Thesis, The Pennsylvania State University, 1993.

3. Young, A.T., "Rayleigh Scattering," *Applied Optics*, vol. 20, no. 4, 1981.

4. Philbrick, C. R., D. B. Lysack, T. D. Stevens. P. A. T. Haris, and Y. -C. Rau, "Atmospheric Measurements Using the LAMP Lidar during the LADIMAS Campaign," Presented at the Sixteenth International Laser Radar conference, sponsored by AMS, USAF, OSA, and NASA, Cambridge, MA, July 20-24, 1992.

5. Rajan, S., G. R. Evansiko, T.J. Kane, and C.R Philbrick, "Aerosol Mapping of the Atmosphere Using a Multiple Wavelength Polarization Lidar," Presented at the Combined Optical-Microwave Earth and Atmospheric Sensing Conference, sponsored by the IEEE, Albuquerque, NM, March 22-25, 1993.

6. Zaccanti, G., P. Bruscaglioni, M. Gurioli, and P. Sansoni, "Laboratory Simulations of Lidar Returns from Clouds: Experimental and Numerical Results," *Applied Optics*, vol. 32, no. 9, March 20, 1993.

7. Ackerman, T.P., B.A. Albrecht, M.A. Miller, E. Clothiaux, R.M. Peters, and W. Syrett, "Remote Sensing of Cloud Properties Using a 94 GHz Radar," Presented at the Combined Optical-Microwave Earth and Atmospheric Sensing Conference, sponsored by the IEEE, Albuquerque, NM, March 22-25, 1993.

8. Beer, F.P. and E.R. Johnston Jr., *Vector Mechanics for Engineers: Statics and Dynamics*, Fourth Edition, McGraw-Hill Book Co., New York, NY, 1984.

9. Parker Hannifin Corporation, Compumotor Division, *Positioning Control Systems and Drives*, Rohnert Park, CA, 1992.

10. Beer, F.P. amd E.R. Johnston Jr.,*Mechanics of Materials*, McGraw-Hill Book Co., New York, NY, 1981.

11. Ingersoll-Rand, The Torrington Company, *Service Catalog*, Torrington, CT, 1988.

12. Swanson Analysis Systems, Inc., *ANSYS Command Reference Guide*, Revision 4.4, Houston, PA, 1989.

Appendix A

SPREADSHEETS TO CALCULATE INERTIA AND TORQUE

This appendix contains the spreadsheets used to calculate the inertia of the support table and equipment and the torque to rotate it about the axes shown in the appropriate figure. The calculations shown in these spreadsheets are for the fork concept as it was analyzed in Chapter 2 and is an example of the calculations for the other concepts. The calculations for the other concepts used these spreadsheets for analysis, but the results of their analysis are not shown for brevity.

The coordinates of the equipment on the optical table, their dimensions and weight are input to the spreadsheet. The total weight of the layout is then calculated with a 5% addition of uncertainties. The position of the rotation axis is then entered to the spreadsheet. With this information, the center of mass of the layout is calculated with the equations discussed in Chapter 2. Page 2 of inertia.xls calculates the inertia of each piece of equipment and the inertia matrix of the system about the center of mass. The inertia matrix about the rotation axis is then calculated.

Torque.xls is linked to inertia.xls to get the mass moment of inertia about the rotation axis. The inputs to the spreadsheet are the inertia of the motor, the gear reduction box ratio, the gear reduction box inertia, the rotation rate, and the time for the layout to reverse direction. The static torque about the rotation is calculated for rotation about the three orthogonal axes. The dynamic torque for a single axis rotation is then calculated. The value that is highlighted in the dark border is the critical value for the conceptual analysis.

All dimensions are in inches

Item	Description	Distance from front edge of support table to leading edge of body in x direction	Distance from center line of support table to center of body in y direction	Distance from center line of support table to bottom/top edge of body in z direction	Length	Width (Radius)	Height	Weight (pounds)
1	Telescope	15.40	0.00	3.00	42.00	9.50	-	83.00
2	Data Acquisition	57.40	0.00	10.00	10.00	3.00	3.00	25.00
3	Support table	0.00	0.00	0.00	60.00	30.00	4.00	175.00
4	Surelight II Laser	24.00	0.00	-2.75	30.30	7.00	6.25	52.00
5	Beam Expander	11.00	0.00	-2.00	12.00	3.00	3.00	15.00
6	Energy monitor	0.00	0.00	-2.00	6.00	3.00	3.00	2.00

height of telescope above the support table	1.00
height of laser above the support table	0.75
x position of rotation axis from leading edge of support plate	30.00
y position of rotation axis from leading edge of support plate	0.00
z position of rotation axis from centerline of support plate	0.00

Weight	352.00
+5% miscellaneous	17.60
Total weight	369.60

system weight 369.60

c.m. in x dir. from leading edge of support plate	34.39
c.m. in y dir. from leading edge of support plate	0.00
c.m. in z dir. from centerline of support plate	2.60

distance from rotation axis to c.m. in x-y plane	4.39
distance from rotation axis to c.m. in x-z plane	5.10
distance from rotation axis to c.m. in y-z plane	2.60

	x-direction	y-direction	z-direction
c.m.1 to c.m.sys	23.01	0.00	9.90
c.m.2 to c.m.sys	28.01	0.00	8.90
c.m.3 to c.m.sys	-4.39	0.00	-2.60
c.m.4 to c.m.sys	8.76	0.00	-8.47
c.m.5 to c.m.sys	-17.39	0.00	-6.10
c.m.6 to c.m.sys	-31.39	0.00	-6.10

xbar of system	4.39
ybar of system	0.00
zbar of system	2.60

inertia.xls

inertia.xls

Ixx	Ixy	Ixz
	Iyy	Iyz
		Izz

inertia matrices are in lb-in2
to get inertia matrices in correct units for mass
divide by 386.2 in/sec2

1 c.m. is u the length of telescope from front

u= 0.666667

3745.38	0.00	0.00
	18140.69	0.00
		18140.69

2 c.m. is center of the data acquisition system

37.50	0.00	0.00
	227.08	0.00
		227.08

3 c.m. is center of the support table

13358.33	0.00	0.00
	52733.33	0.00
		65625.00

4 c.m. u" towards the back of the laser from the center of the optical head along the longitudinal axis

u= 0

381.60	0.00	0.00
	4147.66	0.00
		4190.72

5 c.m. is at the center of the beam expander

22.50	0.00	0.00
	191.25	0.00
		191.25

6 c.m. is at the center of Energy Monitor

3.00	0.00	0.00
	7.50	0.00
		7.50

moments of inertia about center of mass of pointed system

17548.3125	0	25255.921
	75447.515	0
		88382.244

moments of inertia of pointed system about rotation axes origin

20041.81899	0	29466.31
	85050.4398	0
		95491.662

	lb-in2
Inertia of motor	3.25
gear reduction ratio (N2/N1)	20
inertia of gear reduction box	0.1569
Static torque about x axis (in-lb)	48
Static torque about y axis (in-lb)	94.19714698
Static torque about z axis (in-lb)	81.05
load to motor inertia ratio	65.42341522

Motor Static torques with factor of safety of 1.5

in-lb
72
141.2957205
121.575

omega	10	degrees/sec =	0.174532778 rad/sec
turn-around time	0.1	seconds	

for single axis rotation manuever

	Mxx	**Myy**	**Mzz**
Dynamic torque is in in-lb for rotation about x axis	9.644936137		
Dynamic torque is in in-lb for rotation about y axis		39.02384646	
Dynamic torque is in in-lb for rotation about z axis			43.74247825

Motor Dynamic torques with factor of safety of 1.5

in-lb

14.4674042	0	0
0	0	0
0	0	0
0	0	0
0	0	0
0	58.53576969	0
0	0	0
0	0	0
0	0	0
0	0	0
0	0	65.61371737

Appendix B

FORTRAN PROGRAMS TO CALCULATE THE TORQUE REQUIRED FOR A DUAL AXIS ROTATION

This program momentt.for uses Equations 27, 28, and 29 and the program momentf.for uses Equations 33, 34, 35, and 36 to calculate the torque required to rotate the radar and lidar systems and the reaction loads on the fork component from the table component due to its rotation. The user of each program is asked to choose which system they wish to analyze, the radar or lidar system. Data files exist that contain the pertinent mass moment of inertia of the system and fork and are imported by the program. The user is then asked to give the increment over which to step the angular position of the radar or lidar system. The next values to be inputted are the motor reversing time and the choice of having only the lidar or radar system rotating, only the fork component rotating, or both of the components rotating simultaneously. The final inputs to the program are the angular velocities for the lidar or radar component and the angular velocity of the fork component.

The outputs of the program are: feedback of the inputs; the maximum torque at each axis; the angular acceleration that is calculated from the program; and data files containing the variation of torque with angular position.

When the user chooses to have either one or both components rotating, they are selecting the analysis to be carried out assuming that the system will reverse direction at all angular positions. This is able to be accomplished because the torque is not dependent on the previous torque calculation. The four output files are (x is either l or r, depending on the choice of lidar or radar analysis): xtresult.dat and xfresult.dat, a feedback of the inputs and the maximum values for the torques and their corresponding angular positions; xttable.dat is a file containing the torques in the table reference frame, M_{t_1}, M_{t_2}, and M_{t_3}, and the corresponding table angular position, θ (It was found that

and xffork.dat are files containing the torque in the fork reference frame, M_{f_1}, M_{f_2}, and M_{f_3}, and the corresponding table angular positions (It was found that these torques does not vary for different values of the fork angular position, ϕ); xfnewton.dat is a file containing the reaction moments, M_1, M_2, and, M_3, experienced by the ground. The files were plotted for the lidar system with a motor reversing time of 0.1 seconds for the table rotation, 0.2 seconds for the fork rotation, and both axes reversing simultaneously. Figure B1 shows the variation in the torques in the table reference frame for the lidar system. It is easily seen that the torques vary greatly as a function of table angular position. Figure B2 shows the variation in the torques in the fork reference frame for the radar system. Large variations also occur here for varying table position. Figures B3 and B4 show the three-dimensional variation in the inertial torque that is experienced by the ground, M_1 and M_2. The vertical component of the inertial torque, M_3, was not plotted since it is identical to M_{f_3}. Although there are large differences between the two torques, the maximum values are the same as presented in Chapter 3.

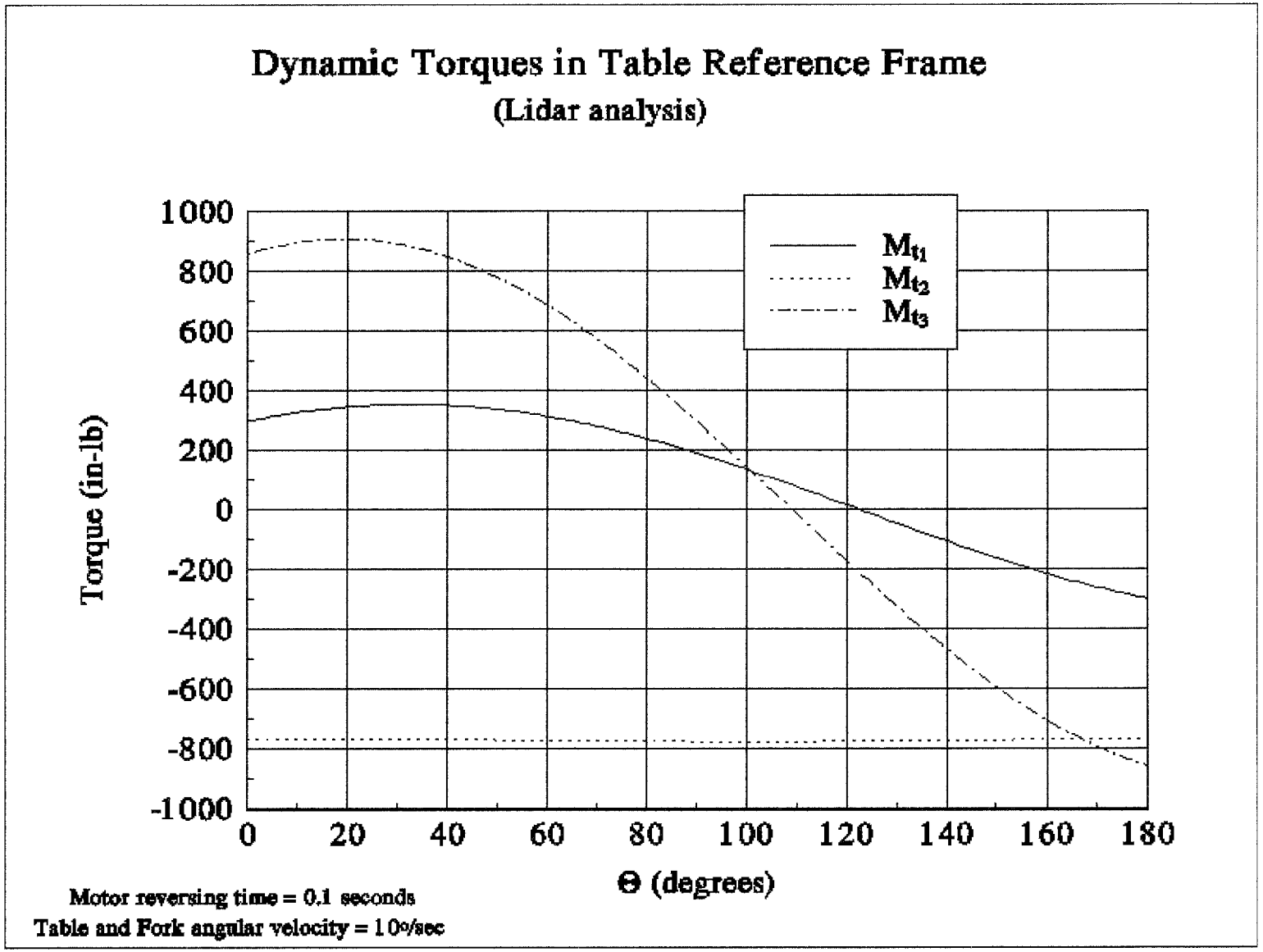

Figure B1: Torque in Table Reference Frame for Lidar Analysis

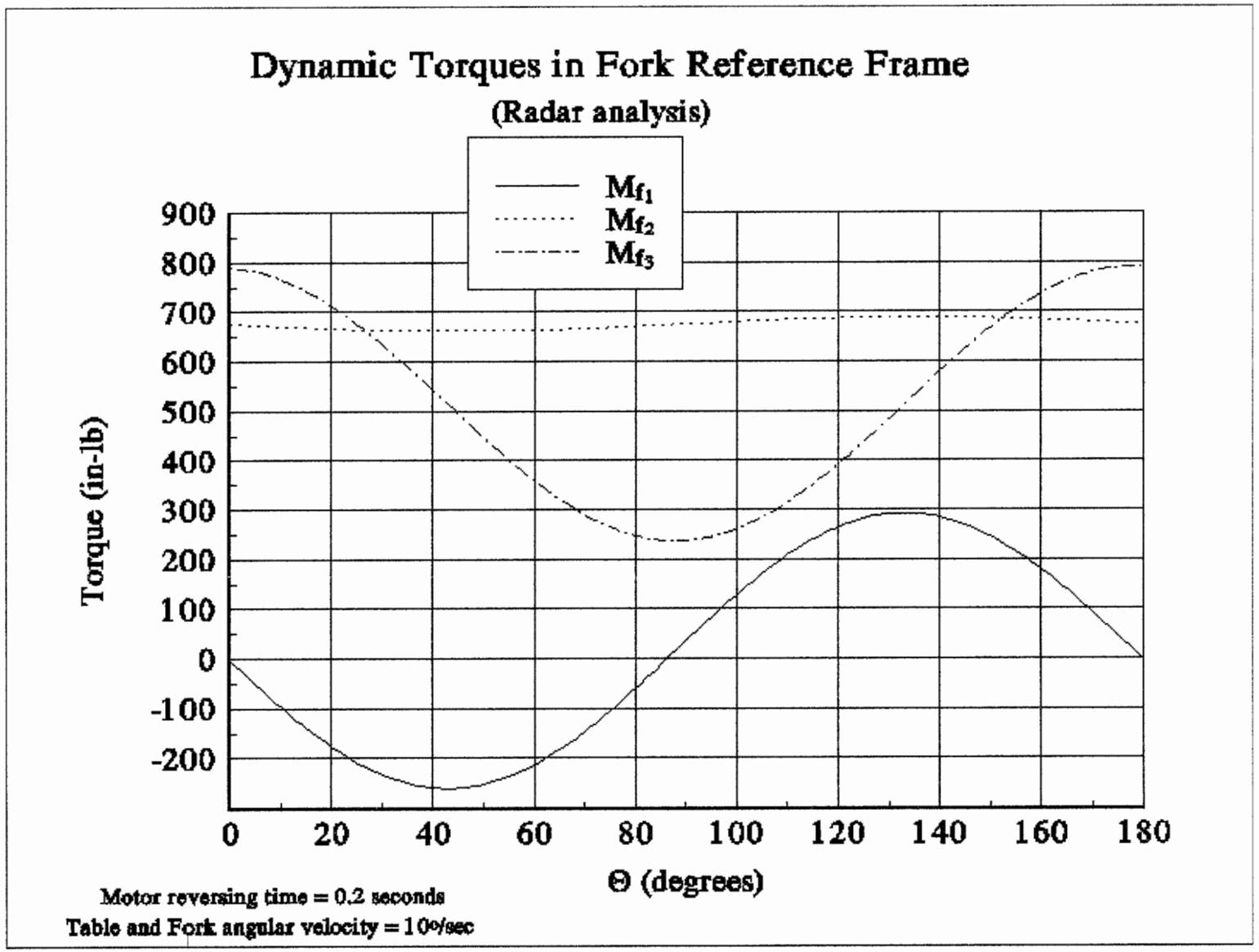

Figure B2: Torque in Fork Reference Frame for Radar Analysis

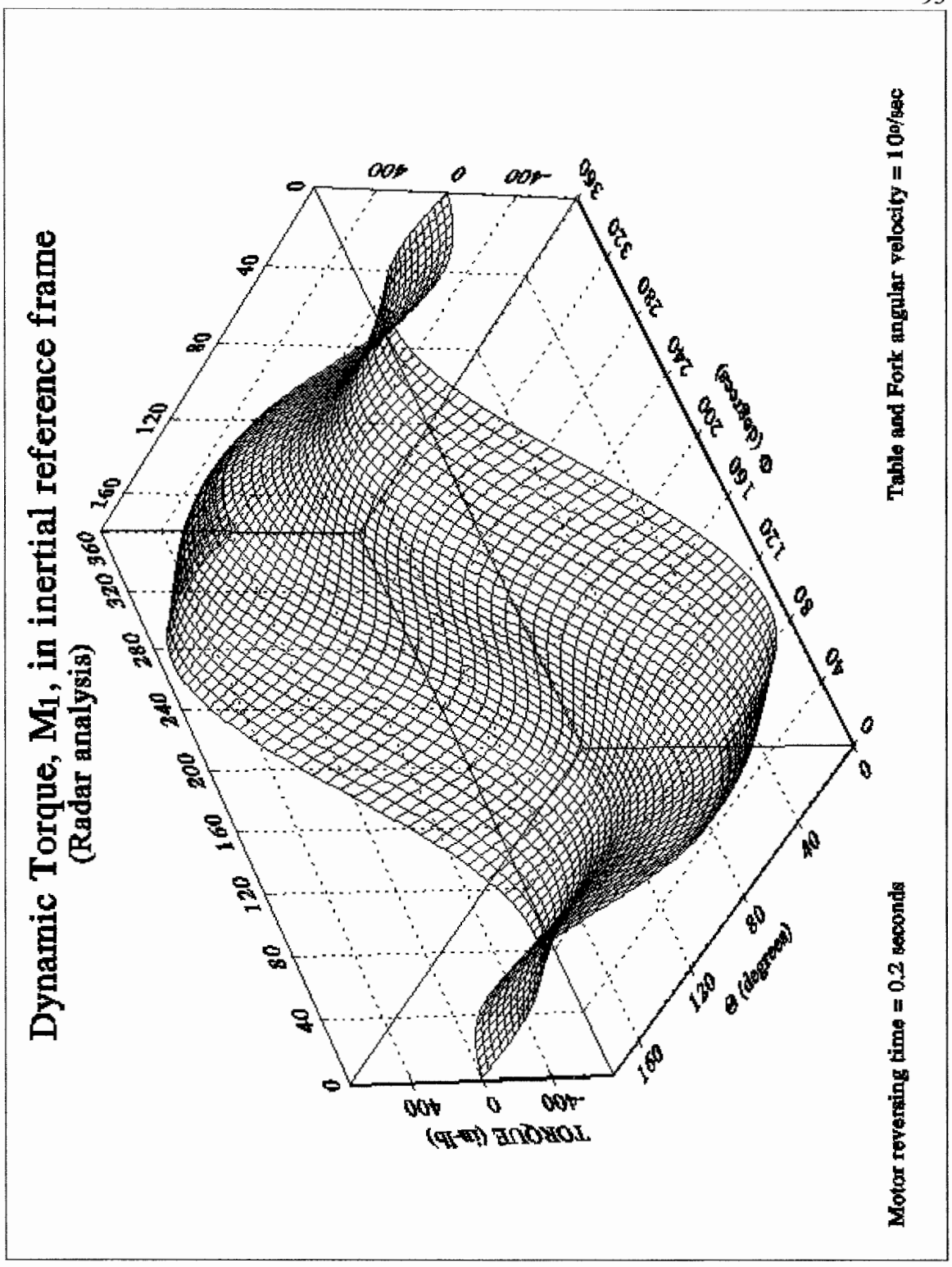

Figure B3: Torque, M_1, in Inertial Reference Frame for Radar Analysis

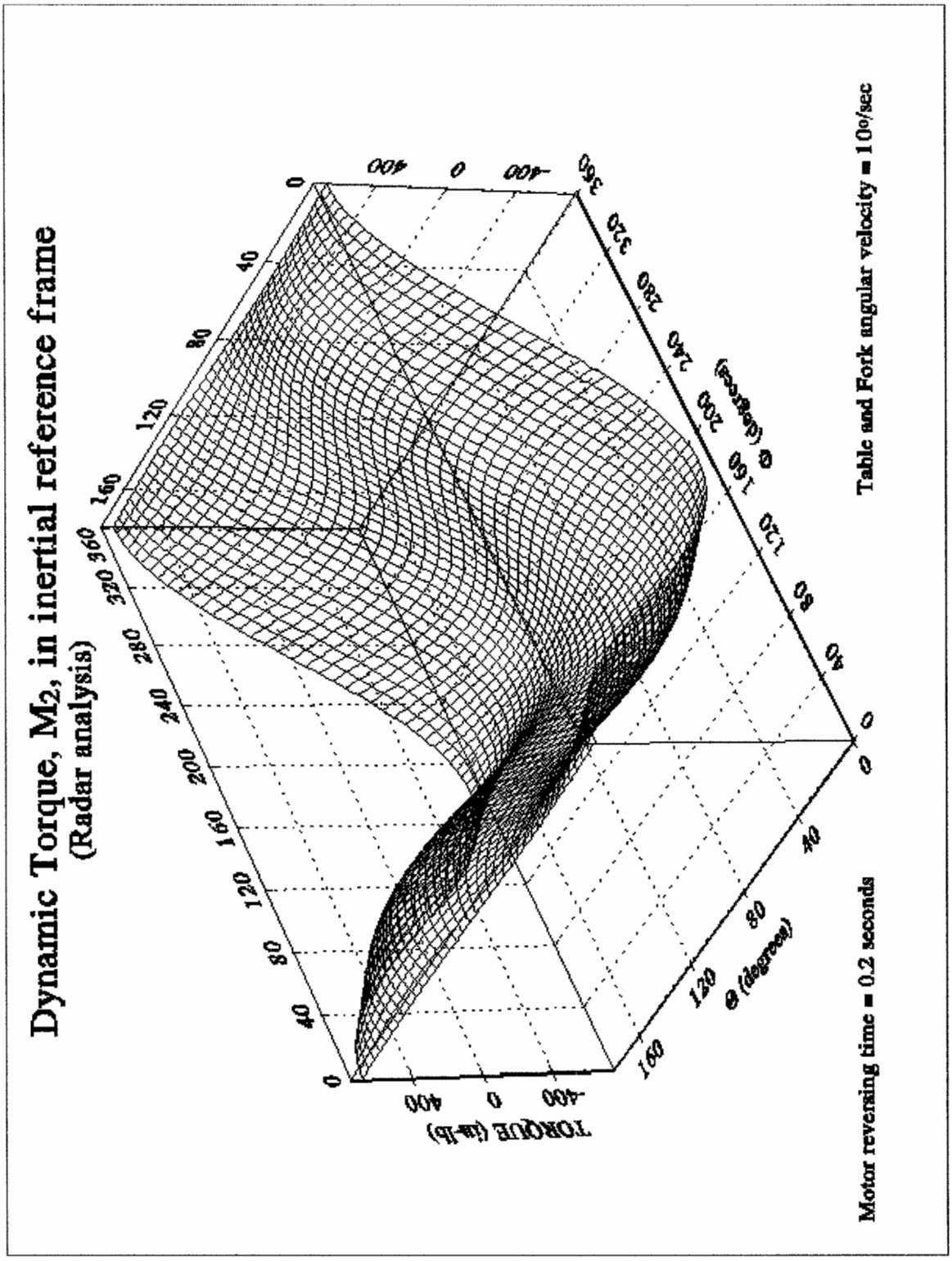

Figure B4: Torque, M_2, in Inertial Refeerence Frame for Radar Analysis

Momentt.for FORTRAN program to analyze the table component rotation

```
* MOMENTT.FOR
*
* CALCULATES THE MOMENTS FOR DUAL AXIS ROTATIONS OF THE
* TABLE COMPONENT IN TABLE, FORK, AND INERTIAL COORDINATES
* IT ALSO CALCULATES THE MAXIMUM TORQUES FOR THE TABLE
* AND INERTIAL COORDINATE SYSTEM
* AS WELL AS THEIR VARIATION WITH POSITION
* A FILE CONTAINING THE INERTIA OF THE TABLE, FORK, GEARBOXES,
AND MOTORS
* MUST EXIST (LIDAR.DAT & RADAR.DAT) IN ORDER
* FOR THE PROGRAM TO RUN

      IMPLICIT DOUBLE PRECISION(A-Z)
      INTEGER DEC,I,J,END
      DIMENSION IT(3,3),IF(3,3)
      DIMENSION ITS(3,3),ITT(3,3)
      CHARACTER*10 OUTF
      CHARACTER*11 IN,OUTT
      CHARACTER*12 OUTRES
      DEGRAD(X) = X*3.14159265359/180.000
      RADDEG(X) = X*180.000/3.14159265359

* ASK FOR THE SYSTEM THAT YOU WISH TO ANALYZE
      WRITE(*,*)'WHAT SYSTEM DO YOU WISH TO STUDY? (RADAR OR LIDAR)'
      READ(*,*) IN(1:5)
      IN(6:10)='.DAT'

* DEFINE THE INCREMENT TO ITERATE THE ANGLES OVER
      WRITE(*,*)'WHAT IS THE INCREMENT? (IN DEGREES)'
      READ(*,*) T
      END=180./T

* DEFINE A TEST POINT FOR FINDING THE MAXIMUM VALUES
      TF1MAX=0.0000000
      TF2MAX=0.0000000
      TF3MAX=0.0000000
      T1MAX=0.0000000
      T2MAX=0.0000000
      T3MAX=0.0000000

      OUTT(1:1)=IN(1:1)
      OUTF(1:1)=IN(1:1)
      OUTRES(1:1)=IN(1:1)
```

```
      OUTT(2:11)='TTABLE.DAT'
      OUTF(2:10)='TFORK.DAT'
      OUTRES(2:12)='TRESULT.DAT'
      OPEN(UNIT=12,FILE=IN,STATUS='OLD')
      OPEN(UNIT=13,FILE=OUTT,STATUS='UNKNOWN')
      OPEN(UNIT=14,FILE=OUTF,STATUS='UNKNOWN')
      OPEN(UNIT=16,FILE=OUTRES,STATUS='UNKNOWN')

* DEFINE THE INERTIA OF THE MASS TO BE MOVED

* READ IN TABLE INERTIAS IN ITS COORDINATE SYSTEM
      READ(12,*) IT(1,1),IT(1,2),IT(1,3)
      READ(12,*) IT(2,1),IT(2,2),IT(2,3)
      READ(12,*) IT(3,1),IT(3,2),IT(3,3)

* READ IN THE FORK INERTIAS IN ITS COORDINATE SYSTEM
      READ(12,*) IF(1,1),IF(1,2),IF(1,3)
      READ(12,*) IF(2,1),IF(2,2),IF(2,3)
      READ(12,*) IF(3,1),IF(3,2),IF(3,3)

* TIME FOR REVERSING OF MOTORS, THE GEAR RATIO, AND ANALYSIS
SELECTION

      WRITE(*,*)'PLEASE ENTER THE MOTOR REVERSING TIME'
      READ(*,*) REVTIM
      WRITE(*,*)'TABLE REVERSAL ENTER 1,FORK REVERSAL ENTER 2,
     * OR BOTH ENTER 3'
      READ(*,*) DEC

* DEFINE INITIAL ANGLES

      THETA=0.00000000000

* SCALE INERTIA OF TABLE FOR GEAR RATIO AND STORE THE ORIGINAL
INERTIA
* IN A STORAGE MATRIX

      DO 10 I=1,3
        DO 20 J=1,3
          ITS(I,J)=IT(I,J)
 20     CONTINUE
 10   CONTINUE
```

```
* DEFINE UNCHANGED TRANSFORMED INERTIA MATRIX OF TABLE IN
FORK COORDINATES

      ITT(1,2)=ITS(1,2)
      ITT(2,1)=ITS(2,1)
      ITT(2,2)=ITS(2,2)
      ITT(2,3)=ITS(2,3)
      ITT(3,2)=ITS(3,2)

* THETA IS THE ANGLE OF THE NORMAL OF THE TABLE FROM ZENITH
* (THE INERTIAL Z AXIS) OR IT CAN BE DESCRIBED AS THE ELEVATION
COORDINATE

      IF(DEC.EQ.2)THEN
        THDOT=0.00000000000
        THDOTT=0.00000000000
      ELSE
        WRITE(*,*) 'PLEASE ENTER THE ELEVATION ANGULAR VELOCITY'
        READ(*,*) THDOT
        THETA=DEGRAD(THETA)
        THDOT=DEGRAD(THDOT)
        THDOTT=ABS(2*THDOT/REVTIM)
      ENDIF

      IF(DEC.EQ.1)THEN
        PHIDOT=0.00000000000
        PHDOTT=0.00000000000
      ELSE
        WRITE(*,*) 'PLEASE ENTER THE AZIMUTH ANGULAR VELOCITY'
        READ(*,*) PHIDOT
        PHIDOT=DEGRAD(PHIDOT)
        PHDOTT=ABS(2.*PHIDOT/REVTIM)
      ENDIF

* ITERATE THROUGH DIFFERENT VALUES OF THETA AND PHI TO GET
MOMENT PROFILE

      DO 30 I=1,END+1

* DEFINE INTERMEDIATE VALUES FOR CALCULATIONS

        A=-PHDOTT*SIN(THETA)+PHIDOT*THDOT*COS(THETA)
        B=PHDOTT*COS(THETA)-PHIDOT*THDOT*SIN(THETA)
        C=IT(3,1)*PHIDOT*SIN(THETA)+IT(3,2)*THDOT+
```

```
     *    IT(3,3)*PHIDOT*COS(THETA)
          D=IT(2,1)*PHIDOT*SIN(THETA)-IT(2,2)*THDOT-
     *    IT(2,3)*PHIDOT*COS(THETA)
          E=-IT(1,1)*PHIDOT*SIN(THETA)+IT(1,2)*THDOT-
     *    IT(1,3)*PHIDOT*COS(THETA)

* DEFINE THE MOMENTS INDIVIDUALLY IN THE TABLE COORDINATE
SYSTEM

          MT1=-IT(1,1)*A+IT(1,2)*THDOTT-IT(1,3)*B-
     *    THDOT*C-PHIDOT*COS(THETA)*D
          MT2=IT(2,1)*A-IT(2,2)*THDOTT-IT(2,3)*B+
     *    PHIDOT*SIN(THETA)*C+PHIDOT*COS(THETA)*E
          MT3=IT(3,1)*A+IT(3,2)*THDOTT+IT(3,3)*B-
     *    PHIDOT*SIN(THETA)*D+THDOT*E

* CONVERT MOMENTS TO IN-LB

          MT1=MT1/386.2
          MT2=MT2/386.2
          MT3=MT3/386.2

* DEFINE THE MOMENTS IN THE FORK COORDINATE SYSTEM

          MF3=COS(THETA)*MT3+SIN(THETA)*MT1
          MF2=-MT2
          MF1=-COS(THETA)*MT1+SIN(THETA)*MT3

* DETERMINE THE MAXIMUM TORQUE AND ITS CORRESPONDING ANGLE
AND MOTOR
* LOCATION FOR THE TABLE IN THE TABLE REFERENCE FRAME

          IF(ABS(MT1).GT.T1MAX)THEN
            T1MAX=ABS(MT1)
            TH1MX=RADDEG(THETA)
          ENDIF
          IF(ABS(MT2).GT.T2MAX)THEN
            T2MAX=ABS(MT2)
            TH2MX=RADDEG(THETA)
          ENDIF
          IF(ABS(MT3).GT.T3MAX)THEN
            T3MAX=ABS(MT3)
            TH3MX=RADDEG(THETA)
          ENDIF
```

```
* DETERMINE THE MAXIMUM TORQUE AND ITS CORRESPONDING ANGLE
AND MOTOR
* LOCATION FOR THE TABLE IN THE FORK REFERENCE FRAME

      IF(ABS(MF1).GT.TF1MAX)THEN
        TF1MAX=ABS(MF1)
        THF1MX=RADDEG(THETA)
      ENDIF
      IF(ABS(MF2).GT.TF2MAX)THEN
        TF2MAX=ABS(MF2)
        THF2MX=RADDEG(THETA)
      ENDIF
      IF(ABS(MF3).GT.TF3MAX)THEN
        TF3MAX=ABS(MF3)
        THF3MX=RADDEG(THETA)
      ENDIF


       WRITE(13,7)RADDEG(ABS(THETA)),MT1,MT2,MT3
       WRITE(14,7)RADDEG(ABS(THETA)),MF1,MF2,MF3

      THETA=THETA+DEGRAD(T)

 30   CONTINUE

     WRITE(16,*)'THE SYSTEM BEING ANALYZED IS THE: ',IN(1:6)

     WRITE(*,*)'THE MAXIMUM MT1 IS:', T1MAX
     WRITE(*,*)'IT OCCURS AT THETA=',TH1MX
     WRITE(16,*)'THE MAXIMUM MT1 IS:',T1MAX
     WRITE(16,*)'IT OCCURS AT THETA=',TH1MX
     WRITE(*,*)'THE MAXIMUM MT2 IS:', T2MAX
     WRITE(*,*)'IT OCCURS AT THETA=',TH2MX
     WRITE(16,*)'THE MAXIMUM MT2 IS:',T2MAX
     WRITE(16,*)'IT OCCURS AT THETA=',TH2MX
     WRITE(*,*)'THE MAXIMUM MT3 IS:', T3MAX
     WRITE(*,*)'IT OCCURS AT THETA=',TH3MX
     WRITE(16,*)'THE MAXIMUM MT3 IS:',T3MAX
     WRITE(16,*)'IT OCCURS AT THETA=',TH3MX

     WRITE(*,*)'THE MAXIMUM MF1 IS:', TF1MAX
     WRITE(*,*)'IT OCCURS AT THETA=',THF1MX
```

```
      WRITE(16,*)'THE MAXIMUM MF1 IS:',TF1MAX
      WRITE(16,*)'IT OCCURS AT THETA=',THF1MX
      WRITE(*,*)'THE MAXIMUM MF2 IS:', TF2MAX
      WRITE(*,*)'IT OCCURS AT THETA=',THF2MX
      WRITE(16,*)'THE MAXIMUM MF2 IS:',TF2MAX
      WRITE(16,*)'IT OCCURS AT THETA=',THF2MX
      WRITE(*,*)'THE MAXIMUM MF3 IS:', TF3MAX
      WRITE(*,*)'IT OCCURS AT THETA=',THF3MX
      WRITE(16,*)'THE MAXIMUM MF3 IS:',TF3MAX
      WRITE(16,*)'IT OCCURS AT THETA=',THF3MX

      WRITE(16,*)'THE MOTOR REVERSING TIME IS:',REVTIM
      WRITE(16,*)'THE ELEVATION ANGULAR VELOCITY IS DEG/SEC:',
     * RADDEG(THDOT)
      WRITE(16,*)'THE AZIMUTH ANGULAR VELOCITY IS DEG/SEC:',
     * RADDEG(PHIDOT)
      WRITE(*,*)'THE ELEVATION ANGULAR ACCELERATION IS (DEG/SEC^2):',
     * RADDEG(THDOTT)
      WRITE(16,*)'THE ELEVATION ANGULAR ACCELERATION IS
(DEG/SEC^2):',
     *  RADDEG(THDOTT)
      WRITE(*,*)'THE AZIMUTH ANGULAR ACCELERATION IS (DEG/SEC^2):',
     *  RADDEG(PHDOTT)
      WRITE(16,*)'THE AZIMUTH ANGULAR ACCELERATION IS (DEG/SEC^2):',
     *  RADDEG(PHDOTT)
 7    FORMAT(F5.1,1X,F9.1,1X,F9.1,1X,F9.1)
 8    FORMAT(F5.1,1X,F5.1,1X,F9.1,1X,F9.1,1X,F9.1)
      END
```

Momentf.for FORTRAN program to analyze the fork component rotation

```
* MOMENTF.FOR
*
* CALCULATES THE MOMENTS FOR DUAL AXIS ROTATIONS OF THE
* FORK DESIGN IN FORK, AND INERTIAL COORDINATES
* IT ALSO CALCULATES THE MAXIMUM TORQUES FOR THE FORK
* AND INERTIAL COORDINATE SYSTEM
* AS WELL AS THEIR VARIATION WITH POSITION
* A FILE CONTAINING THE INERTIA OF THE TABLE, FORK, GEARBOXES,
AND MOTORS
* MUST EXIST (LIDAR.DAT & RADAR.DAT) IN ORDER

      IMPLICIT DOUBLE PRECISION(A-Z)
      INTEGER DEC,I,J,END
      DIMENSION IT(3,3),IF(3,3)
      DIMENSION ITS(3,3),ITT(3,3)
      CHARACTER*10 OUTF
      CHARACTER*11 IN
      CHARACTER*12 OUT,OUTRES
      DEGRAD(X) = X*3.14159265359/180.000
      RADDEG(X) = X*180.000/3.14159265359

* ASK FOR THE SYSTEM THAT YOU WISH TO ANALYZE
      WRITE(*,*)'WHAT SYSTEM DO YOU WISH TO STUDY? (RADAR OR LIDAR)'
      READ(*,*) IN(1:5)
      IN(6:10)='.DAT'

* DEFINE THE INCREMENT TO ITERATE THE ANGLES OVER
      WRITE(*,*)'WHAT IS THE INCREMENT? (IN DEGREES)'
      READ(*,*) T
      END=180./T

* DEFINE A TEST POINT FOR FINDING THE MAXIMUM VALUES
      TF1MAX=0.0000000
      TF2MAX=0.0000000
      TF3MAX=0.0000000
      T1MAX=0.0000000
      T2MAX=0.0000000
      T3MAX=0.0000000

      OUTF(1:1)=IN(1:1)
      OUT(1:1)=IN(1:1)
      OUTRES(1:1)=IN(1:1)
      OUTF(2:10)='FFORK.DAT'
```

```
      OUT(2:12)='FNEWTON.DAT'
      OUTRES(2:12)='FRESULT.DAT'
      OPEN(UNIT=12,FILE=IN,STATUS='OLD')
      OPEN(UNIT=14,FILE=OUTF,STATUS='UNKNOWN')
      OPEN(UNIT=15,FILE=OUT,STATUS='UNKNOWN')
      OPEN(UNIT=16,FILE=OUTRES,STATUS='UNKNOWN')

* DEFINE THE INERTIA OF THE MASS TO BE MOVED

* READ IN TABLE INERTIAS IN ITS COORDINATE SYSTEM
      READ(12,*) IT(1,1),IT(1,2),IT(1,3)
      READ(12,*) IT(2,1),IT(2,2),IT(2,3)
      READ(12,*) IT(3,1),IT(3,2),IT(3,3)

* READ IN THE FORK INERTIAS IN ITS COORDINATE SYSTEM
      READ(12,*) IF(1,1),IF(1,2),IF(1,3)
      READ(12,*) IF(2,1),IF(2,2),IF(2,3)
      READ(12,*) IF(3,1),IF(3,2),IF(3,3)

* TIME FOR REVERSING OF MOTORS, THE GEAR RATIO, AND ANALYSIS
SELECTION

      WRITE(*,*)'PLEASE ENTER THE MOTOR REVERSING TIME'
      READ(*,*) REVTIM
      WRITE(*,*)'TABLE REVERSAL ENTER 1,FORK REVERSAL ENTER 2,
     * OR BOTH ENTER 3'
      READ(*,*) DEC

* DEFINE INITIAL ANGLES

      THETA=0.00000000000
      PHI=0.0000000000

* SCALE INERTIA OF TABLE FOR GEAR RATIO AND STORE THE ORIGINAL
INERTIA
* IN A STORAGE MATRIX

      DO 10 I=1,3
        DO 20 J=1,3
          ITS(I,J)=IT(I,J)
 20     CONTINUE
 10   CONTINUE
```

```
* DEFINE UNCHANGED TRANSFORMED INERTIA MATRIX OF TABLE IN
FORK COORDINATES

      ITT(1,2)=ITS(1,2)
      ITT(2,1)=ITS(2,1)
      ITT(2,2)=ITS(2,2)
      ITT(2,3)=ITS(2,3)
      ITT(3,2)=ITS(3,2)

* THETA IS THE ANGLE OF THE NORMAL OF THE TABLE FROM ZENITH
* (THE INERTIAL Z AXIS) OR IT CAN BE DESCRIBED AS THE ELEVATION
COORDINATE

      IF(DEC.EQ.2)THEN
        THDOT=0.00000000000
        THDOTT=0.00000000000
      ELSE
        WRITE(*,*) 'PLEASE ENTER THE ELEVATION ANGULAR VELOCITY'
        READ(*,*) THDOT
        THETA=DEGRAD(THETA)
        THDOT=DEGRAD(THDOT)
        THDOTT=ABS(2*THDOT/REVTIM)
      ENDIF

* PHI IS THE ANGLE BETWEEN THE INERTIAL Y AXIS AND THE CURRENT
* TABLE MOUNT LOCATION OR IT CAN BE DESCRIBED AS THE AZIMUTH
COORDINATE

      IF(DEC.EQ.1)THEN
        PHIDOT=0.00000000000
        PHDOTT=0.00000000000
      ELSE
        WRITE(*,*) 'PLEASE ENTER THE AZIMUTH ANGULAR VELOCITY'
        READ(*,*) PHIDOT
        PHI=DEGRAD(PHI)
        PHIDOT=DEGRAD(PHIDOT)
        PHDOTT=ABS(2.*PHIDOT/REVTIM)
      ENDIF

* ITERATE THROUGH DIFFERENT VALUES OF THETA AND PHI TO GET
MOMENT PROFILE

      DO 30 I=1,END+1
```

```
* DEFINE INTERMEDIATE VALUES FOR CALCULATIONS

      A=-IT(1,1)*PHIDOT*SIN(THETA)-THDOT*IT(1,2)-
     *   PHIDOT*COS(THETA)*IT(1,3)
      B=IT(1,3)*PHIDOT*SIN(THETA)-THDOT*IT(2,3)+
     *   PHIDOT*COS(THETA)*IT(3,3)
      C=IT(1,3)*(PHDOTT*SIN(THETA)+PHIDOT*THDOT*COS(THETA))+
     *   IT(2,3)*THDOTT+
     *   IT(3,3)*(PHDOTT*COS(THETA)-PHIDOT*THDOT*SIN(THETA))
      D=-IT(1,1)*(PHDOTT*SIN(THETA)+PHIDOT*THDOT*COS(THETA))+
     *   IT(1,2)*THDOTT-
     *   IT(1,3)*(PHDOTT*COS(THETA)-PHIDOT*THDOT*SIN(THETA))
      E=-IT(1,2)*(PHDOTT*SIN(THETA)+PHIDOT*THDOT*COS(THETA))+
     *   IT(2,2)*THDOTT+
     *   IT(2,3)*(PHDOTT*COS(THETA)-PHIDOT*THDOT*SIN(THETA))
      F=-2*IT(1,2)*PHIDOT*THDOT*COS(THETA)-
     *   IT(2,3)*PHIDOT*THDOT*SIN(THETA)-
     *   IT(1,3)*PHIDOT*THDOT*SIN(THETA)

* DEFINE THE MOMENTS INDIVIDUALLY IN THE TABLE COORDINATE
SYSTEM

      MF1=-THDOT*SIN(THETA)*A+THDOT*COS(THETA)*B-
     *   IF(1,3)*PHDOTT-COS(THETA)*D+SIN(THETA)*C
      MF2=E-IF(2,3)*PHDOTT+F
      MF3=THDOT*COS(THETA)*A-THDOT*SIN(THETA)*B+IF(3,3)*PHDOTT+
     *   SIN(THETA)*D+COS(THETA)*C

* CONVERT MOMENTS TO IN-LB

      MF1=MF1/386.2
      MF2=MF2/386.2
      MF3=MF3/386.2


* DEFINE MOMENTS IN INERTIAL COORDINATES
* ITERATE OVER PHI

      PHI=0.00000
      DO 40 J=1,2*END+1

        M1=COS(PHI)*MF1-SIN(PHI)*MF2
        M2=SIN(PHI)*MF1+COS(PHI)*MF2
        M3=MF3
```

```
      PHI=DEGRAD(T)+PHI
      WRITE(15,8)RADDEG(ABS(THETA)),RADDEG(ABS(PHI)),M1,M2,M3

* DETERMINE THE MAXIMUM TORQUE AND ITS CORRESPONDING ANGLE
AND MOTOR
* LOCATION FOR THE INERTIAL SYSTEM

      IF(ABS(M1).GT.T1MAX)THEN
        T1MAX=ABS(M1)
        TH1MX=RADDEG(THETA)
        PH1MX=RADDEG(PHI)
      ENDIF
      IF(ABS(M2).GT.T2MAX)THEN
        T2MAX=ABS(M2)
        TH2MX=RADDEG(THETA)
        PH2MX=RADDEG(PHI)
      ENDIF
      IF(ABS(M3).GT.T3MAX)THEN
        T3MAX=ABS(M3)
        TH3MX=RADDEG(THETA)
        PH3MX=RADDEG(PHI)
      ENDIF

 40   CONTINUE

* DETERMINE THE MAXIMUM TORQUE AND ITS CORRESPONDING ANGLE
AND MOTOR
* LOCATION FOR THE FORK SYSTEM

      IF(ABS(MF1).GT.TF1MAX)THEN
        TF1MAX=ABS(MF1)
        THF1MX=RADDEG(THETA)
      ENDIF
      IF(ABS(MF2).GT.TF2MAX)THEN
        TF2MAX=ABS(MF2)
        THF2MX=RADDEG(THETA)
      ENDIF
      IF(ABS(MF3).GT.TF3MAX)THEN
        TF3MAX=ABS(MF3)
        THF3MX=RADDEG(THETA)
      ENDIF

      WRITE(14,7)RADDEG(ABS(THETA)),MF1,MF2,MF3
```

```
      THETA=THETA+DEGRAD(T)

30    CONTINUE

      WRITE(16,*)'THE SYSTEM BEING ANALYZED IS THE: ',IN(1:6)

      WRITE(*,*)'THE MAXIMUM M1 IS:', T1MAX
      WRITE(*,*)'IT OCCURS AT THETA=',TH1MX
      WRITE(*,*)'AND A PHI=',PH1MX
      WRITE(16,*)'THE MAXIMUM M1 IS:',TF1MAX
      WRITE(16,*)'IT OCCURS AT THETA=',TH1MX
      WRITE(16,*)'AND A PHI=',PH1MX
      WRITE(*,*)'THE MAXIMUM M2 IS:', T2MAX
      WRITE(*,*)'IT OCCURS AT THETA=',TH2MX
      WRITE(*,*)'AND A PHI=',PH2MX
      WRITE(16,*)'THE MAXIMUM M2 IS:',T2MAX
      WRITE(16,*)'IT OCCURS AT THETA=',TH2MX
      WRITE(16,*)'AND A PHI=',PH2MX
      WRITE(*,*)'THE MAXIMUM M3 IS:', T3MAX
      WRITE(*,*)'IT OCCURS AT THETA=',TH3MX
      WRITE(*,*)'AND A PHI=',PH3MX
      WRITE(16,*)'THE MAXIMUM M3 IS:',T3MAX
      WRITE(16,*)'IT OCCURS AT THETA=',TH3MX
      WRITE(16,*)'AND A PHI=',PH3MX

      WRITE(*,*)'THE MAXIMUM MF1 IS:', TF1MAX
      WRITE(*,*)'IT OCCURS AT THETA=',THF1MX
      WRITE(16,*)'THE MAXIMUM MF1 IS:',TF1MAX
      WRITE(16,*)'IT OCCURS AT THETA=',THF1MX
      WRITE(*,*)'THE MAXIMUM MF2 IS:', TF2MAX
      WRITE(*,*)'IT OCCURS AT THETA=',THF2MX
      WRITE(16,*)'THE MAXIMUM MF2 IS:',TF2MAX
      WRITE(16,*)'IT OCCURS AT THETA=',THF2MX
      WRITE(*,*)'THE MAXIMUM MF3 IS:', TF3MAX
      WRITE(*,*)'IT OCCURS AT THETA=',THF3MX
      WRITE(16,*)'THE MAXIMUM MF3 IS:',TF3MAX
      WRITE(16,*)'IT OCCURS AT THETA=',THF3MX

      WRITE(16,*)'THE MOTOR REVERSING TIME IS:',REVTIM
      WRITE(16,*)'THE ELEVATION ANGULAR VELOCITY IS DEG/SEC:',
     *  RADDEG(THDOT)
      WRITE(16,*)'THE AZIMUTH ANGULAR VELOCITY IS DEG/SEC:',
     *  RADDEG(PHIDOT)
      WRITE(*,*)'THE ELEVATION ANGULAR ACCELERATION IS (DEG/SEC^2):',
```

```
    * RADDEG(THDOTT)
      WRITE(16,*)'THE ELEVATION ANGULAR ACCELERATION IS
(DEG/SEC^2):',
    *  RADDEG(THDOTT)
      WRITE(*,*)'THE AZIMUTH ANGULAR ACCELERATION IS (DEG/SEC^2):',
    *  RADDEG(PHDOTT)
      WRITE(16,*)'THE AZIMUTH ANGULAR ACCELERATION IS (DEG/SEC^2):',
    *  RADDEG(PHDOTT)
 7   FORMAT(F5.1,1X,F9.1,1X,F9.1,1X,F9.1)
 8   FORMAT(F5.1,1X,F5.1,1X,F9.1,1X,F9.1,1X,F9.1)
     END
```

Input files for the different components

LIDAR.dat

```
20978.713 0 33127.949
0 85986.258 0
33127.949 0 95490.587
71612615.261 0 0
0 40129.533 63655.875
0 63655.875 77577.803
```

RADAR.dat

```
25072.133 0 0
0 85792.133 0
0 0 97093.333
71612615.261 0 0
0 40129.533 63655.875
0 63655.875 77577.803
```

Output file from Momentt.for

LTRESULT.dat

```
THE SYSTEM BEING ANALYZED IS THE: LIDAR.
THE MAXIMUM MT1 IS:     72.924440567904000
IT OCCURS AT THETA=    149.000000000000000
THE MAXIMUM MT2 IS:    159.369125422349000
IT OCCURS AT THETA=    156.000000000000000
THE MAXIMUM MT3 IS:    183.511993331470000
IT OCCURS AT THETA=    160.000000000000000
```

THE MAXIMUM MF1 IS: 91.728710355710200
IT OCCURS AT THETA= 24.000000000000000
THE MAXIMUM MF2 IS: 159.369125422349000
IT OCCURS AT THETA= 156.000000000000000
THE MAXIMUM MF3 IS: 196.999179113017000
IT OCCURS AT THETA= 159.000000000000000
THE MOTOR REVERSING TIME IS: 0.500000000000000
THE ELEVATION ANGULAR VELOCITY IS DEG/SEC: 10.000000000000000
THE AZIMUTH ANGULAR VELOCITY IS DEG/SEC: 10.000000000000000
THE ELEVATION ANGULAR ACCELERATION IS (DEG/SEC^2):
40.000000000000000
THE AZIMUTH ANGULAR ACCELERATION IS (DEG/SEC^2):
40.000000000000000

Output file from Momentf.for

RFRESULT.dat
THE SYSTEM BEING ANALYZED IS THE: RADAR.
THE MAXIMUM M1 IS: 112.396511788794000
IT OCCURS AT THETA= 45.000000000000000
AND A PHI= 345.000000000000000
THE MAXIMUM M2 IS: 119.304312899944000
IT OCCURS AT THETA= 45.000000000000000
AND A PHI= 255.000000000000000
THE MAXIMUM M3 IS: 315.752089059923000
IT OCCURS AT THETA= 0.000000000000000
AND A PHI= 5.000000000000000
THE MAXIMUM MF1 IS: 112.396511788794000
IT OCCURS AT THETA= 45.000000000000000
THE MAXIMUM MF2 IS: 40.015596552079600
IT OCCURS AT THETA= 0.000000000000000
THE MAXIMUM MF3 IS: 315.752089059923000
IT OCCURS AT THETA= 0.000000000000000
THE MOTOR REVERSING TIME IS: 0.500000000000000
THE ELEVATION ANGULAR VELOCITY IS DEG/SEC: 10.000000000000000
THE AZIMUTH ANGULAR VELOCITY IS DEG/SEC: 10.000000000000000
THE ELEVATION ANGULAR ACCELERATION IS (DEG/SEC^2):
40.000000000000000
THE AZIMUTH ANGULAR ACCELERATION IS (DEG/SEC^2):
40.000000000000000

Appendix C

ANSYS FINITE ELEMENT ANALYSIS OF THE FORK COMPONENT

This appendix contains the batch file for input to ANSYS to complete a deflection, rotation, and reaction force analysis of the fork component and the output. Several assumptions that were used in the analysis are: the shaft that is rotating the table is assumed to go all the way across the fork component; the loads in the fork coordinates that were calculated in the dual axis rotation analysis, are considered the largest expected loads; the English units (pounds and inches) that are used throughout the thesis were converted to SI units (kilograms and meters) for easy calculation of the masses and gravity; and the fork shaft is cantilevered at the base to apply a boundary condition. The reaction forces, deflections, and rotations at the support points for the table are output and are considered the critical output from this analysis.

ANSYS batch file (fork.in)

```
/prep7
/title,VSM analysis
et,1,4          * 3-D elastic beam for frame
et,2,4          * 3-D elastic beam for shaft
et,3,4          * 3-D elastic beam for base
et,4,21         * point mass for motor
r,1,3.7097E-3,13.21317989E-6,13.21317989E-6,0.1524,0.1524
              * define properties of element 1
keyopt,1,6,1
mp,ex,1,69.6385E9      * young's modulus
mp,dens,1,2768         * density
mp,gxy,1,25.5115E9     * shear modulus
r,2,4.56066E-3,1.6549E-6,1.6549E-6,0.0381,0.0381
                    * define properties of element 2
keyopt,2,6,1
mp,ex,2,69.6385E9      * young's modulus
mp,dens,2,2768         * density
mp,gxy,2,25.5115E9     * shear modulus
r,3,50.6707479E-3,204.317123E-6,204.317123E-6,0.2540,0.2540
                    * define properties of element 3
keyopt,3,6,1
mp,ex,3,69.6385E9      * young's modulus
mp,dens,3,2768         * density
mp,gxy,3,25.5115E9     * shear modulus
r,4,0.954947           * define properties of element 4
                    * mass
keyopt,4,3,2
n,1,-0.625475,1.651,0  * define position of nodes
n,51,-0.625475,0.381,0
fill,1,51
n,76,0,0.381,0
fill,51,76
n,101,0.625475,0.381,0
fill,76,101
n,151,0.625475,1.651,0
fill,101,151
n,152,0,0.3556,0
n,175,0,0,0
fill,152,175
type,1                 * select element 1
mat,1
real,1
e,1,2                  * place elements
```

```
egen,50,1,1,1
e,51,52
egen,50,1,51,51
e,101,102
egen,50,1,101,101
type,2              * select element 2
mat,2
real,2
e,1,151              * place element
type,3              * select element 3
mat,3
real,3
e,76,152             * place elements
e,152,153
e,153,154
e,154,155
e,155,156
e,156,157
e,157,158
e,158,159
e,159,160
e,160,161
e,161,162
e,162,163
e,163,164
e,164,165
e,165,166
e,166,167
e,167,168
e,168,169
e,169,170
e,170,171
e,171,172
e,172,173
e,173,174
e,174,175
type,4              * select element 4
real,4
e,133               * place elements
e,134
e,135
e,136
e,137
e,138
```

```
e,139
e,140
e,141
e,142
e,143
e,144
e,145
e,146
e,147
e,148
e,149
e,150
e,151
save
nsel,node,175,175
d,all,all              *clamp the rotation of the frame
nall
f,1,fz,102.304         * horizontal load at node 1
f,1,fy,-782.848        * vertical load at node 1
f,1,mz,-836.046        * torque due to table at node 1
f,151,fz,-102.304      * horizontal load at node 154
f,151,fy,-862.912      * vertical load at node 154
f,151,mz,836.046       * torque due to table at node 154
f,151,mx,131.733       * reaction torque at node 154
acel,0,9.81,0          * apply gravity field
lwrite
afwrite
finish
/input,27              *solve problem
finish
/post1
/output,fork,out
set,1
prrfor                 *print reaction forces at base
nsel,node,1,1          *print displacement of left support
prdisp
nsel,node,all,all
nsel,node,151,151      *print displacement of left support
prdisp
finish
/eof
```

ANSYS output file

```
USE LOAD STEP    1  ITERATION    0  SECTION   1  FOR LOAD CASE    1


GEOMETRY STORED FOR   175  NODES   194  ELEMENTS
 TITLE= VSM analysis

DISPLACEMENT STORED FOR  175 NODES

ITERATION SUMMARY INFORMATION STORED

NODAL FORCES STORED FOR  194 ELEMENTS

REACTIONS STORED FOR   6 REACTIONS

FOR LOAD STEP=    1  ITERATION=    1  SECTION=   1
 TIME=  0.000000E+00   LOAD CASE=  1
 TITLE= VSM analysis

 PRINT REACTION FORCES PER NODE
1          ANSYS - ENGINEERING ANALYSIS SYSTEM  REVISION 4.4      A 16   PENN STATE
MAY 1,1990
    ANSYS(R)  COPYRIGHT(C) 1971, 1978, 1982, 1983, 1985, 1987, 1989, 1990   SWANSON
ANALYSIS SYSTEMS, INC. AS UNPUBLISHED WORK.
    PROPRIETARY DATA - UNAUTHORIZED USE, DISTRIBUTION OR DUPLICATION IS
PROHIBITED.  ALL RIGHTS RESERVED.
    FOR SUPPORT CALL JIM CARRAS       PHONE 814/865-1444      TWX

 VSM analysis                                              1.7229  MAY 19,1993 CP=     17.940
**UNIVERSITY VERSION FOR EDUCATIONAL PURPOSES ONLY**

      ***** POST1 REACTION FORCE LISTING *****

 LOAD STEP    1  ITERATION=    1  SECTION=  1
 TIME=   0.00000E+00    LOAD CASE=  1

 THE FOLLOWING X,Y,Z FORCES ARE IN GLOBAL COORDINATES

   NODE     FX           FY           FZ           MX           MY           MZ
   175  0.23785105E-07   2884.7711     0.60472303E-08 -131.73300     -127.97719      161.40793

 TOTAL    0.23785105E-07   2884.7711     0.60472303E-08 -131.73300     -127.97719      161.40793

 NSEL  FOR LABEL= NODE  FROM     1 TO     1 BY    1

    1  NODES (OF    175  DEFINED) SELECTED BY  NSEL  COMMAND.

 PRINT NODAL DISPLACEMENTS
```

```
1          ANSYS - ENGINEERING ANALYSIS SYSTEM  REVISION 4.4      A 16   PENN STATE
MAY 1,1990
    ANSYS(R)  COPYRIGHT(C) 1971, 1978, 1982, 1983, 1985, 1987, 1989, 1990   SWANSON
ANALYSIS SYSTEMS, INC. AS UNPUBLISHED WORK.
    PROPRIETARY DATA - UNAUTHORIZED USE, DISTRIBUTION OR DUPLICATION IS
PROHIBITED.  ALL RIGHTS RESERVED.
    FOR SUPPORT CALL JIM CARRAS       PHONE 814/865-1444      TWX

 VSM analysis                                          1.7230  MAY 19,1993 CP=     17.980
 **UNIVERSITY VERSION FOR EDUCATIONAL PURPOSES ONLY**

       ***** POST1 NODAL DISPLACEMENT LISTING *****

 LOAD STEP    1  ITERATION=    1  SECTION=  1
 TIME=  0.00000E+00     LOAD CASE=  1

 THE FOLLOWING X,Y,Z DISPLACEMENTS ARE IN GLOBAL COORDINATES

   NODE     UX           UY           UZ           ROTX         ROTY         ROTZ
    1  0.39125873E-04 -0.80068314E-04  0.18829971E-03  0.16011697E-03  0.56583445E-04 -
0.40274147E-03

 MAXIMUMS
 NODE        1            1            1            1            1            1
 VALUE   0.39125873E-04 -0.80068314E-04  0.18829971E-03  0.16011697E-03  0.56583445E-04 -
0.40274147E-03

 NSEL  FOR LABEL= NODE  FROM     0 TO     0 BY    1

 ***WARNING ***                        CP=     18.020   TIME=  1.72298
 STARTING RANGE FOR NODE SELECTS MUST BE GREATER THAN ZERO.
 COMMAND IGNORED.

 NSEL  FOR LABEL= NODE  FROM   151 TO   151 BY    1

    1  NODES (OF    175  DEFINED) SELECTED BY  NSEL  COMMAND.

 PRINT NODAL DISPLACEMENTS
1          ANSYS - ENGINEERING ANALYSIS SYSTEM  REVISION 4.4      A 16   PENN STATE
MAY 1,1990
    ANSYS(R)  COPYRIGHT(C) 1971, 1978, 1982, 1983, 1985, 1987, 1989, 1990   SWANSON
ANALYSIS SYSTEMS, INC. AS UNPUBLISHED WORK.
    PROPRIETARY DATA - UNAUTHORIZED USE, DISTRIBUTION OR DUPLICATION IS
PROHIBITED.  ALL RIGHTS RESERVED.
    FOR SUPPORT CALL JIM CARRAS       PHONE 814/865-1444      TWX

 VSM analysis                                          1.7230  MAY 19,1993 CP=     18.050
 **UNIVERSITY VERSION FOR EDUCATIONAL PURPOSES ONLY**

       ***** POST1 NODAL DISPLACEMENT LISTING *****

 LOAD STEP    1  ITERATION=    1  SECTION=  1
```

```
 TIME=   0.00000E+00     LOAD CASE=  1

 THE FOLLOWING X,Y,Z DISPLACEMENTS ARE IN GLOBAL COORDINATES

   NODE     UX           UY           UZ           ROTX         ROTY         ROTZ
    151   0.36870888E-04 -0.10915808E-03  0.85300736E-04  0.14516819E-03  0.56583445E-04
0.34752135E-03

 MAXIMUMS
 NODE       151          151          151          151          151          151
 VALUE    0.36870888E-04 -0.10915808E-03  0.85300736E-04  0.14516819E-03  0.56583445E-04
0.34752135E-03


 ***** ROUTINE COMPLETED *****  CP =       18.070

 /EOF ENCOUNTERED ON FILE18


 PREP7 AFWRITE OR SFWRITE WARNING MESSAGES =   0
 NUMBER OF SOLUTION PHASE WARNING MESSAGES =   0


 ***** RUN COMPLETED *****  CP=      18.1600   TIME=    1.7231
```

Appendix D

MANUFACTURING DRAWINGS OF THE VOLUME SCANNING MECHANISM

This appendix contains the detailed manufacturing drawings for the volume scanning mechanism. Figure D1 and D2 give further views of the VSM from that shown in Chapter 4. Figures D3 through D6 show the assembly drawings for the mounting brackets for the lidar and radar systems. The support brackets are the brackets that extend from the side of the fork system without the GME assembly. The difference between the two brackets is that the lidar mounting plate was made to be bolted around the optical table and the radar mounting plate was made to be mounted to a flat plate on the radar housing unit. The remaining figures show the drawings for the individual pieces that are required for the two identical VSM's.

Figures D7 and D8 are the plates that will hold the base square tubing, Figure D11, in place and create a flat surface for ground placement of the VSM. Figures D9 and D10 show the horizontal and vertical plates used to mount the fork motor to the large bottom plate, Figure D8.

Figure D12 shows the plate is used to help distribute the load carried through the cylindrical base to the base square tubing. This plate is attached to the square tubing, the base capping cylinder, Figure D13, and the angle irons used to link the plate with the base square tubing.

Figure D14 shows how the base bearing holding cylinder was manufactured. This cylinder is the casing that will house the radial bearings for the fork shaft, Figure D16. The fork shaft is press fit into the bearings and the shaft mounting cylinder, Figure D15, is bolted to the top of the shaft. The bottom of the shaft is bolted to the motor to fork shaft interface to allow an easy link between the gme shaft and the fork shaft. This arrangement is then prepared to be bolted to the "u-shaped" portion of the fork component.

Figure D18 shows the angle that was used to bolt the base configuration with the bottom square tubing of the "u-shaped" portion of the fork component, Figure D22. The bottom of the "u-shaped" portion is welded to the support and motor side square tubing, Figures D21 and D23. To increase the strength of the joint angle supports, Figure D24, are welded at the corners of the "u-shaped" portion on both sides of the u shaped portion.

To mount the table rotation motors to the fork component, four motor mounting blocks, Figure D19, are bolted to the inside of the motor square tubing inside the section where a wall has been removed, see Figure D23. A motor mounting plate made to accept the GME combination, Figure D20, is bolted to the blocks after the gme combination is mounted to the plate.

The motor shaft and key for both the lidar and radar systems, Figures D25 and D26, were welded into the appropriate mounting bracket. The shaft that did not need to be prepared for linking to a motor was made as shown in Figure D27. The radar system used the radar mounting plate, Figure D28, to mount both shafts to the radar system. The lidar system used a lidar mounting bracket, Figure D29, to attach both shafts to the lidar system.

These drawings were used by metal machinists to produce the parts and preassemble parts of the VSM. Due to the time required to manufacture the parts -- 5 weeks -- complete assembly of both VSM's was not accomplished.

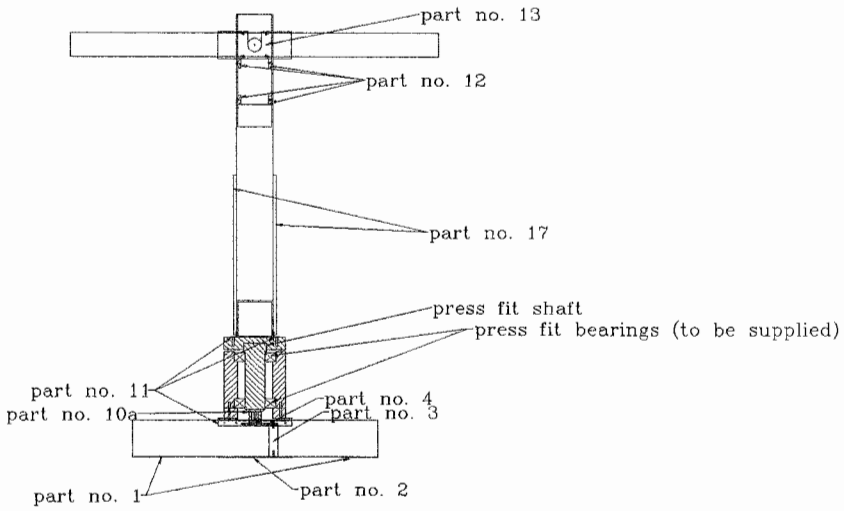

Figure D1: Volume Scanning Mechanism (Side View)

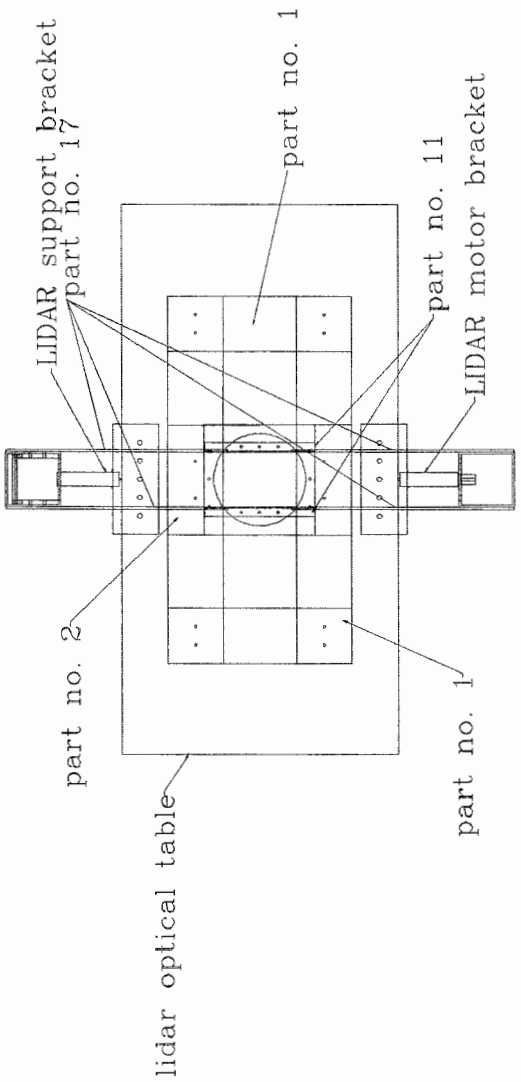

Figure D2: Volume Scanning Mechanism (Top View)

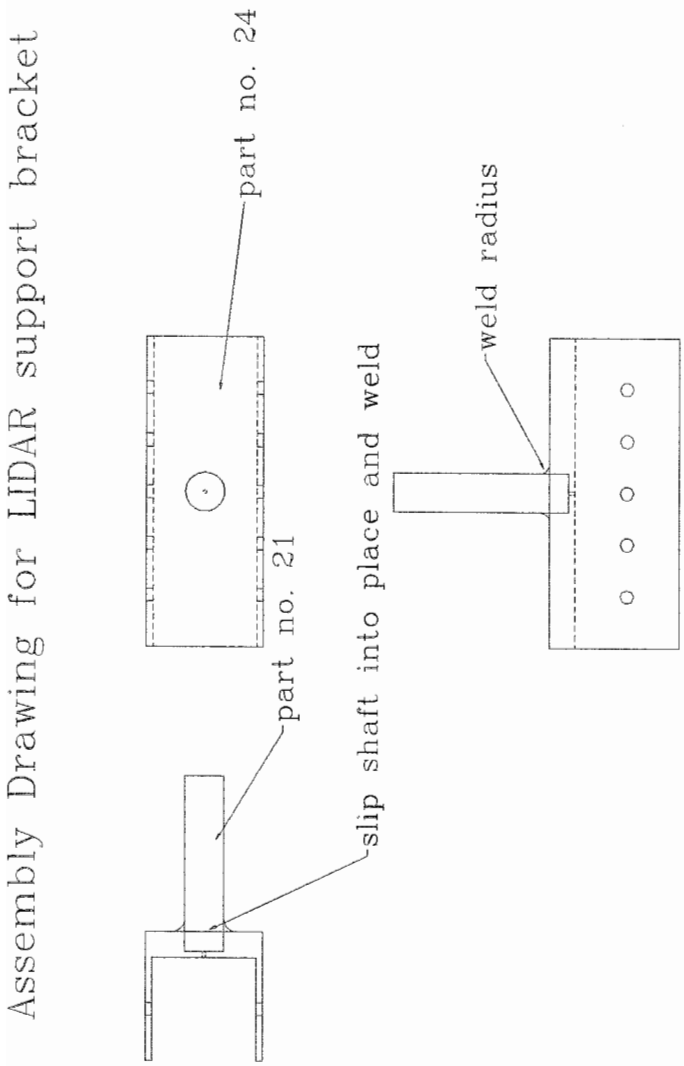

Figure D3: LIDAR Support Bracket

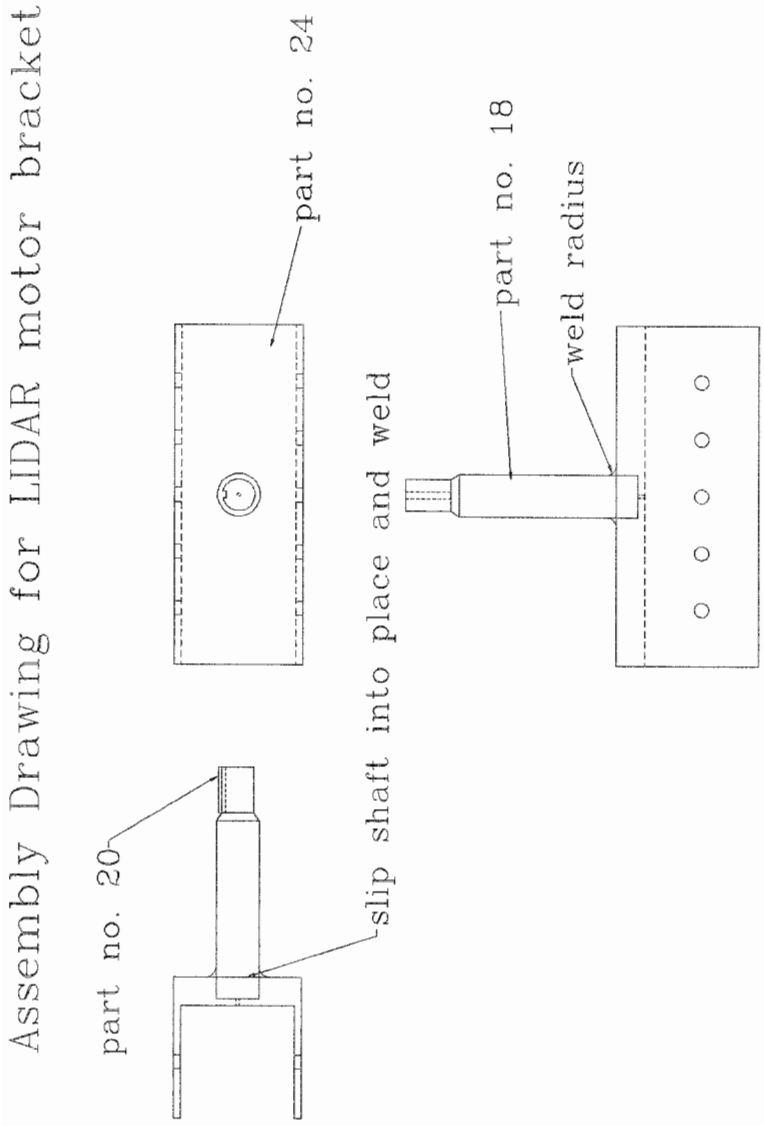

Figure D4: LIDAR Motor Bracket

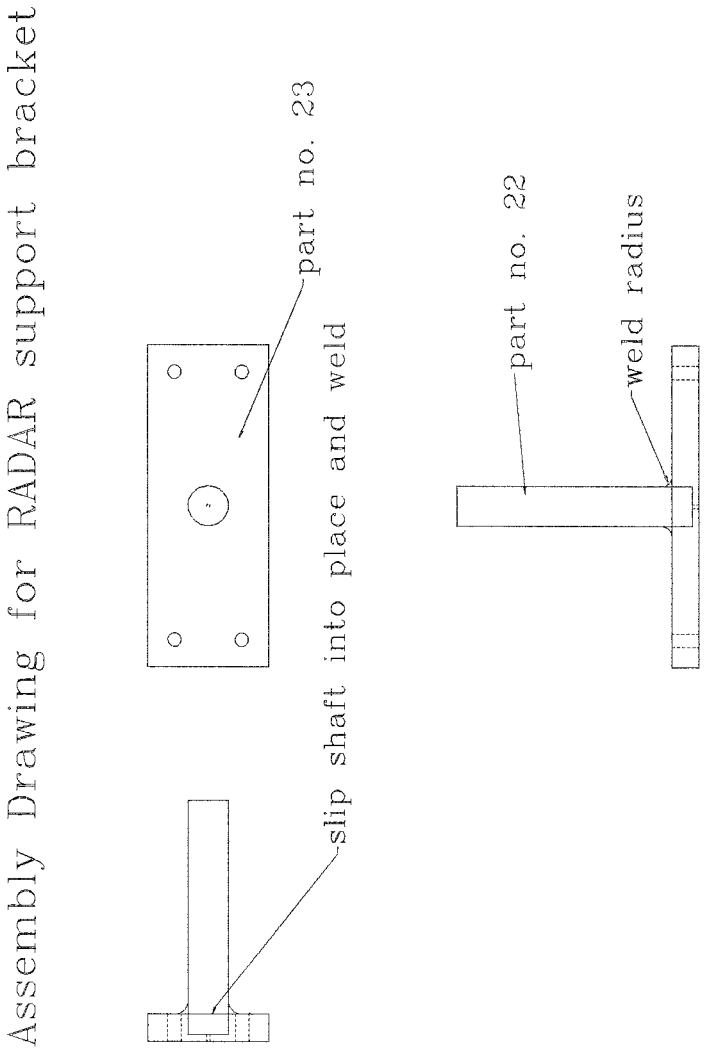

Figure D5: RADAR Support Bracket

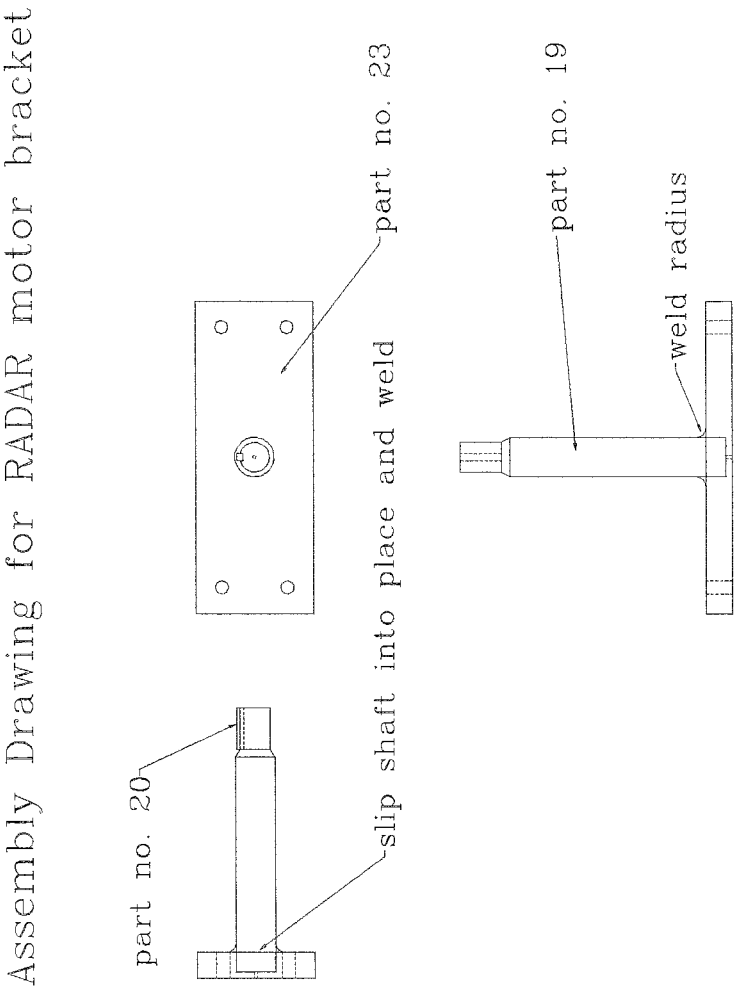

Figure D6: RADAR Motor Bracket

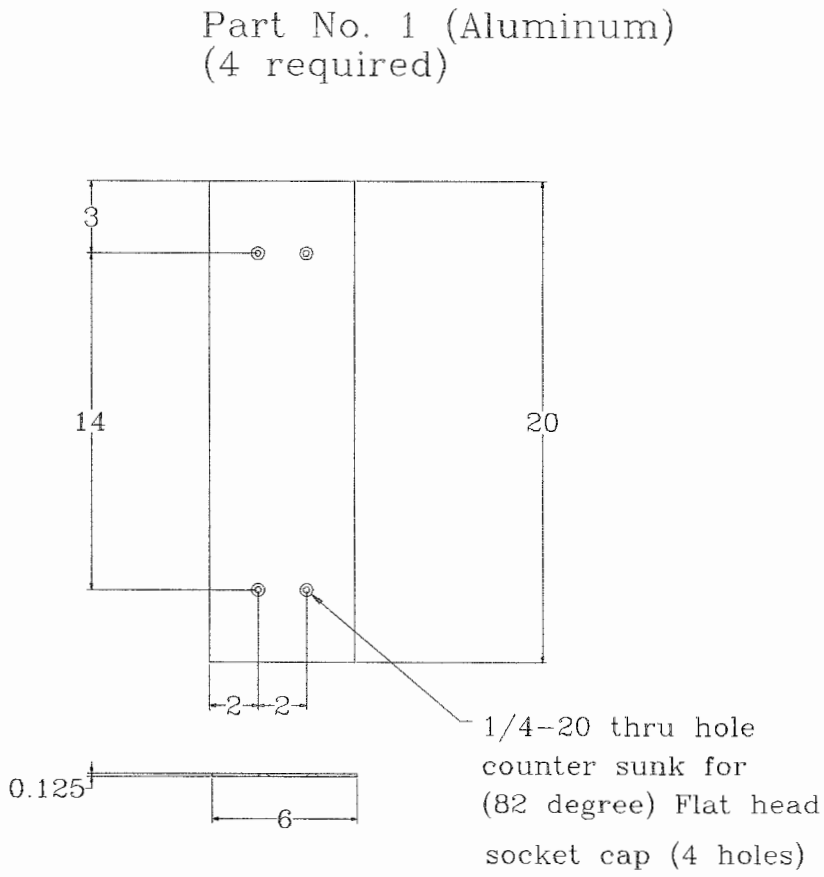

Figure D7: Part No. 1 Small Bottom Plate

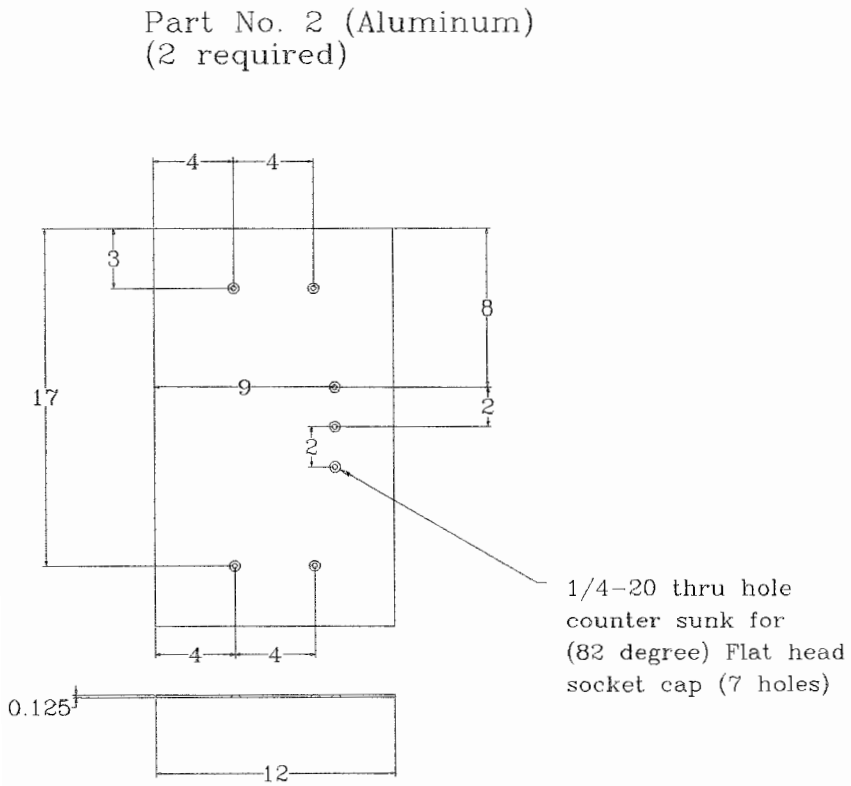

Figure D8: Part No. 2 Large Bottom Plate

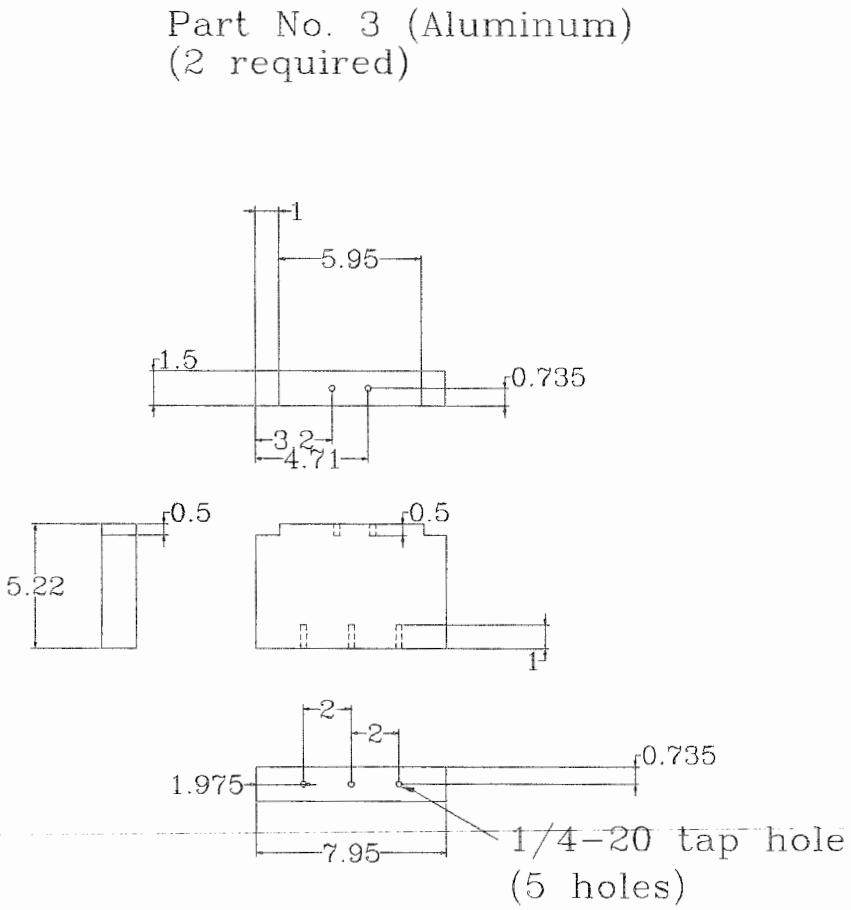

Figure D9: Part No. 3 Fork Motor Vertical Plate

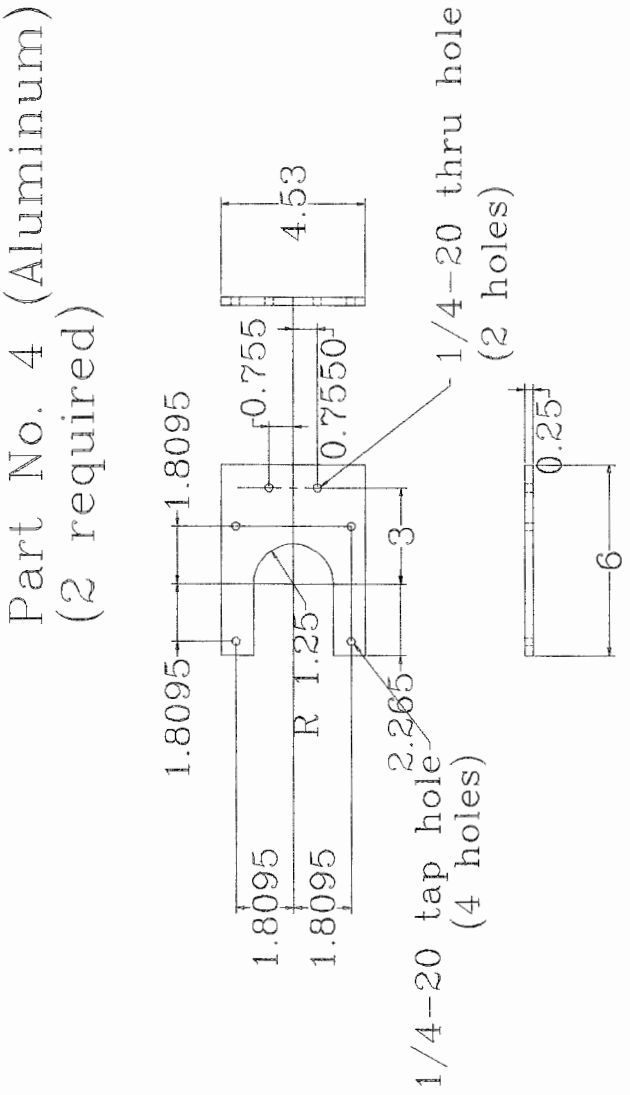

Figure D10: Part No. 4 Fork Motor Horizontal Plate

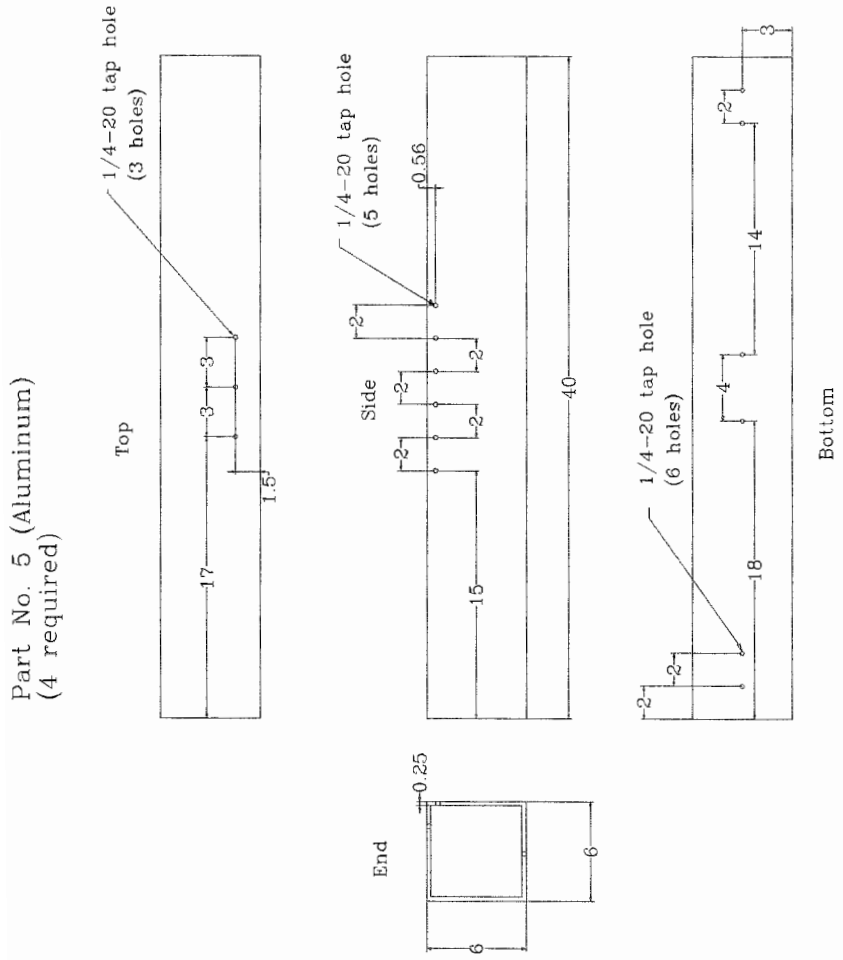

Figure D11: Part No. 5 Base Square Tubing

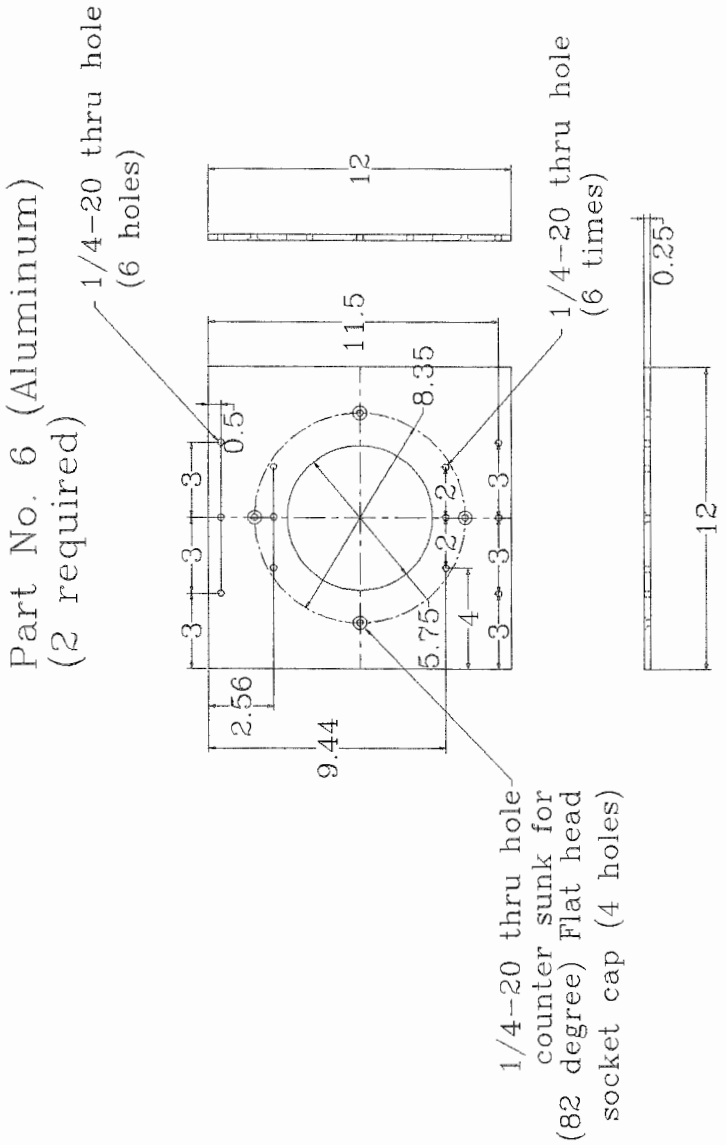

Figure D12: Part No. 6 Base Load Distribution Plate

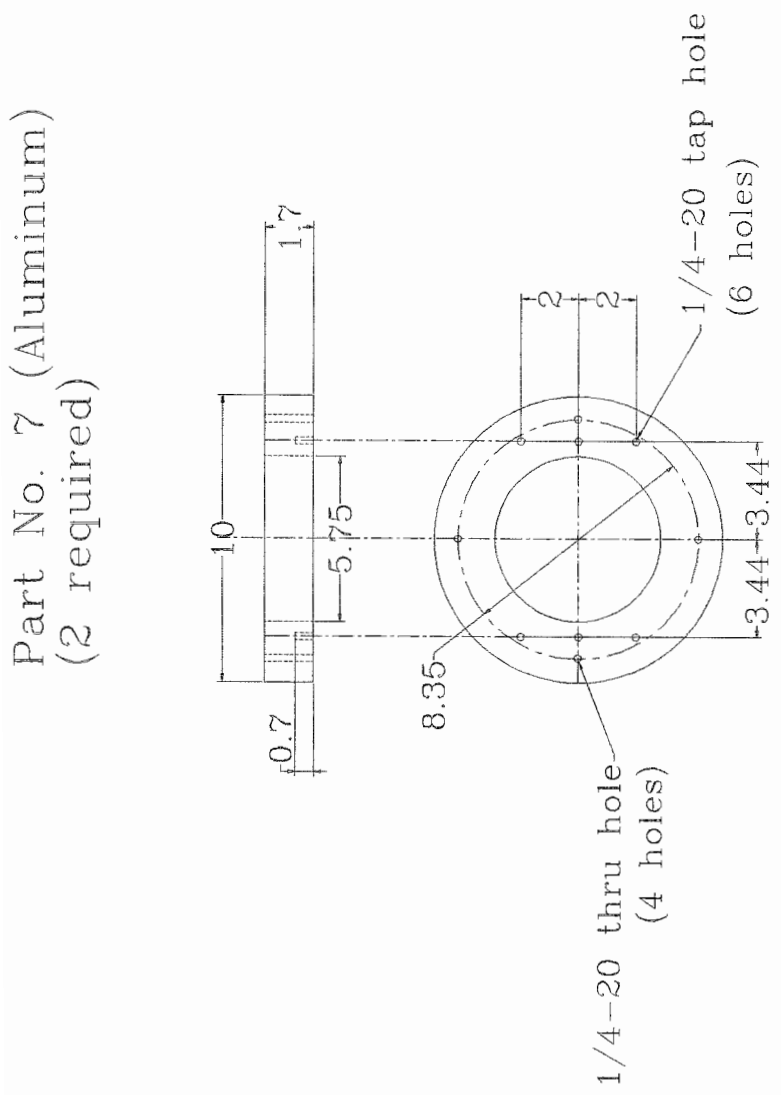

Figure D13: Part No. 7 Base Capping Cylinder

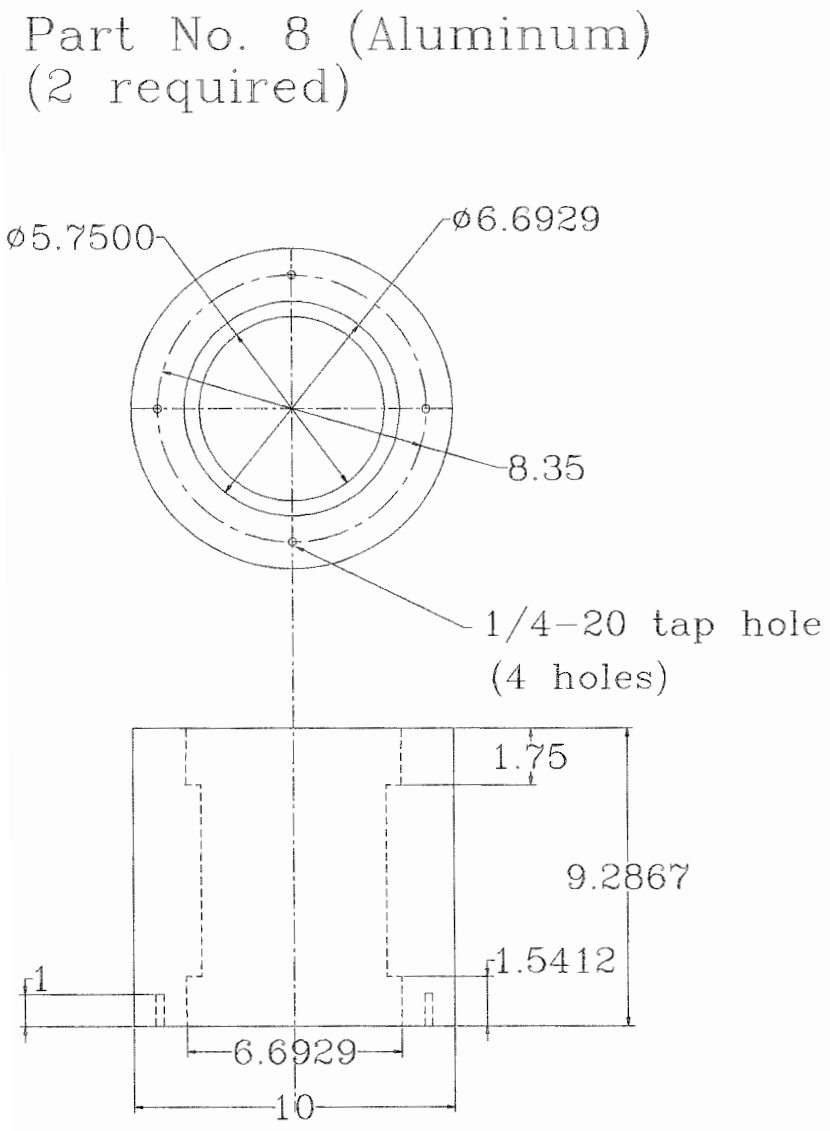

Figure D14: Part No. 8 Base Bearing Holding Cylinder

Part No. 9 (Aluminum)
(2 required)

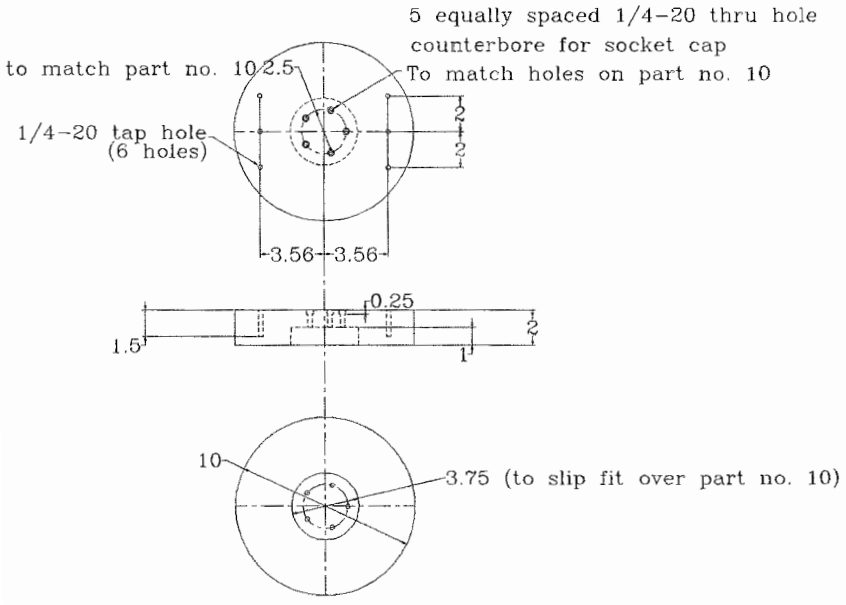

Figure D15: Part No. 9 Shaft Mounting Cylinder

Part No. 10 (Aluminum)
(2 required)

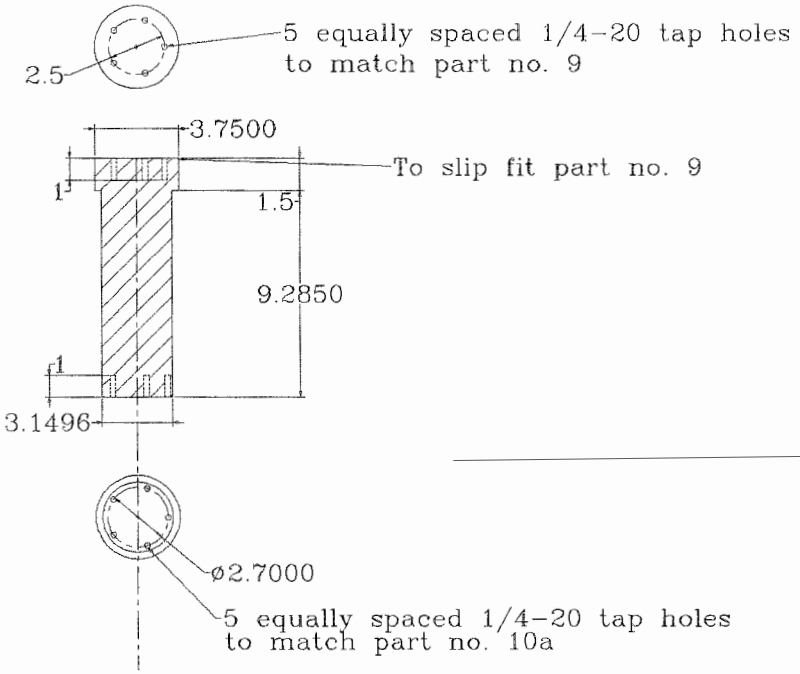

Figure D16: Part No. 10 Fork Shaft

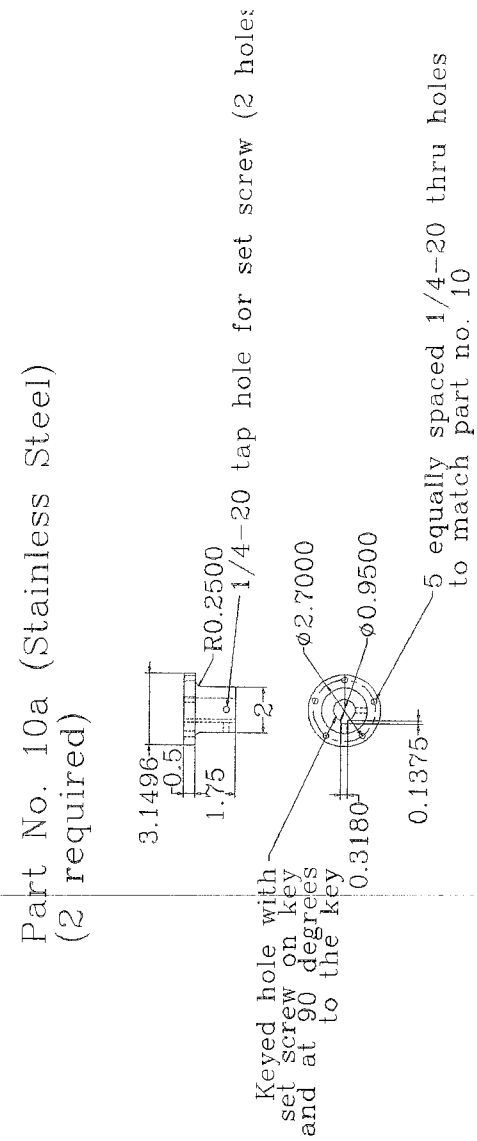

Figure D17: Part No. 10a Motor to Fork Shaft Interface

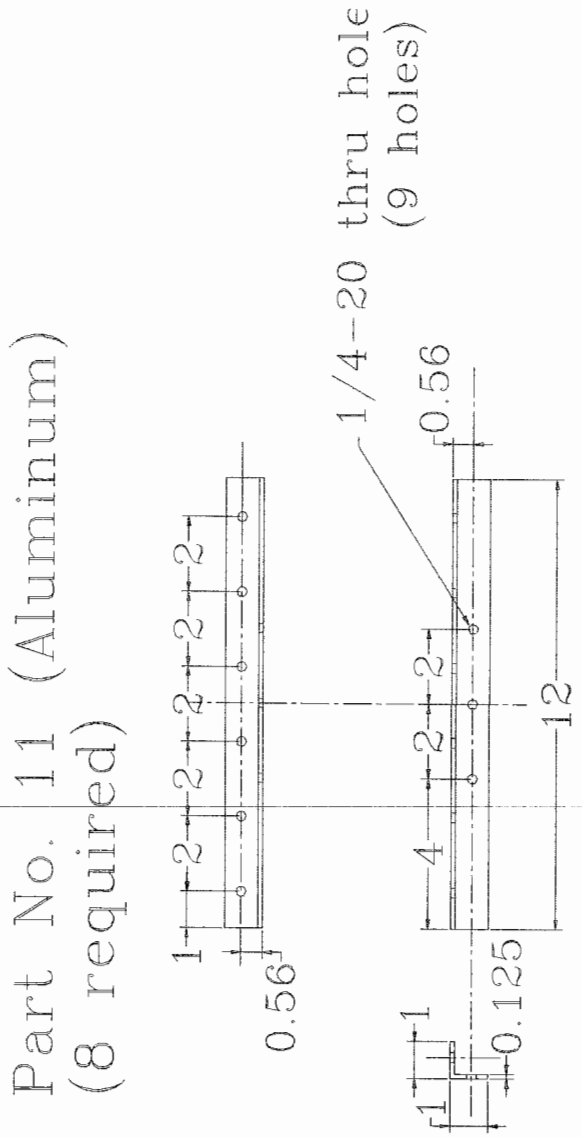

Figure D18: Part No. 11 Base to U Shaped Portion Mounting Bracket

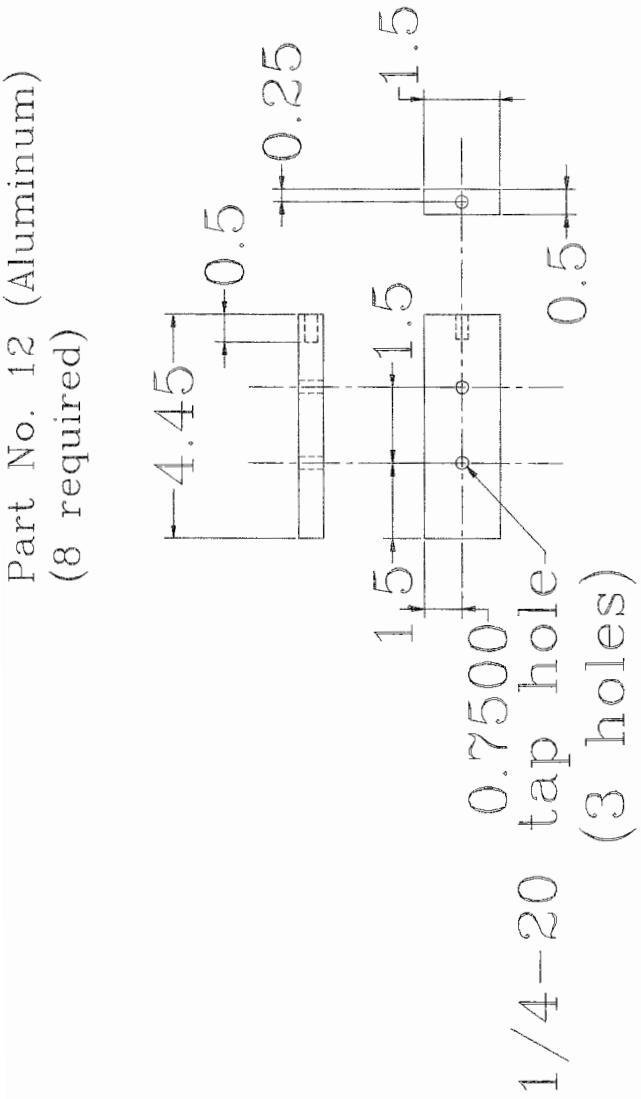

Figure D19: Part No. 12 Table Motor Mounting Block

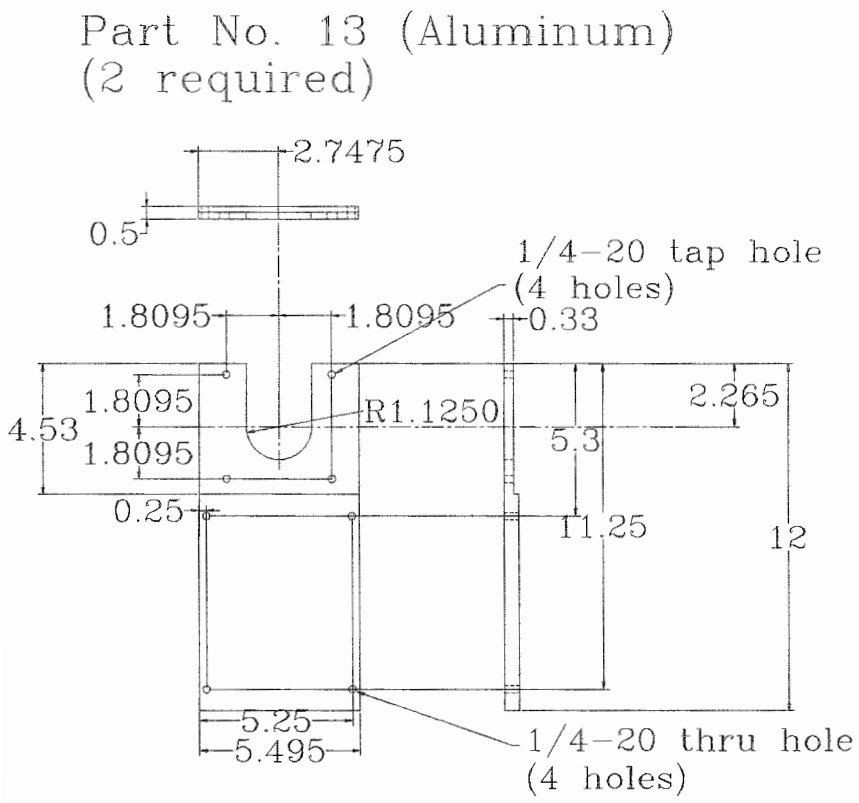

Figure D20: Part No. 13 Table Motor Mounting Plate

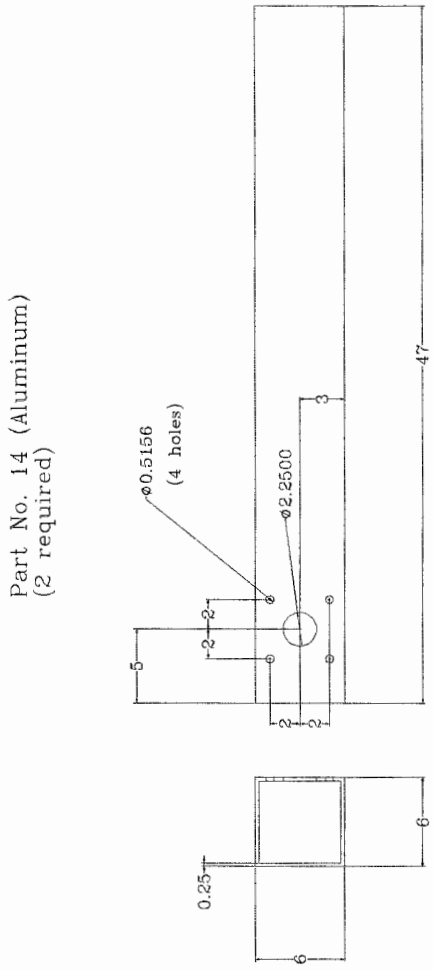

Figure D21: Part No. 14 U Shaped Portion Support Side Square Tubing

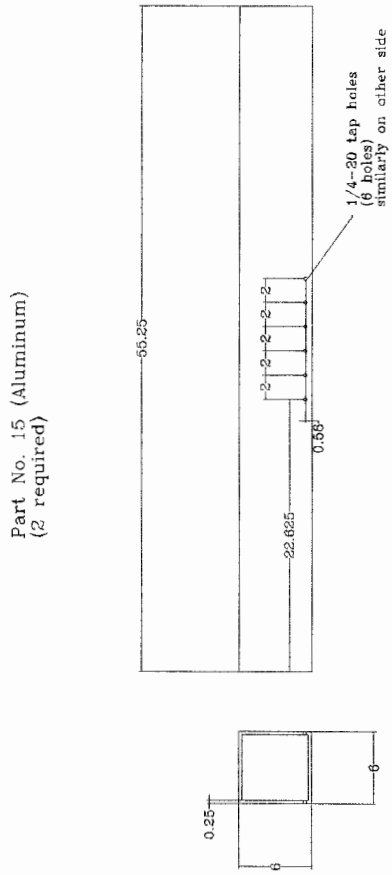

Figure D22: Part No. 15 U Shaped Portion Bottom Square Tubing

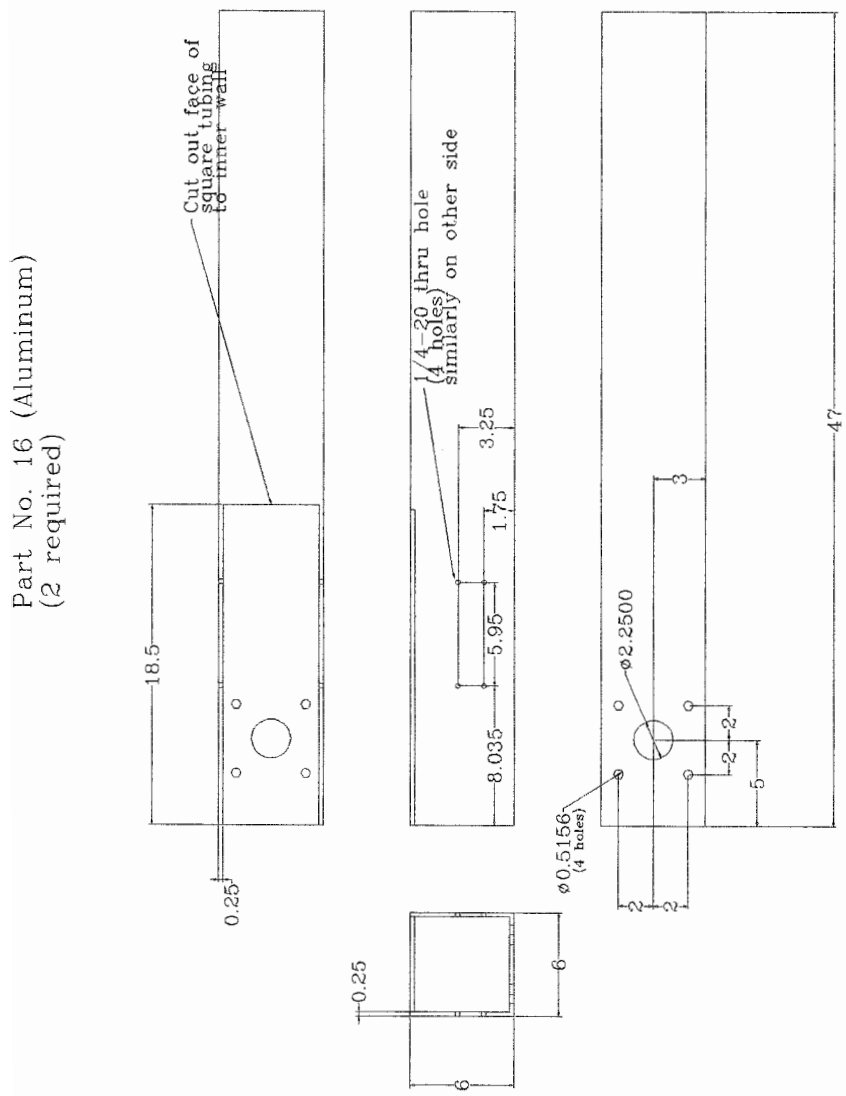

Figure D23: Part No. 16 U Shaped Portion Motor Side Square Tubing

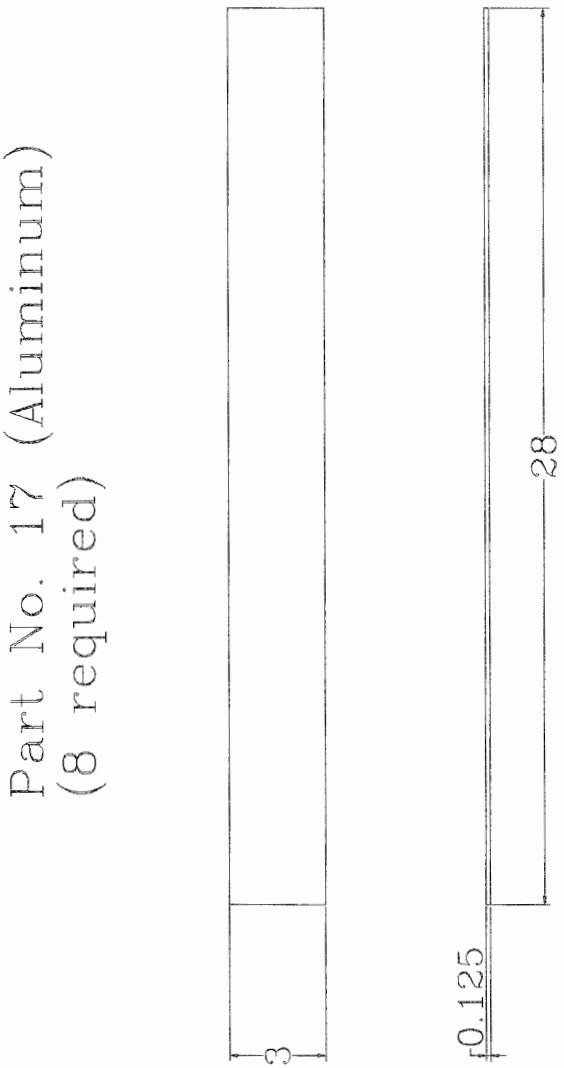

Figure D24: Part No. 17 U Shaped Portion Angle Supports

Part No. 18 & 19 (Aluminum)
(1 each required)

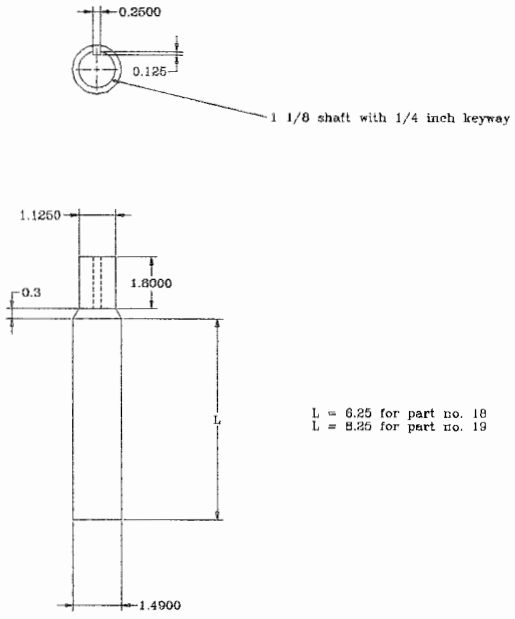

Figure D25: Part No. 18 & 19 LIDAR and RADAR Motor Shafts

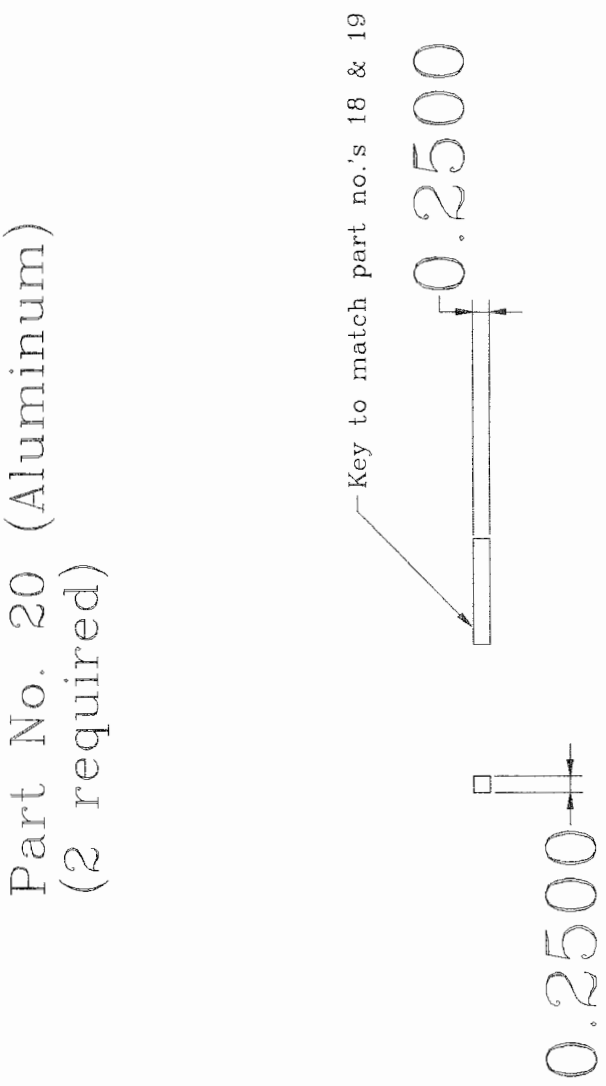

Figure D26: Part No. 20 LIDAR and RADAR Keys for Shafts

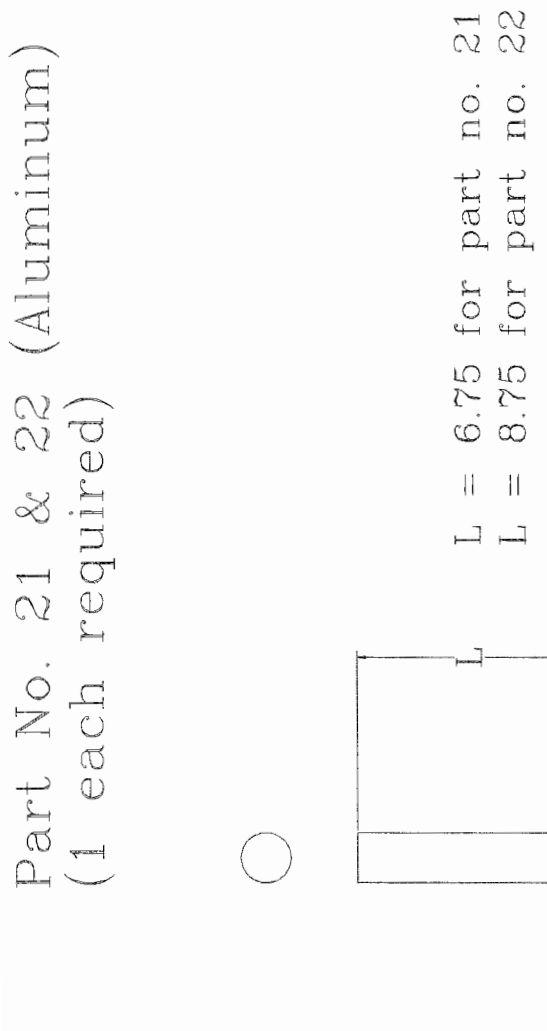

Figure D27: Part No. 21 & 22 LIDAR and RADAR Support Shafts

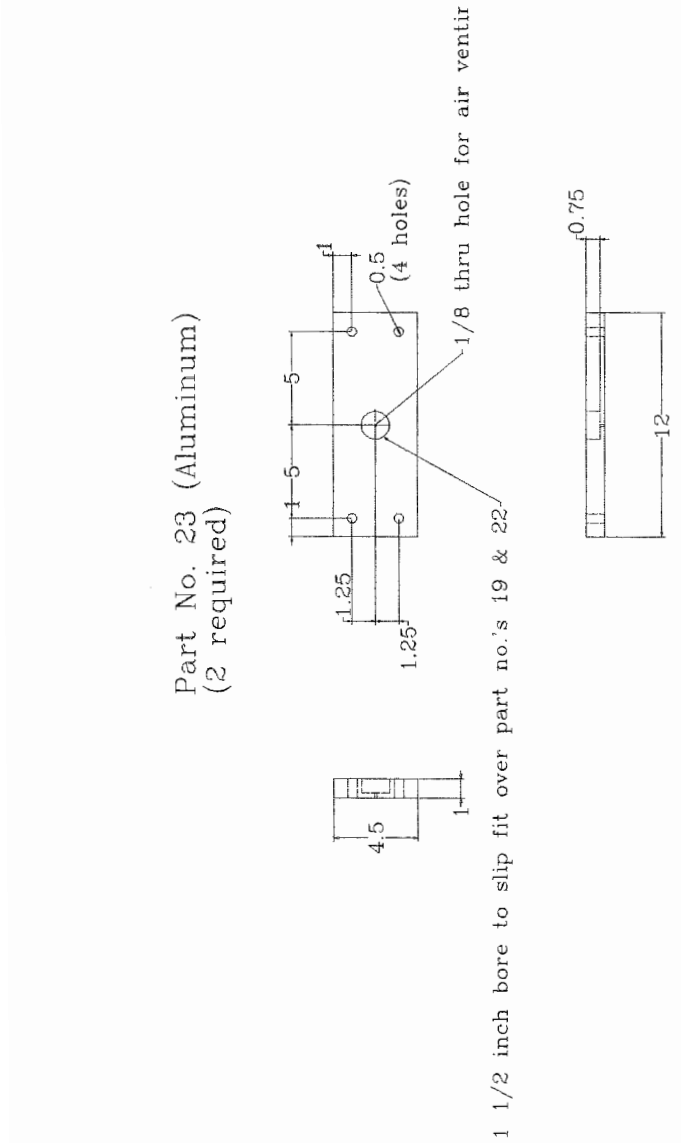

Figure D28: Part No. 23 RADAR Table Mounting Plate

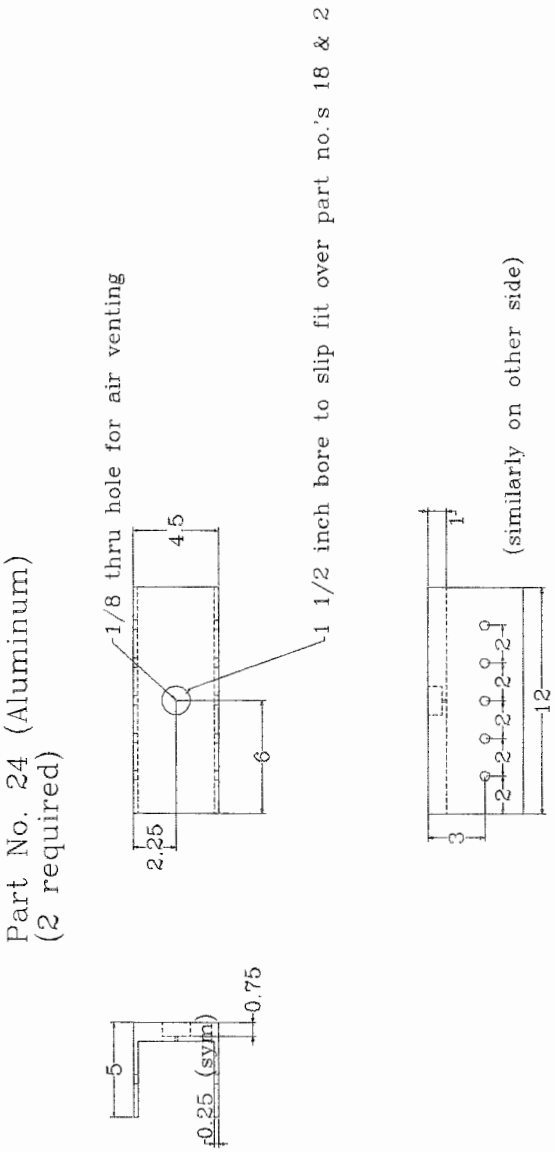

Figure D29: Part No. 24 LIDAR Table Mounting Bracket